EXPERIMENTS WITH GEOMETRIC NON-LINEAR COUPLING FOR ANALYTICAL VALIDATION

THESIS

Jonathan D. Boston

AFIT/GAE/ENY/10-M04

DEPARTMENT OF THE AIR FORCE
AIR UNIVERSITY

AIR FORCE INSTITUTE OF TECHNOLOGY

Wright-Patterson Air Force Base, Ohio

AFIT/GAE/ENY/10-M04

EXPERIMENTS WITH GEOMETRIC NON-LINEAR COUPLING FOR ANALYTICAL VALIDATION

THESIS

Presented to the Faculty

Department of Aeronautics and Astronautics

Graduate School of Engineering and Management

Air Force Institute of Technology

Air University

Air Education and Training Command

In Partial Fulfillment of the Requirements for the

Degree of Master of Science in Aeronautical Engineering

Jonathan D. Boston, BS

March 2010

AFIT/GAE/ENY/10-M04

EXPERIMENTS WITH GEOMETRIC NON-LINEAR COUPLING FOR ANALYTICAL VALIDATION

Jonathan D. Boston, BS

Approved:

//signed//	17 Mar 2010
Lt Col Eric D. Swenson (Chairman)	Date
//signed//	17 Mar 2010
Dr. Donald Kunz (Member)	Date
//signed//	17 Mar 2010
Dr. Maxwell Blair (Member)	Date

Abstract

This study was focused on obtaining accurate experimental data for the validation of the geometrically exact beam theory from a series of experiments in which high quality surface shape and deflection data was collected. Many previous experiments have experienced issues with data collection or test articles which the researchers were unable to overcome. The test program was performed in two stages: qualification and joined-wing. The qualification stage validated the experimental procedures on simple 72 in long aluminum beams with 8 in x 0.5 in cross-sections. The joined-wing stage was the primary experiment focused on obtaining quality data for use in validation and each joined-wing had an overall length of 57 in. The fore wing was designed with a chord of 8 in and a thickness of 0.5 in; the aft wing was designed with a chord of 6 in and a thickness of 0.5 in. These dimensions were chosen so the joined-wing produced a non-linear bend-twist couple before permanent deformation. The bend-twist couple in a solid cross-section aluminum joined-wing was successfully captured with surface shape, deflection points, and strain data.

To God and my Wife

Acknowledgements

I would like to express my appreciation to my research advisor, Lt Col Eric Swenson, for his guidance and support throughout this research. I would also like to thank my sponsor, Dr. Max Blair, for the support, perspective, and guidance he provided during this endeavor.

I would like to also thank those who made the experiments possible, including Chris Zickenfoose for his laboratory support and Jason "Turk" Vangel for his fabrication efforts. Without these and many others, this research would not have been possible.

Finally, I would like to thank my wife for all her support during this thesis. Her understanding, encouragement, and patience made this paper possible.

Jonathan D. Boston

Table of Contents

Page

List of Figures

Page

Page

Page

List of Tables

EXPERIMENTS WITH GEOMETRIC NON-LINEAR COUPLING FOR ANALYTICAL VALIDATION

I. Problem Statement

The joined-wing concept is being evaluated by the Air Force Research Laboratories (AFRL) for use in High Altitude Long Endurance (HALE) Intelligence, Surveillance and Reconnaissance (ISR) aircraft, similar in design to the Boeing SensorCraft, represented in Fig. 1.1. The joined-wing concept was patented by Wolkovich, who in 1986 presented his concept as a viable alternative to conventional aircraft. He cited light weight and high wing stiffness among the chief benefits. Many researchers have and still are working on analyzing and optimizing his initial concept. [19]

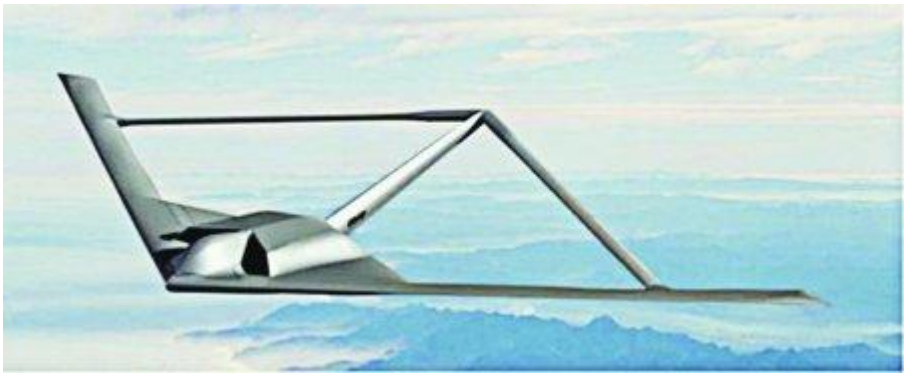

Figure 1.1: Boeing SensorCraft Concept. [16]

While significant work has been performed analytically and aerodynamically on the joined-wing, experimental validation of the structural response is lacking. Part of this lack of experimentation stems from the difficulty of performing the experiment and the fidelity of current analytical tools. When optimizing a joined-wing aircraft design, the unique bend-twist deformations require non-linear analyses, which significantly increase solution time over linear analyses. Analytical tools are being created using a newer beam theory which has shown great promise to significantly decrease solution time for optimization. One of the primary tools is geometrically exact beam theory (GEBT). [10]

GEBT is a reformulation of the basic beam equations that avoids the limiting approximations in Euler-Bernoulli beam theory. However, GEBT, like any other new theory, should be validated experimentally.

Other sources of geometric non-linearities include the following: large displacements, follower forces, and coupling. Large displacements violate the linear assumptions which simplify the equations. Follower forces change directions as a structure is loaded, which requires non-linear analyses. Coupling includes any two effects that depend on each other as a load is applied, such as global and local buckling in a hollow beam or the bend-twist in the joined-wing design.

The goals of this research are to provide experimental data on simple joined-wing test articles that will allow researchers to validate tools like GEBT for use in the design of joined-wing HALE aircraft, to develop a standard set of experimental procedures for testing joined-wings in the lab, and to compare experimental data with analytical results.

This research begins with an overview of previous work done on joined-wing aircraft. Next, the design and setup of the experiments for this research are discussed in detail. There are two stages to the experiment: qualification and joined-wing. The qualification stage involves simple wings and is for the development of the standard set of experimental procedures. The joined-wing stage is the primary experimental stage and produces the experimental measurements for use in validation. Last, the results of the experiments are discussed as well as preliminary finite element (FE) models and their analyses. All FE analyses require a non-linear solver: the qualification models because of large deformations and non-linear geometric couplings, and the joined-wing models because of the bend-twist coupling.

II. Background

This research is the result of several previous and ongoing research projects, including the novel joined-wing design and development of conceptual analysis tools such as GEBT. In this chapter, the joined-wing aircraft, previous experimental work, and previous analytical work are discussed.

2.1 The Joined-Wing Aircraft

Throughout the history of aircraft design, unique concepts have been tried by designers with the goal of better aircraft design. The joined-wing is no exception; however, it wasn't until 1986, when Wolkovich [19] published his research into his patented concept, that aircraft designers started to seriously consider the joined-wing. Wolkovich's research showed that a joined-winged aircraft could compete with traditional aircraft designs due to light weight, high wing stiffness, low induced drag, good transonic area distribution, high trimmed C_L max, reduced wetted area and parasite drag, direct lift control capability, direct sideforce control capability, and good stability and control. Initial optimization studies showed that while there were benefits of the joined-wing concept, there were no direct cost savings for a mid-ranged transport aircraft. Still, it was suggested in these studies that a different mission might provide better performance. [8, 9]

These is ongoing joined-wing research being performed in support of the AFRL SensorCraft HALE concept. [2] HALE ISR aircraft typically need very high aspect ratio wings to gain the efficiency needed to stay aloft for extended periods of time. Long wings also provide increased benefit of allowing large radar antennas to be carried internally. However, high aspect ratio wings tend to be very flexible, especially in the relatively light-weight HALE design. The joined-wing is naturally stiff and therefore an obvious design option for high aspect ratio wings. However, the load paths in the joined wing are not conventional and lead to geometric non-linear responses.

2.2 Previous Experimental Studies

Several studies have been performed to experimentally acquire static load data for the joined-wing. Each experiment has experienced issues which the researcher was unable

to overcome. Bond [3] performed research in capturing the non-linear deformations using a complex rib and spar test article shown in Fig. 2.1.

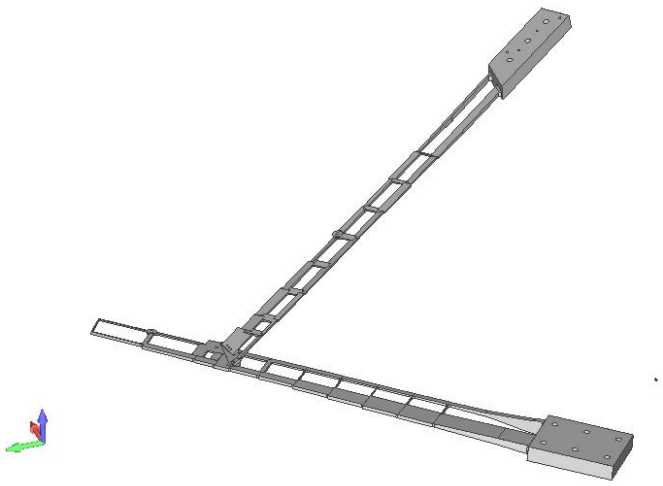

Figure 2.1: Test Article by Bond. [3]

Analysis of the experimental results collected from this test article revealed rotation and translation in the assumed rigid boundary conditions. While this did not invalidate the research performed, it decreased the usability of the collected data, since the boundary condition movement would also need to be modeled to use this data in validation of code. The test also revealed that the wing skins increased the stiffness to the point that the non-linear effects were not seen, and the skins were removed for the experiment. Third, displacement data was collected at only three points on the experiment. While these three points could be used to help compare to analytical models, they were not sufficient to capture the full shape of the joined-wing as it deformed. Finally, fourteen stage gages were placed on the test article to measure strain. The strain gage data highlighted issues with the boundary conditions.

A second experimental study was performed by Green, Keller, and this author [4] on a simple aluminum plate joined-wing test article produced by Simpson for AFRL. Figure 2.2 shows the test article and corresponding FE model. This experiment was this author's first attempt to record surface shapes and match them to different FE models. Green *et al.* had issues in tuning the FE model to the experimental results, and it was concluded that the test article had been permanently deformed during the testing.

The welded joint between the fore and aft wings was also found to be cracked after the testing. This permanent deformation was not recorded in the data and therefore most of the test data had an unknown zero load offset. This accidental permanent deformation highlighted the need to methodically re-record the unloaded test article for data comparison and ensure that applied loads do not yield the structure.

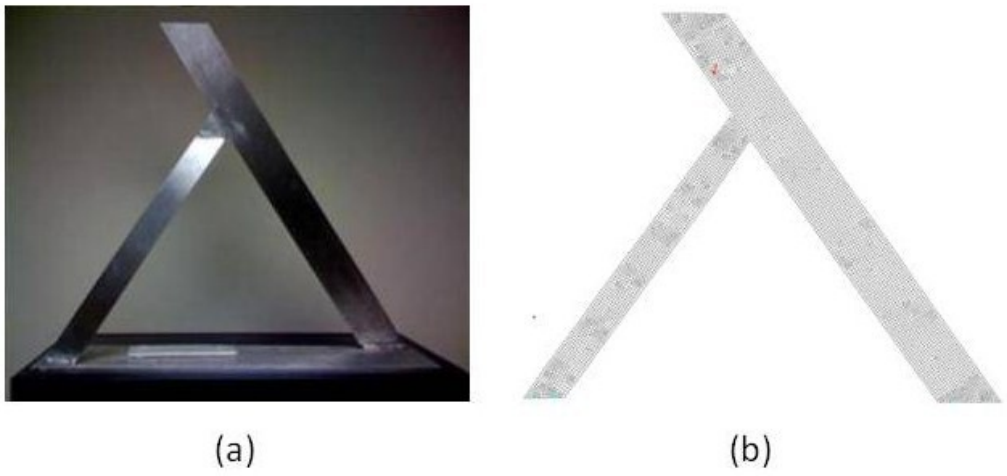

Figure 2.2: 1 Meter Joined-wing (a) Test Article and (b) FE Model. [4]

Patil [17] tested a joined-wing configuration, but did not see non-linear deformations before material yield. He showed that a joined-wing is significantly stiffer than a single wing model. For Patil's experiment, two joined-wings were constructed, both out of 1 in x 1/8 in aluminum bars. The main wing was 20 in long. A single wing was also constructed to serve as a comparison. The first joined-wing was planar and the second non-planar, as depicted in Fig. 2.3.

The non-planar wing showed the least amount of tip and joint deflection, while the single wing showed many times more. The planar wing's deflection was between the non-planar joined-wing and the single wing. This research points out that not all joined-wings exhibit non-linear deformations before material yield; the cross-section contributes greatly to the type of deformations which will be seen.

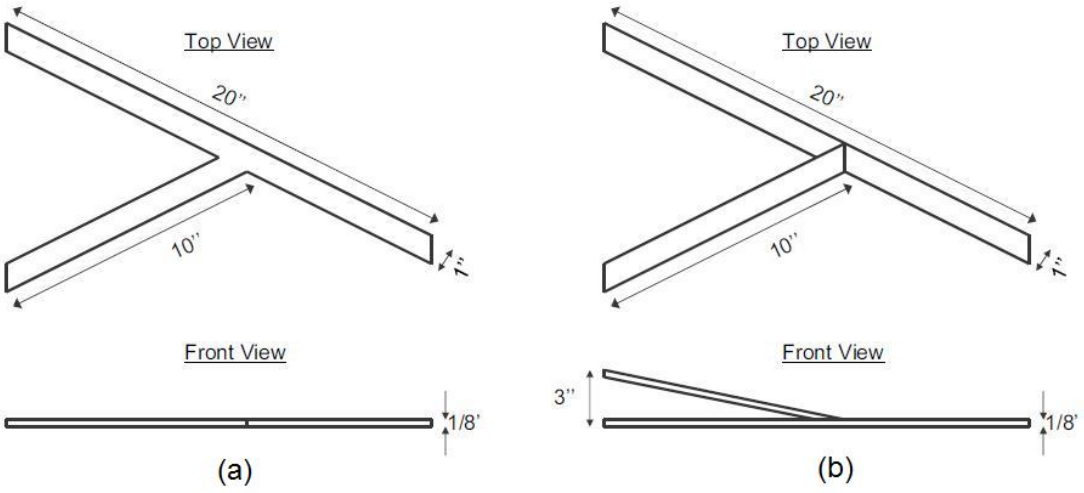

Figure 2.3: Two Joined-wing Cases: (a) Planar and (b) Non-planar. [17]

2.3 Previous Analytical Work

Most joined-wing concepts have been analytically tested due to the lower costs associated with computer simulation in comparison to building and testing a physical test article. Computer simulations allow many different cases to be tested and compared; however, unless the simulation has been validated, few quantitative results can be accurately determined.

Several researchers at the University of Cincinnati used FE analysis (FEA) to model various joined-wing configurations and to compare different FEA solvers. Models were created to accurately represent the internal and external structure of the joined-wing. Marisarla [14] constructed the FE model with skins, ribs, and stringers, as depicted in Fig. 2.4. However, most of the analyses were performed assuming small (linear) deformations. Also, much time was spent converting the model for use with several different FEA solvers so as to compare results between the solvers to see how closely they matched. His research showed the importance of knowing how to correctly use the FEA tools available. It also showed that, had experimental data been available, much of the guesswork would have been removed, as the answer would have been known.

Narayanan [15], also from the University of Cincinnati, used FEA to analyze an aerodynamically shaped joined-wing model. He compared the results of two models and

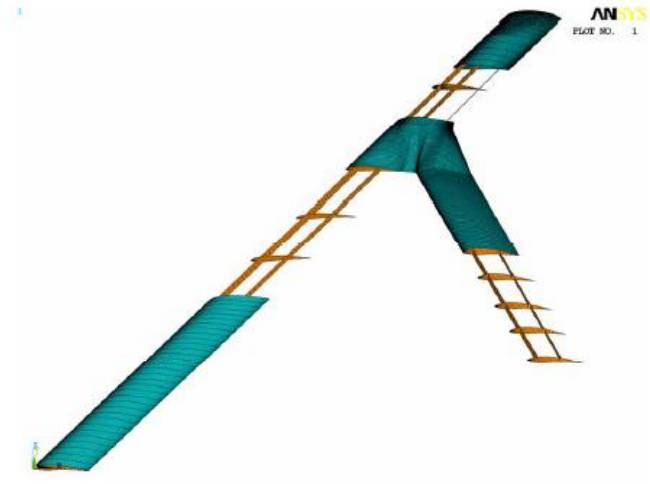

Figure 2.4: Detailed Joined-wing FEM. [14]

both linear and non-linear solutions. The models were constructed out of shell elements, one having unstructured elements and the other structured elements. The unstructured model was similar to Marisarla's joined-wing in Fig. 2.4. The structured model is shown in Fig. 2.5 with the skins removed. Narayanan concluded that when linear and non-linear solutions were compared, the solutions diverged as the loads increased. This showed that the joined-wing models required a non-linear solver to accurately predict the deformations. The non-linear solutions also predicted skin buckling at the higher loads. Narayanan concluded that non-linear solvers are required to accurately predict joined-wing deflections and stresses.

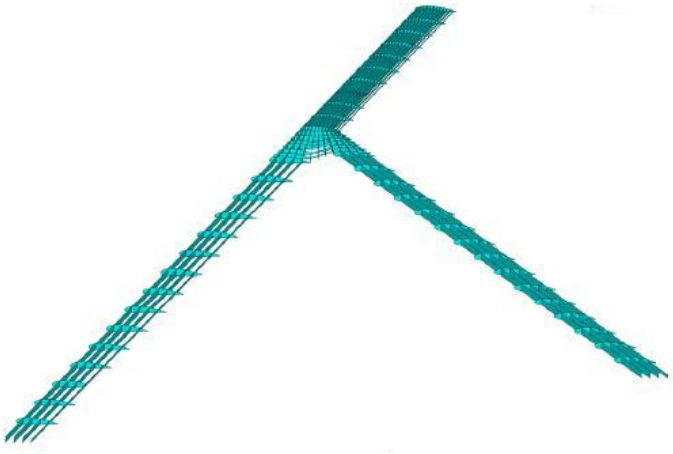

Figure 2.5: Plate Joined-wing FEM - Skins Removed to Show Detail. [15]

Rasmussen [18] investigated many joined-wing configurations in search of the weight optimal joined-wing. Fore and aft wing sweep, vertical displacement, and joint location were considered. It was discovered that there are several locally optimal wing configurations, depending on the critical failure mode. The two main configurations differed as to whether the fore and aft wings were in-plane with each other or at opposite dihedral angles. With a vertical separation between the wings, there are more issues of global wing buckling versus local skin buckling with the in-plane wings. The non-linear responses were also examined and it was determined critical to include non-linear analyses in the optimization of the joined-wing. This research highlights the buckling expected with a joined-wing and the need for non-linear analysis.

Kaloyanova [13] focused on modeling a joined-wing HALE aircraft as a semi-monocoque structure as opposed to the easier but less accurate method of modeling the aircraft as a monocoque structure. A semi-monocoque model includes the internal structure of the aircraft as part of the load bearing structure. A monocoque model has the skin carrying the entire load. An initial analysis was performed on the structure using aerodynamic loads obtained from a computational fluid dynamics (CFD) model. The structural model's responses showed that the aft wing stresses were significantly higher than yield for the material. A simple optimization was completed which yielded a slightly heavier structure that did not yield under the applied aerodynamic load. As with most analytical case studies, this structural model showed that non-linear analysis was needed for the expected loads. Global buckling analyses indicated that the structure was very stable; however, a local buckling analysis was not completed.

Patil [17] performed several analytical studies after performing his experiments. When correlated with linear and non-linear analytical responses to identical loads and boundary conditions, agreement was fairly close until material yield. Both the linear and non-linear cases showed virtually the same answers. Responses were being computed using a distributed load, which showed that the joined wing was significantly stiffened by the aft wing, compared to the single wing model. The non-planar configuration was the stiffest due to the aft wing carrying a compressive load. Patil conducted a further study to see where and when buckling would first occur. The aft wing approached a buckled

state as the aft wing thickness was reduced. The dynamic analysis showed that the non-planar joined wing was significantly stiffer in bending and torsion than the planar joined wing.

Blair, Canfield, and Roberts [2] optimized a non-linear joined-wing HALE aircraft with stress constraints, geometric non-linearities, and aeroelastic trim for the ISR mission and multiple load conditions. The loads applied in these analyses accounted for the expected flight loads the aircraft might see. During the analysis, geometric non-linearity was found below the critical buckling eigenvalue, showing that non-linear analysis was required. The joined-wing aircraft was successfully optimized where mass was minimized for the various load cases. Although confidence was expressed in the theoretical development of the analysis tools, it was noted that no experimental validation has been done on the analytical tools and was highly recommended performing experimental validation.

Adams [1] looked at the Boeing SensorCraft design and outlined the optimal design. He concluded that the initial SensorCraft design was not optimized for geometric and aeroelastic non-linearities. His results indicate that global buckling is typically the critical condition for a weight optimized joined-wing design.

Because the time required to compute non-linear solutions is significant, research is being performed to find ways to perform design optimization without resorting to traditional analytical tools. One approach is to model the slender members of joined wing as beam using the geometrically exact beam theory. Hodges [12] was one of the first to coalesce the various mathematical components that make up the geometrically exact beam theory into a coherent theory without assumptions about the way the beam deforms with relation to the beam axis or the cross section. Recently, Yu provided a general-purpose implementation of the mixed formulation of the geometrically exact beam theory into a computer code called GEBT. Work has been performed by Blair, Yu, Green, and others [10, 20] which uses GEBT to optimize and design joined-wing HALE aircraft. However, little experimental work has been performed to validate these design and analysis tools. Due to this lack of experimental data, this research effort is focused on collecting data for the express purpose of validating GEBT.

III. Test Design and Setup

3.1 Experiment Setup

Due to the limited quantity and quality of current joined-wing experimental data, the primary focus of this research is to collect accurate laboratory data for use in validating analytical models. This experiment is separated into two distinct stages: qualification and joined-wing.

The qualification stage of this experiment is focused on verifying all experimental procedures, resolving construction issues, and gaining confidence in data collection and analysis. Because of the nature of the construction techniques and the amount of data collected and analyzed, the qualification stage is a risk reduction measure for the joined-wing stage through development of standardized experimental procedures and verification of the design. This data is also used as a first step in validating the analytical code. The joined-wing stage is the primary experiment of this research effort and incorporates lessons learned from procedures evaluated during the qualification stage to facilitate ease of data collection and analysis.

3.1.1 Qualification Test Articles. For the qualification stage, there are three test articles, all of which are 72 in long. The first test article is a solid 6061 aluminum beam with a cross-section of 8 in x 0.5 in, as shown in Fig. 3.1(a). The second test article is built from two 2024 aluminum spars with cross-sections of 0.5 in x 0.5 in spaced 7 in apart, connected by two 0.02 in thick 2024 aluminum skins, as shown in Fig. 3.1(b). The test article is held together at the top and bottom by 1018 low carbon steel inserts, as shown as the black area in Fig. 3.1(b). These inserts act as springs to avoid large stress concentrations in the skin and also form the rest of the box structure of the test article. The third test article is identical to the second, except the skins are bonded to a foam insulation core that fills the entire hollow region of the cross-section, as shown by the light colored area in Fig. 3.1(c). The foam is designed to prevent the rapid onset of skin buckling. Table 3.1 lists the test articles and their key features.

The top and bottom mounting structure of the experimental test articles is constructed from 4130 steel to provide rigid attachment points that are independent of the

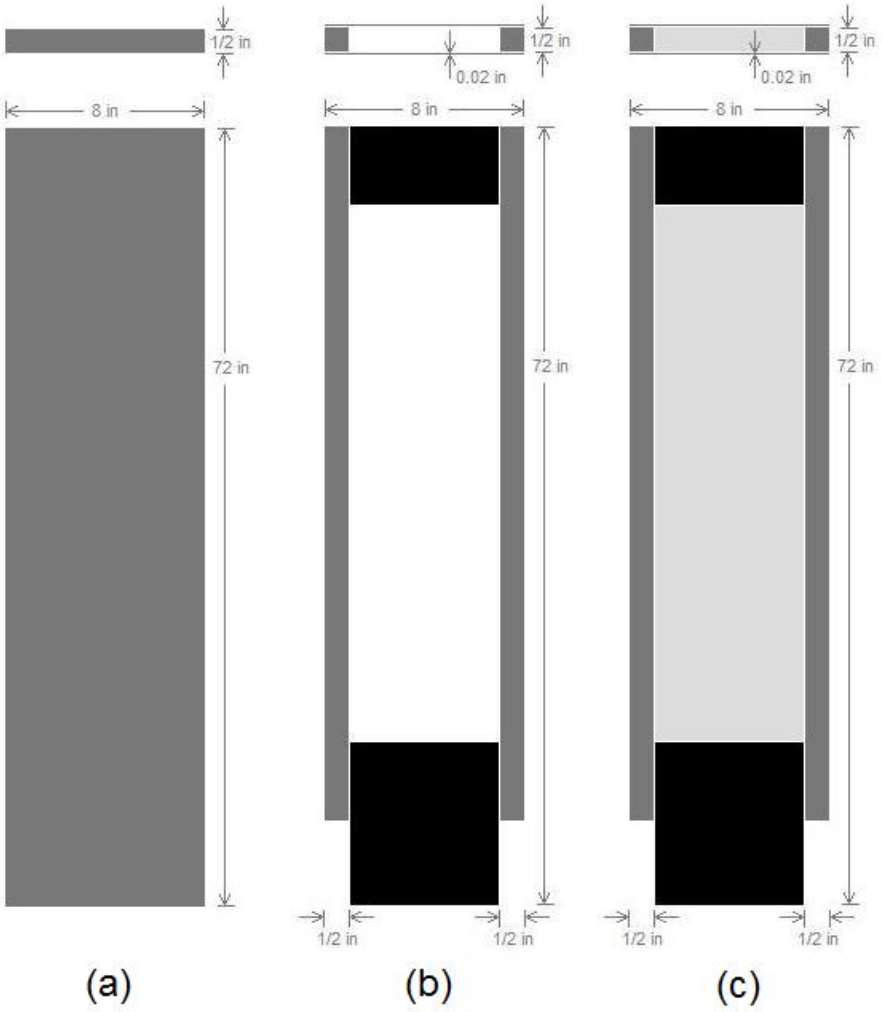

Figure 3.1: Qualification Test Articles - (a) Solid, (b) Hollow, and (c) Foam Filled.

Table 3.1: Key Features of Qualification Test Articles.

Name	Span (in)	Chord (in)	Thickness (in)	Skin thickness (in)	Core material
Solid	72	8	0.5	N/A	Aluminum Solid
Hollow	72	8	0.54	0.02	None
Foam-Filled	72	8	0.54	0.02	Insulation Foam

test article. The top mounting structure, Fig. 3.2(a), provides a common cable attachment point for load application. The bottom mounting structure, Fig. 3.2(b), holds the test article fixed against unwanted movement or rotations. The load is applied through a cable system which has an integral load cell to accurately measure these loads. The forces are assumed to be applied in the direction defined by the tip of the top mounting structure and the top pulley location, as shown in Fig. 3.3. This force direction is approximately horizontal when the test article is unloaded and is recorded during the test to allow better optimization of the FE model.

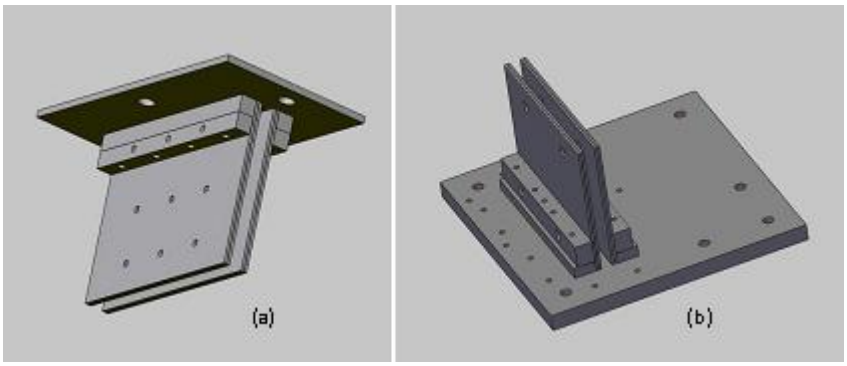

Figure 3.2: Mounting Structure - (a) Top and (b) Bottom.

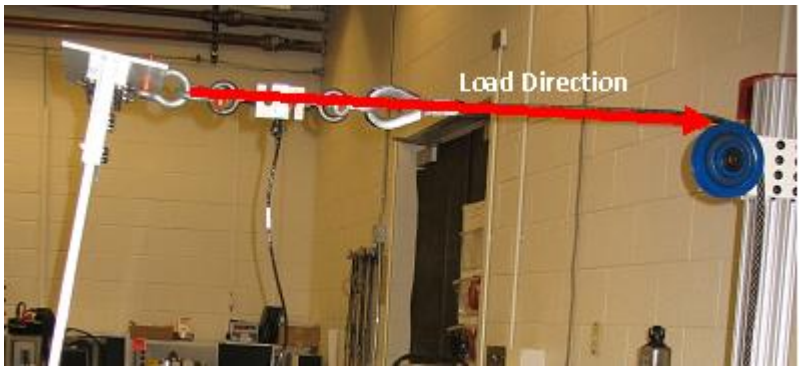

Figure 3.3: Load Direction.

The qualification test articles are tested in two directions, around the x-and z-axes, as shown in Fig. 3.4. Traditionally, cantilevered beams are loaded in the direction with the lowest rigidity, in this case around the x-axis. However, since there are non-linear instabilities in bending along the stiffer direction that are similar to the joined-wing, tests are conducted around the z-axis and compared to the analytical models. The x-

axis bending will be referred to as lateral bending, and the z-axis bending will be referred to as transverse bending.

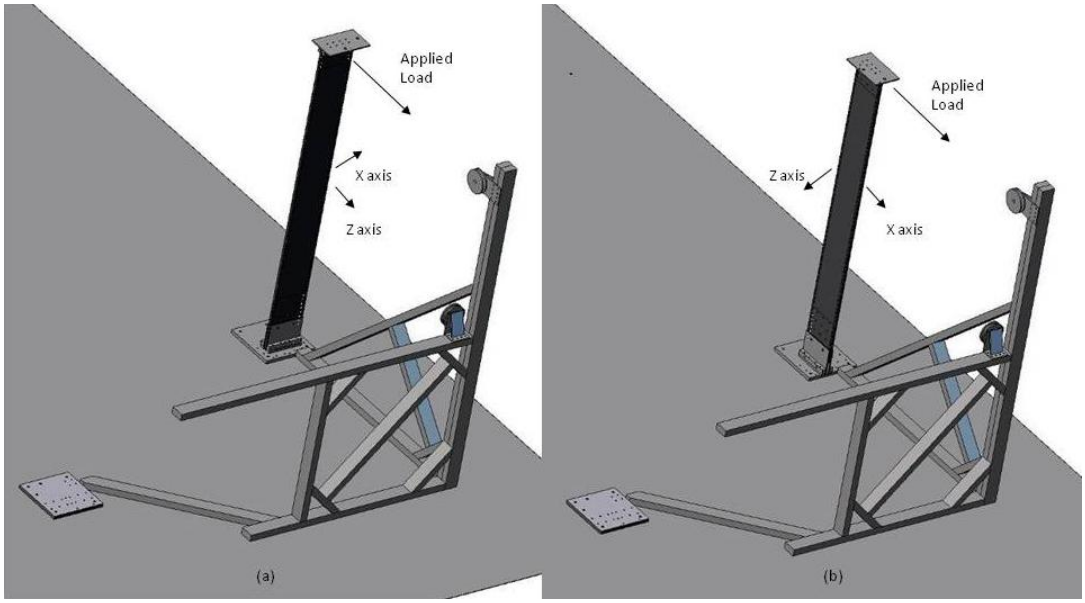

Figure 3.4: Bending Around the (a) Lateral and (b) Transverse Bending Directions.

The transverse buckling instability around the z-axis is predicted using the twist-bend buckling theory as presented by Hartog. [11] The critical load before buckling in a simple cantilevered beam is calculated using:

$$P_{cr} = 4.01 \frac{Eht^3}{6l^2} \sqrt{\frac{1}{2\,(1+\nu)}} \tag{3.1}$$

where P_{cr} is the critical buckling load, E is the Young's modulus, h is the width, t is the thickness, l is the length, and ν is Poisson's ratio. For the solid qualification test article, the critical load before the structure buckles is around 1,000 lb, according to Eq. 3.1. Experiments have shown that buckling occurs around this calculated load, as will be discussed in Chapter 4.

3.1.2 Joined-wing Test Design. The second stage of the experiment consists of three joined-wing test articles of which only the solid joined-wing was tested in this research. Figure 3.5 shows the basic test setup, with the fore wing, aft wing, and load direction labeled. As with the qualification test articles, the joined-wing test articles

each have a different type of cross-section property: solid, hollow, and foam-filled. The basic design and construction are the same as the qualification test articles. The most noticeable changes are a difference in the width and angle of the wings. Table 3.2 lists the test articles and their key features.

Table 3.2: Key Features of Joined-wing Test Articles.

Name	Height (in)	Fore Span (in)	Fore Chord (in)	Aft Span (in)	Aft Chord (in)	Wing Thickness (in)	Skin Thickness (in)	Core material
Solid	57	67	8	67	6	0.5	N/A	Aluminum Solid
Hollow	57	67	8	67	6	0.54	0.02	None
Foam-Filled	57	67	8	67	6	0.54	0.02	Insulation Foam

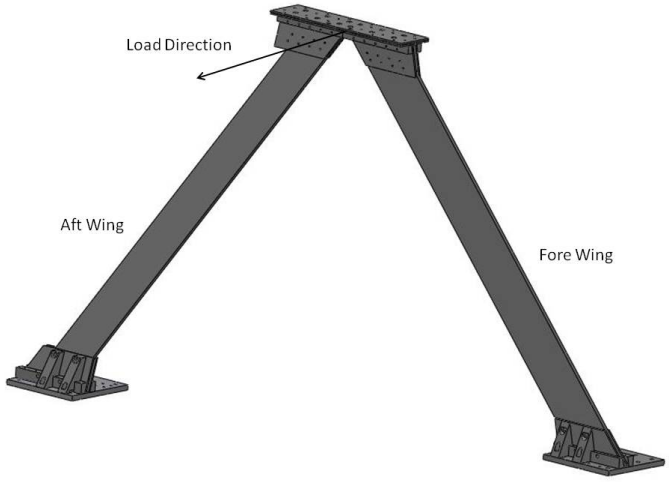

Figure 3.5: Joined-wing Test Article Setup.

The fore and aft wings are of two different chord lengths. The fore wing has a chord of 8 in and the aft wing has a chord of 6 in. The fore and aft chord lengths were derived using trial and error optimization using FE models to match the stresses in the roots of both wings at various load cases and especially near the yield point of the material. This optimization was accomplished by comparing Von Mises stress results from a series of FE models, where the width and skin thickness varied.

Extruded aluminum tubes were originally considered for the wings; however, tubes of the required dimensions and material properties were not commercially available. For the sake of time and budget, a built-up design was selected which allowed the number of different cross-sections to be increased from one to three.

The joined-wing design is centered around three design constraints: boundary conditions, geometric non-linearity, and material yield. First, the boundary conditions must be known to accurately compare the test results to the FE results. Second, the bend-twist coupling had to be seen. This is the geometric non-linearity of the joined-wing design. Third, the experiment could not experience yielding before producing a significant bend-twist coupling. This was the purpose of the optimization described above. These three constraints are not trivial, as seen with previous experiments described in Chapter 2.

As with the qualification test articles, the top (Fig. 3.6(a)) and bottom (Fig. 3.6(b), (c)) mounting structure is made out of 4130 steel to minimize movement in the mounting structure. Throughout all tests, the bottom mounting structure is examined to make sure no undesirable deformations or deflections occur. Since one of the primary purposes of the experiment is to cause the bend-twist couple, the mounting structure must not significantly move or flex as this will change the geometry of the test article and negate the bend-twist coupling.

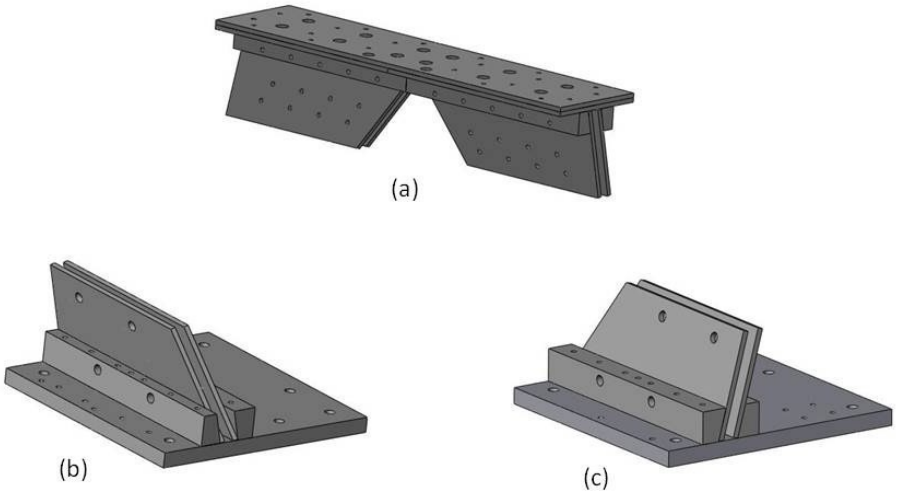

Figure 3.6: Mounting Structure - (a) Top , (b) Bottom Fore, and (c) Bottom Aft.

The load is applied in the same manner as the qualification test articles, approximately perpendicular to the front edge of the joined-wing's top mounting structure and between the top of the joined-wing and the top pulley, which is approximately horizontal when unloaded, as shown in Fig. 3.7. During the experiment, the exact direction and magnitude of the force is recorded for the purposes of accuracy and completeness, in the same methods as the qualification tests.

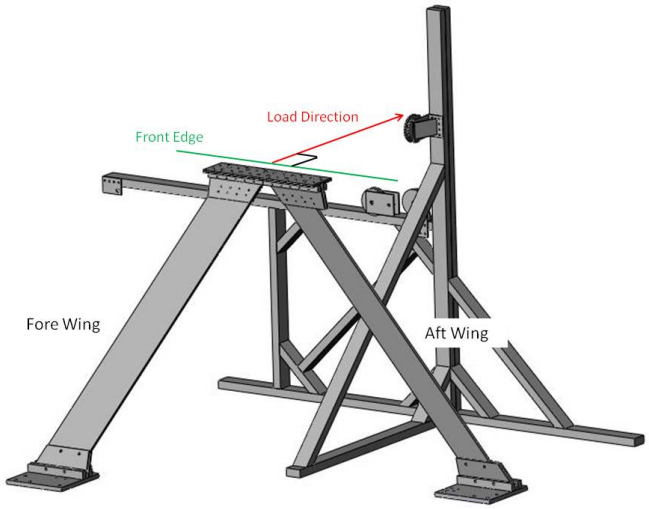

Figure 3.7: Joined-wing with Loading Structure and Loading Direction.

3.1.3 Mounting Structure Design. The mounting structure, as referred to previously, is composed of the base plates (Fig. 3.8), top plates (Fig. 3.9), interface plates (Fig. 3.10), and connector blocks (Fig. 3.11). It was designed to satisfy three key concepts: reusability, rigidity, and commonality. First, parts of the mounting structure needed to be reused between each experimental model. Second, the mounting structure is designed to minimize base rotations and stress concentrations. Third, the mounting structure needed to provide common load application points and conditions.

All connections and interfaces in this experiment are made with bolts. This allows parts to be assembled and disassembled as needed. One alterative is welded joints. While welding the pieces together can potentially provide a stiffer connection between components, welding can cause both material property changes as well as alignment issues.

It was also desired to create a common set of base plates which could be bolted to the floor. Different components bolt onto the base plates without requiring the removal of the base plates from the floor. The vertical bolts, as seen in Fig. 3.8, are designed to allow any test article to be slid onto the base plates and tightened down.

Figure 3.8: Base Plate.

The cable is attached to the top plate on the test article for the purpose of applying the load. Figure 3.9 shows the top plate for the qualification test articles and the joined-wing test articles.

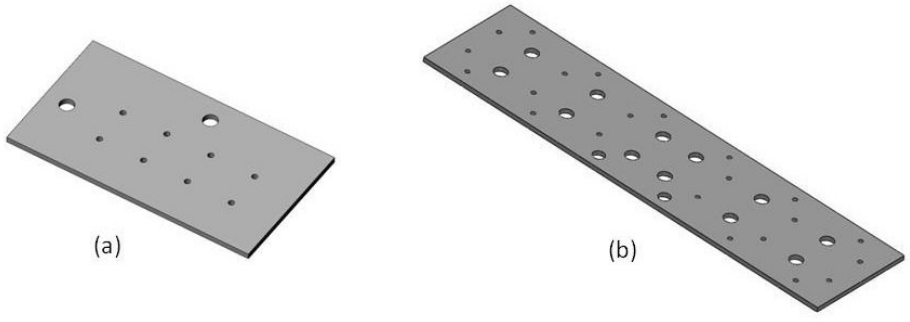

Figure 3.9: Top Plate - (a) Qualification and (b) Joined-wing.

The interface plates, as shown in Fig. 3.10, are between the test article and the top and base plates. These interface plates are designed to flex and distribute the load as it is increased and serve as transitions between the rigid base constraint and the various test articles. The interface plates also provide additional surface area to allow bolting of the test article to the top and base plates. These plates reduce the stress concentration that would be present if they did not flex at all, especially at the base of the experiment. The hollow and foam-filled wings do not use the interface plates at the top because of the low forces applied to these models.

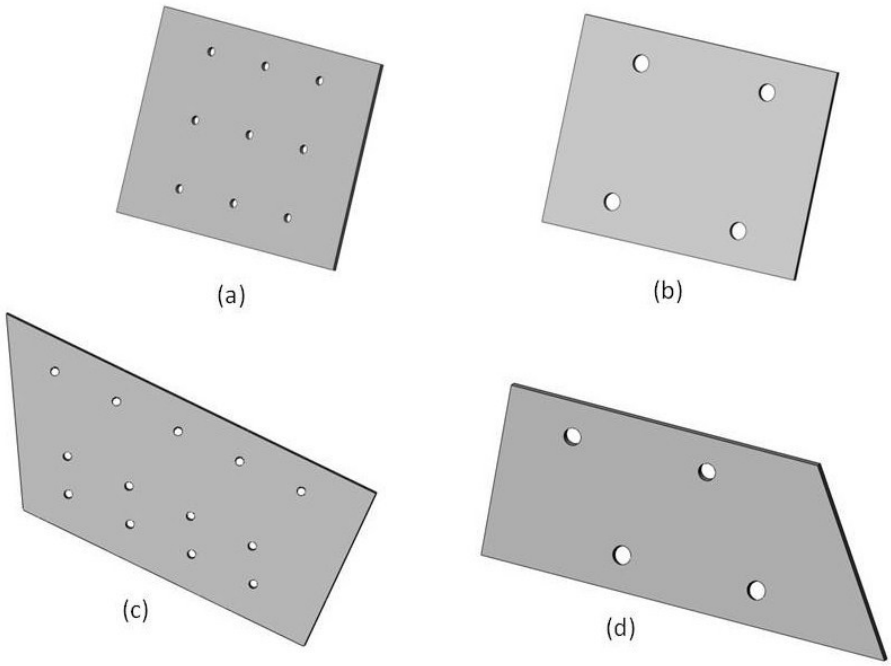

Figure 3.10: Interface Plates - Qualification, (a) Top and (b) Bottom and the Joined-wing, (c) Top and (d) Bottom.

Finally, connecting the interface plates to the top and base plates are connector blocks, shown in Fig. 3.11. These provide rigid locations where the bolts can be fastened and hold the entire support structure together. Without these blocks, there would be no way to connect the interface plates to the base and top plates.

Additionally, for the joined-wing test articles, stiffener blocks (Fig. 3.12) can be placed between the interface plates and the base plate. These stiffener blocks are designed to provide additional stiffness to prevent or minimize base rotation. The joined-wing test article will be tested with and without these stiffener blocks.

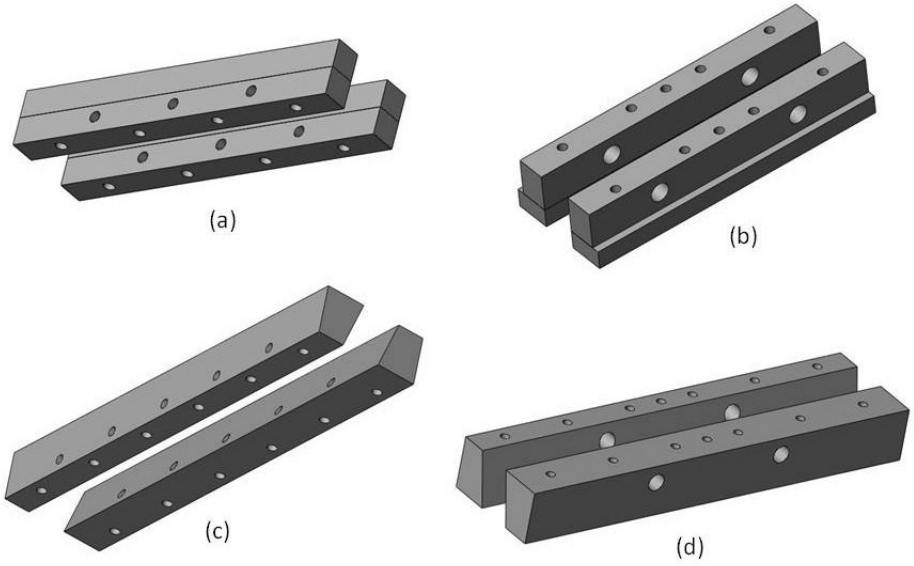

Figure 3.11: Connector Blocks - Qualification, (a) Top and (b) Bottom and the Joined-wing, (c) Top and (d) Bottom.

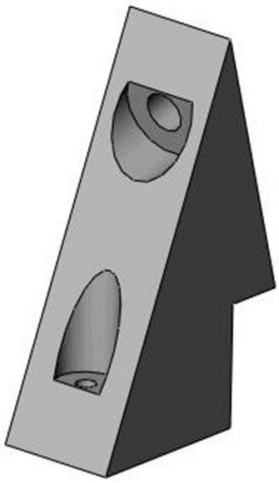

Figure 3.12: Stiffener Blocks.

The base plates are anchored to the floor using 0.5 in concrete anchors. There are six anchors per base plate, each rated to withstand an 8,000 lb pull-out force. The maximum load that can be applied to the test article is 3,000 lb. To estimate the total force on the anchors at the base, a static equilibrium equation is derived to relate the applied force to the resisted force:

$$f_b = \frac{f_e l_e}{l_b} \tag{3.2}$$

where f_b is the force at the base plate, f_e is the force applied to the experiment, l_e is the length of the experiment, and l_b is the distance between the experiment and the bolts.

Using a maximum load of 3,000 lb, an experiment length of 72 in, and a bolt distance from the experiment of 8 in, the anchors have to resist approximately 27,000 lb of total force. Eq. 3.2 does not factor in any other resistances to rotation, which would lower the total force needed; therefore, by having six bolts per base plate, the base plates will not pullout while maintaining a high safety factor. This is the primary constraint and is very important in keeping the end conditions of the experiment known.

3.1.4 Loading Structure. The loading structure, as shown in Fig. 3.13, is required to be able to load the test articles with a known and repeatable load, roughly perpendicular to the test article. This point load is an approximation for the load due to lift on the wing. The loading structure is built primarily of 80/20 extruded aluminum beams, because 80/20 is easy to cut and assemble. There are two load structure configurations of the 80/20 for this project: qualification and joined-wing.

The loading structure is anchored to the floor with concrete anchors at multiple locations to keep it from moving under load. Initially, the anchors were undersized for the maximum load and pulled out under a 1,000 lb load applied to the solid qualification test article. The undersized anchors were replaced with stronger anchors to prevent failure in the future.

Figure 3.13: Loading Structure - (a) Qualification and (b) Joined-wing.

The load is generated using a 3/4 ton hand crank winch and a 1/2 in cable, shown in Fig. 3.14. The cable was sized for the maximum load case while maintaining a safety factor of at least 2.

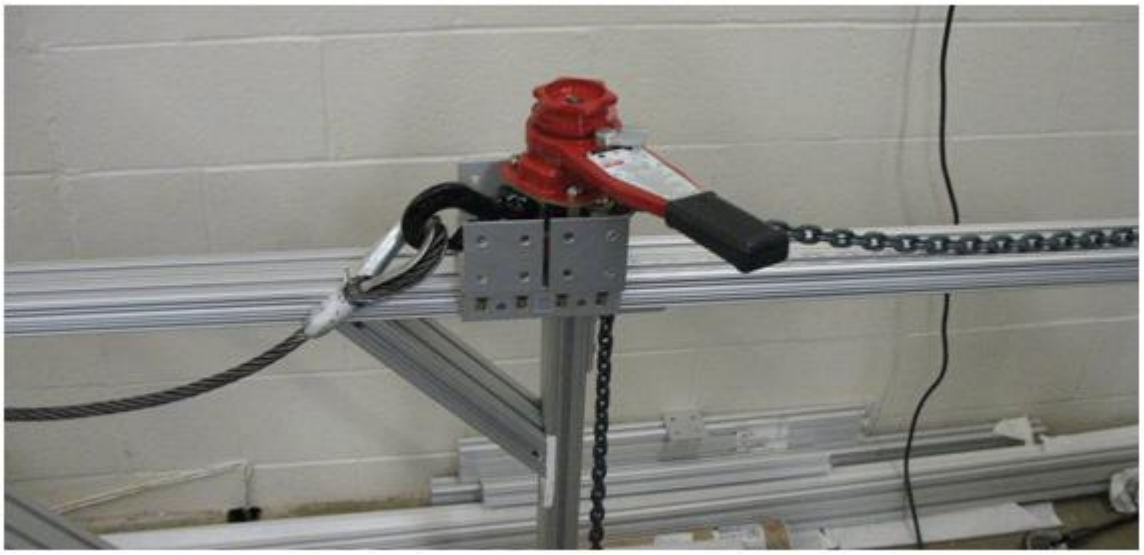

Figure 3.14: Cable and Winch.

The load is measured using a 3,000 lbf Sensortronics S-beam load cell, which has a rated 0.03% full scale nonlinearity and 0.02% full scale hysteresis, or less than 1 lb each for the 3,000 lbf load cell. The load cell is located between the cable and the experiment (Fig. 3.15), resulting in an accurate measurement of the applied force. Because this is an inline load cell, only the magnitude of the force is recorded. The direction is determined from measuring the angle of the cable during the experiment.

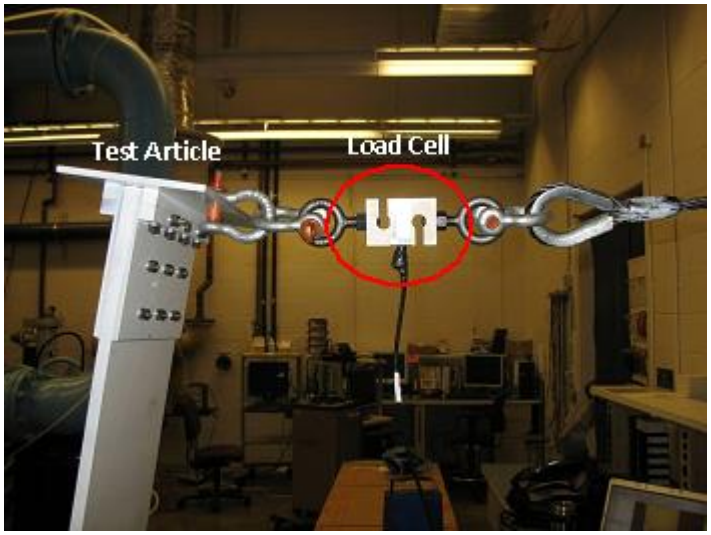

Figure 3.15: Load Cell.

In the case of the solid joined-wing test article, the cable system is designed to be able to apply a maximum load of 3,000 lb through a simple compound pulley system, since the winch is only rated to 1,500 lb. Later, it was found that the compound pulley was not needed to fully load the solid joined-wing test article because the initial joined-wing FE models were predicting a significantly stiffer joined-wing test article.

3.1.5 Strain Gages. Strain gages are applied, in accordance to the manufacturer's specifications, to the regions of the test articles where the FE model predicts the largest stresses. The measured strains will be used to help correlate the analytical and experimental data as well as estimate when material yield is being approached so as to not yield the test articles before testing is complete. For the test articles, single axis gages are used. Figures 3.16 and 3.17 show examples of the FE model predicted strain field for the models along the primary bending direction.

For the solid qualification test article, three strain gages are used, as shown in Fig. 3.18. Two strain gages are located on the face of the model just above the interface plates and are oriented in the primary tension direction to record the strain as the experiment is loaded around the x-axis, as defined in Fig. 3.4 above. The third gage is located on the side of the model to capture the strain when bending around the z-axis.

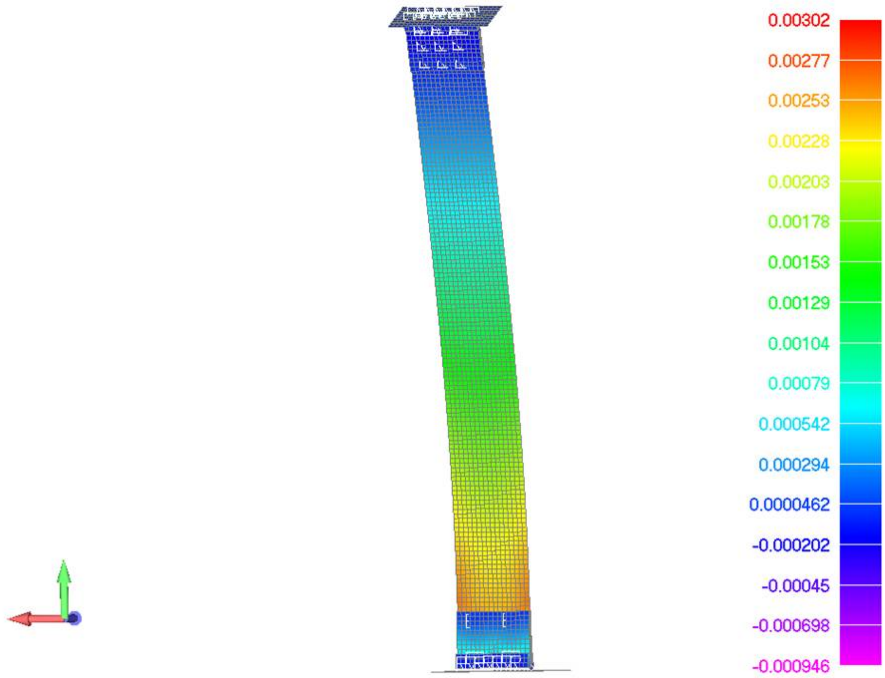

Figure 3.16: FE Model Predicted Strain Field on the Qualification Test Article.

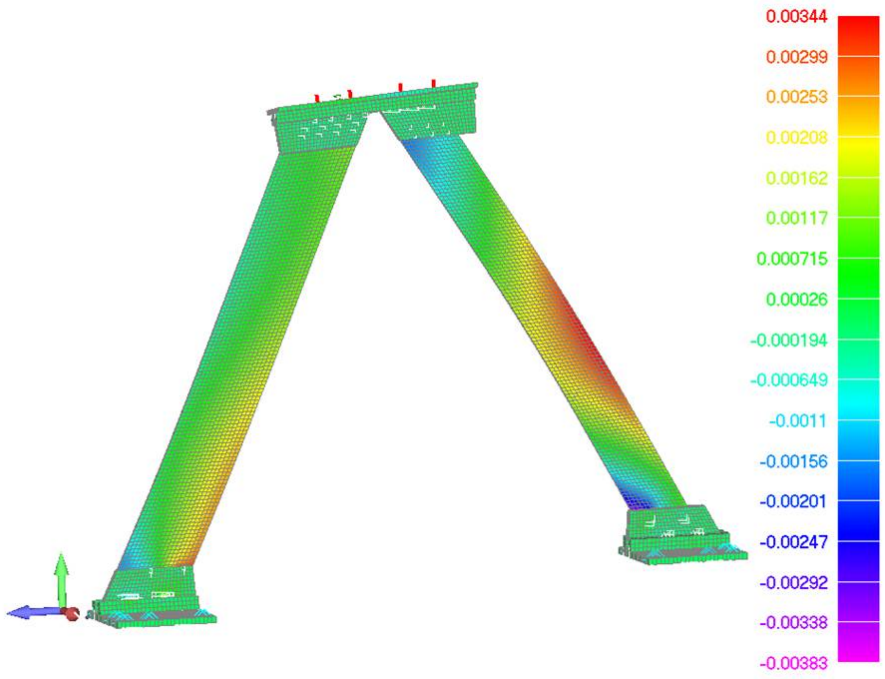

Figure 3.17: FE Model Predicted Strain Field on the Joined-wing Test Article.

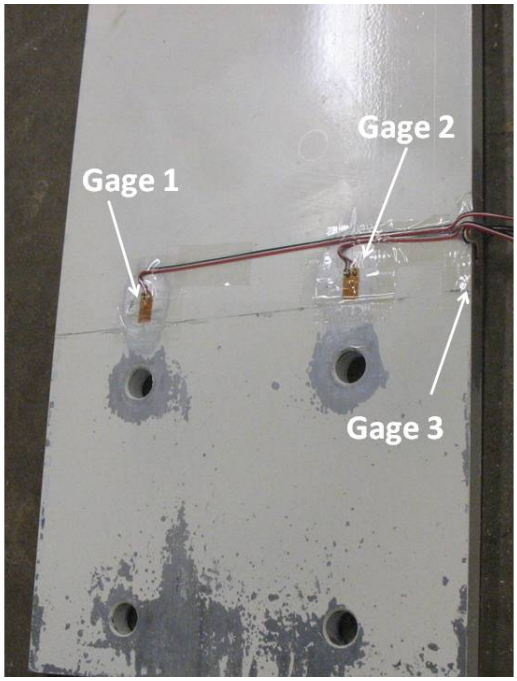

Figure 3.18: Solid Qualification Test Article with Gages.

For the hollow and foam-filled qualification test articles, two strain gages are used, as shown in Fig. 3.19. One is located near the bolts holding the skin to the ribs, just above the bottom steel insert. The second is located on the skin over the steel insert.

For the joined-wing models, gages are placed in the locations of highest or most dynamic strain, as predicted from the preliminary FE model results. A total of four gages will be used, the limitation of the gage reader. Figure 3.20 shows these gages on the solid joined-wing test article.

3.1.6 Measuring Displacements and Rotations. The FARO Photon 80 laser scanner, shown in Fig. 3.21, is used to record deflections of the test articles under various loads. The FARO Laser Tracker, shown in Fig. 3.22, is used to more precisely record point deflections. Both systems use lasers to record the location of the experiment but each uses a completely different method. In both cases, the laser light reflects off a surface and is received back into the scanner. The change in intensity and the time taken are used to calculate the reflectivity and distance of the surface being measured, respectively. The difference lies in how they interpret this returned laser.

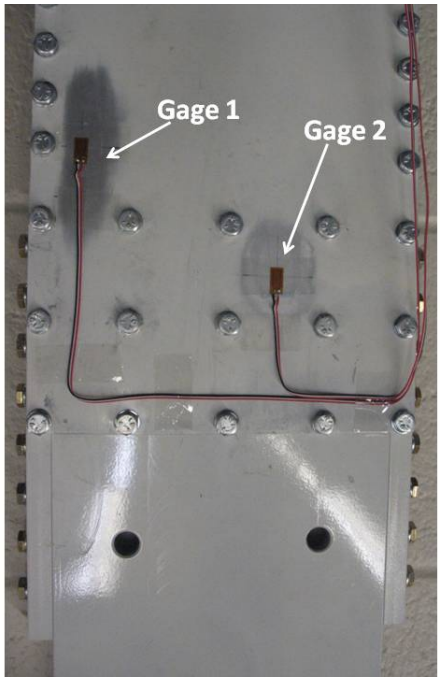

Figure 3.19: Hollow and Foam-filled Qualification Test Article with Gages.

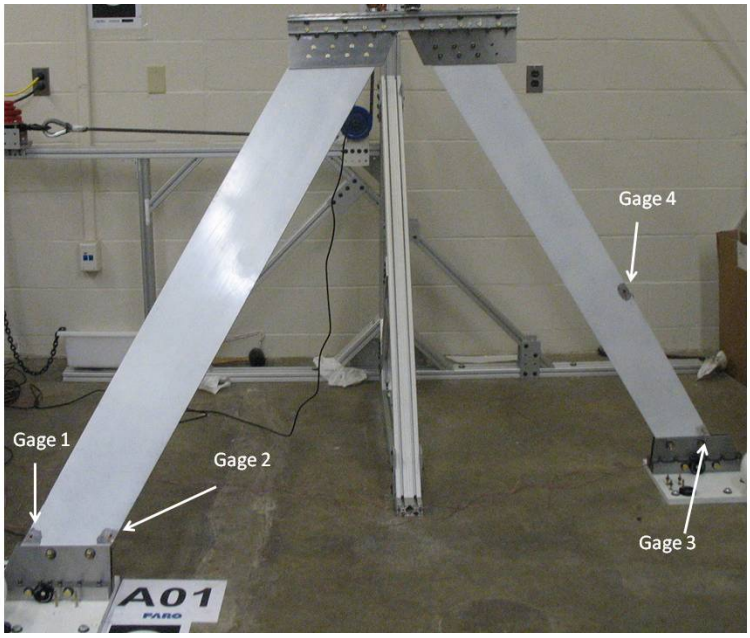

Figure 3.20: Solid Joined-wing Test Article with Gages.

Figure 3.21: FARO Photon 80 Laser Scanner.

Figure 3.22: FARO Laser Tracker.

The FARO Photon 80 laser scanner is designed as a room or complete article scanner. It uses a class 3R 20 mW infrared laser, with a 785 nm wavelength. Because of the class and power of this laser, laser eyewear is required for safe use of the system. The Photon 80 can scan at various levels of detail. For higher accuracy, automatic noise reduction can be activated, lowering the scanning repeatability from 1.5 mm RMS to 0.75 mm RMS at 10 m. The noise compression takes multiple scan points and averages the location and results in higher accuracy and smaller data files. The maximum data collection rate is 120,000 points/s. The Photon 80 can be directed to scan only parts of a room and for these experiments, only the test article is scanned since all other data is removed anyway in post-processing. The Photon 80 records the reflectivity of the surface, and can distinguish between white and black, based on reflectivity. This is helpful in identifying various points on the test article as reference points as well as FARO provided targets. These targets aid in data reduction and correlation. [7]

The FARO Laser Tracker is used to record the deflections; however, this system is limited to basic shapes and specific points. The accuracy is significantly greater than the FARO Photon 80. At 10 m, the accuracy is approximately 0.02 mm. For the purposes of this experiment, the best use of the Laser Tracker is to measure a specific point as it moves under the various load cases. The spherically mounted retroreflectors (SMRs) (Fig. 3.23), which the Laser Tracker tracks for 3D scans, can be put in a known and specific location on the test article. This point can be measured and compared to the corresponding point in the FE model. [6]

To create consistent data sets, several basic steps are performed: initial zero scans, intermediate low load scans, and final zero scans. The initial zero scan is the baseline for deflection measurements. Because of the weight of the load cell and cable, the zero scan is taken without these attached. Although each data scan set should have identical zero scans, a new one is required for each set to make sure the experiment is at zero and to ease the data reduction steps, especially if the laser system has moved or been bumped.

Between each load case, the test articles are unloaded to a relatively low but repeatable load and scanned. The purpose of this low load is to quantify any permanent deformation in the test article. If there is any permanent deformation from the previous

Figure 3.23: FARO Spherically Mounted Retroreflector.

load case, the deflection will show up in the scan and all subsequent data can be corrected by this offset. Ideally, the test article would be returned all the way back to a zero load state, but this is impractical for the design of this set of experiments.

At the end of a set of load cases, the test article is again returned to a zero load state by removing the cable and is scanned. Under certain conditions, such as the first time a model is loaded to a high load, the connections at the base can move slightly. This is due to the tolerances of the bolt holes. Typically, this will only happen once for a set of experiments. It is most evident when high loads are applied. This shifting will be picked up on subsequent near zero load and the final zero load scans. To mitigate the effects of shifting, a recently bolted test article is loaded fairly high and then rescanned at zero before proceeding with the set of load cases.

In addition to laser scan data, several other data sources are recorded. At every load case, the strain readings from the various gages are recorded. A Vishay P3 self-contained strain gage reader is used, as shown in Fig. 3.24. This gage reader is a four channel, battery powered strain gage bridge and amplifier.

The applied load is also recorded, using the previously mentioned Sensortronics load cell attached to an IQ plus 355 Digital Weight Indicator, as shown in Fig 3.25. The

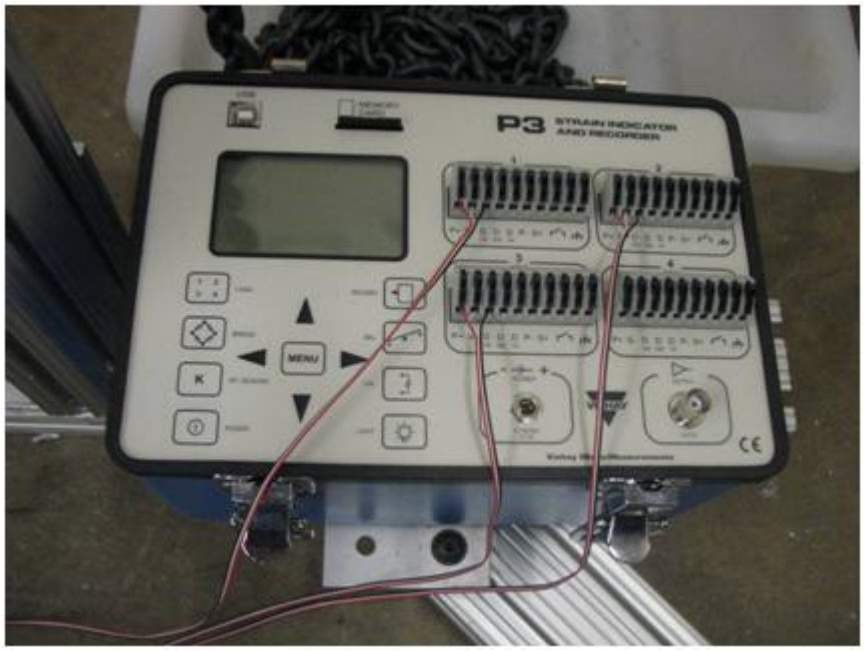

Figure 3.24: Strain Gage Reader.

IQ plus 355 has a linearity of 0.01% and a large digital display for easy-to-read applied loads.

Finally, information such as the direction on the load and the height of the pulley is recorded. The direction of the load is recorded using a digital inclinometer on the cable and at the top of the test article, shown in Fig. 3.26. The inclinometer has an accuracy of $\pm$ 0.7 deg.

The position of the pulley is assumed to be static for the entire data set and is recorded at the beginning using a tape measure.

All angle, strain, and load data are recorded in a spreadsheet. While there are ways to automate the data collection, the relatively small amounts of data and the length of each scan makes it easier to manually record the data than to set up an automatic process.

For safety, the structure is designed to fail in the direction of the load application structure, since the test article has the lowest factor of safety. Also, the strain gages are actively monitored to keep the load below yield for the test article. Safety glasses are

Figure 3.25: Load Cell and Display.

Figure 3.26: Inclinometer on Test Article.

worn when running the experiment and no one is allowed to stand directly in front of or behind the test article when under load.

3.1.7 Material Testing. Knowing the properties of the material tested is important for accurately modeling the experiment. The most important property is the Young's modulus of elasticity. Test samples are cut from excess material from the wings and tested in a MTS tensile test system, as shown in Fig. 3.27, to determine the modulus and yield point on the aluminum. The test sample is referred to as a dogbone, shown in Fig. 3.28. The dogbone has a reduced cross-sectional area in the center that is designed to stretch before the ends of the sample. The measured load versus elongation is converted into a stress-strain relationship which is used to determine the modulus of elasticity. The modulus of elasticity is the slope of the linear portion of the curve.

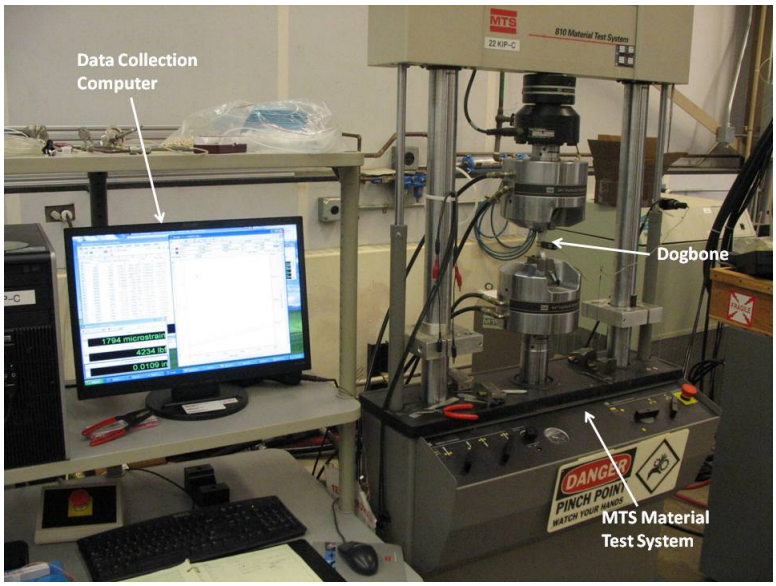

Figure 3.27: Tensile Tester

3.2 Analytical Models

The analytical modeling is done both before and after the experimental testing. Before testing, FE models were used in the experiment design process. After the testing, the FE models are hand tuned to match the measured displacement and strain data. Tuning the FE models is easiest for the qualification models, and lessons learned from the qualification tests are applied to the joined-wing models.

Figure 3.28: Material Dogbone

For all the FE models, several versions of Nastran were used interchangeably: MD Nastran V2007.0, MD Nastran V2008.0, and NX Nastran V5.0. MD Nastran V2007.0 was the primary solver for most analyses. For all linear analyses, solution method 101, SESTATIC, was used. For all non-linear analyses, solution method 106, NLSTATIC, was used.

QUAD4 plate elements are used exclusively to represent the various parts of the model. Both the qualification and joined-wing test articles are modeled separately. While it is easier to ignore the base and top mounting structures, these structures play important roles in the way the structure deforms, especially for the joined-wing. Therefore, the mounting structure is modeled as well as the actual test article.

Connections between components are represented with both rigid links and 6 degree-of-freedom (6DOF) spring elements. If all connections are modeled with rigid links, the model is overly stiff, resulting in lower than measured results. The 6DOF spring elements allow the stiffness to be changed between the components. Varying the stiffness of the 6DOF springs allows the FE model to match with experimental results. For the bolts used to connect the skins to the ribs of the built-up wings, rigid links are still used because of the proximity of the bolts to each other.

The primary assumptions going into the FE modeling process are that the material is homogeneous and that the top and bottom connector bolts will act like stiff springs. Figure 3.29 shows an example of a typical wing FE mesh.

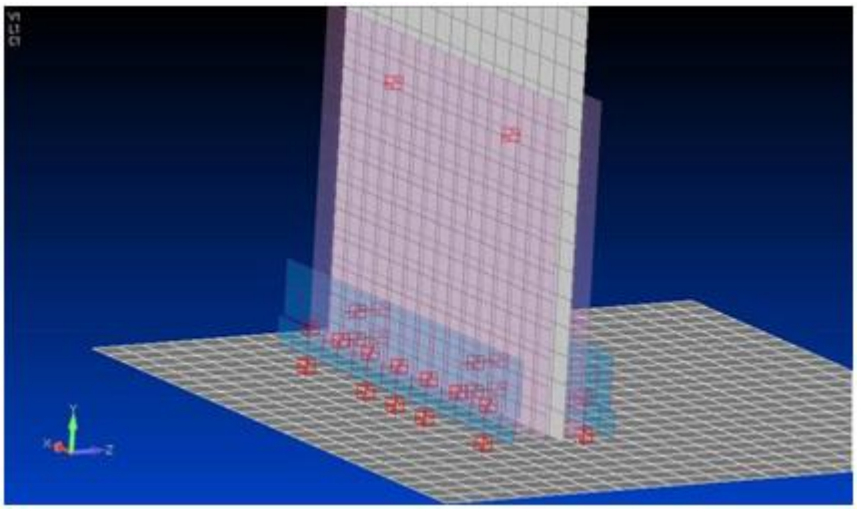

Figure 3.29: Typical FE Mesh.

3.2.1 Linear and Non-linear Solutions. When computing displacement solutions in a FEA program, there are two main solvers: linear and nonlinear. The fastest and easiest solutions come from the linear solver. A linear solution means that the displacements are proportional to the applied load. The assumption of linearity significantly reduces the computations required when compared with non-linear assumptions and allows the analysis to be solved in a single simultaneous equation set. However, solutions by this method only agree with the measured results when deflections are small, since beyond small deflections, the linear assumption does not apply.

A non-linear solver must be used for large deflections and the bend-twist coupling seen in the test articles, especially the joined-wing, because the bend-twist coupling is an inherently non-linear effect. A non-linear solution is computed by increasing small load increments until the solution converges. Because it cannot be assumed that there is a linear relationship between load and displacement, a non-linear solver applies these small load increments, iterates around that load until the solution converges, and then repeats until the full load has been applied. This process is extremely time intensive. For the joined-wing FE model developed in this research, typical solution times on a standard PC is 30 min. On the cluster server, solution time is reduced to 25 min, although the cluster server allows multiple load cases to be solved simultaneously. On the other hand, a linear solver takes about 10 s for the same FE model.

As stated before, the primary purpose of this thesis is to collect displacement, rotation, and strain data that can be used to validate analytical models of joined-wings. Due to the issues and approximations involved in creating FE models, accurate data is vital in validating modeling approaches. Significant effort has been spent on creating faster ways of computing non-linear solutions for the joined-wing, especially for the purpose of optimization. Because of the bend-twist coupling of the joined-wing, time prohibitive non-linear optimizations must be used for accurate predictions. Therefore, various approximations and techniques are used, including geometrically exact beam theory. Such hybrid techniques need accurate experimental data in order to be considered valid and trustworthy methods.

3.2.2 Importing Scan Results. To compare the various forms of experimental results with analytical model predictions, several approaches are taken. The first way is to import the Photon 80 laser scan data directly into the Finite Element Modeling And Postprocessing (FEMAP) program, the pre- and post-processor used in this research, to visually compare measured and predicted deflections and rotations. This is the simplest method, but not the easiest or most accurate due to the differences between the model and measured coordinate systems. In FEMAP, the scanned data has to be manually rotated and translated to match the analytical results. This approach is very slow with a large number of data points.

The FARO Laser Tracker allows precise data to be recorded at specific points on the experiment. While this does not capture the surface shapes, it is easier to import the data and directly compare points on the analytic models to the experimental results. The FARO Photon 80 captures the surface shape at the sacrifice of accuracy. The FARO Photon 80 records the data as a set of points, as shown in Fig. 3.30. The FARO Laser Tracker also records discrete points, but in the scanning stage, these points can be combined into lines, planes, or other objects, as shown in Fig. 3.31.

3.2.3 Reducing the Data. The most significant challenge with the data recorded is that the coordinate systems of the scanner and FE model are not the same. After recording surface scans with the Photon 80 and discrete point measurements with the

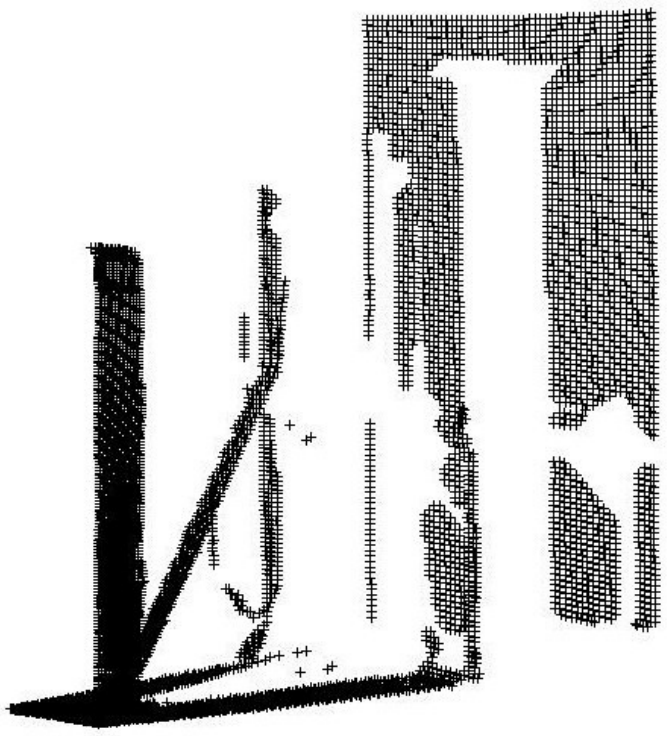

Figure 3.30: Example of FARO Photon 80 Scan Data of the Qualification Test Article.

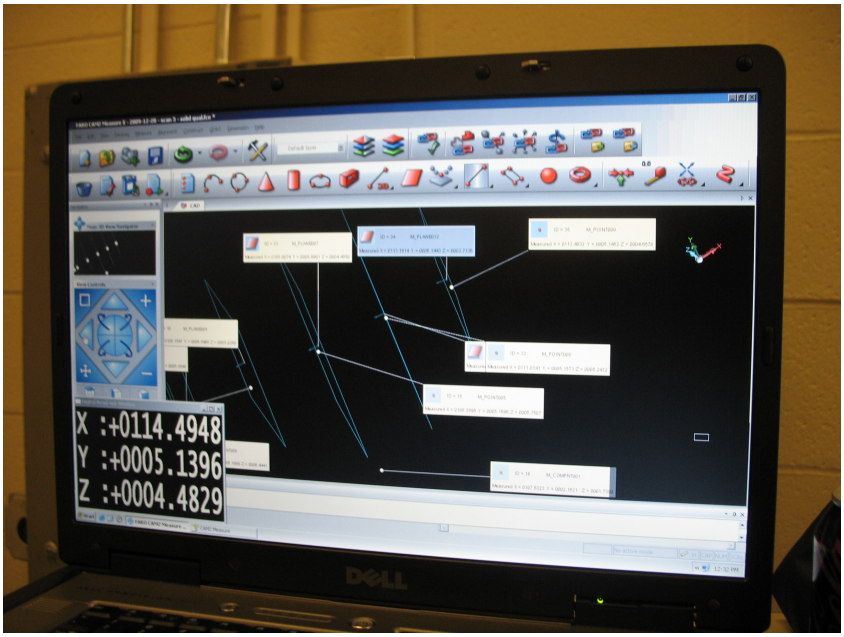

Figure 3.31: Example of FARO Laser Tracker Scan Data of the Qualification Test Article.

Laser Tracker, the measured data is aligned with the known geometry from the FE model, using PolyWorks®, a screen shot of which is shown in Fig. 3.32. PolyWorks® is designed to make it easy to import, align, and edit measurement data from a variety of laser scanning tools, including the Laser Tracker and Photon 80.

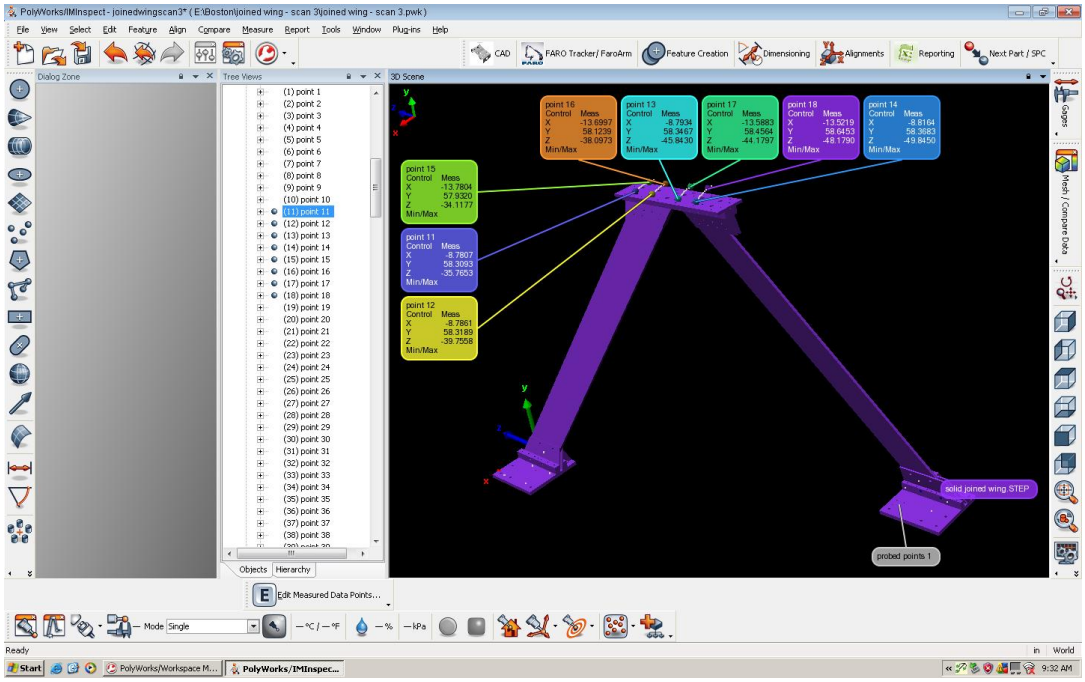

Figure 3.32: PolyWorks® Screenshot.

This alignment requires a two step process. Known geometry on the test article's bottom mounting structure is scanned with the Laser Tracker for aligning the Laser Tracker coordinate system with the FE model. Spherical targets (Fig. 3.33) around the testing area are also scanned with the Laser Tracker. These are used to align the Photon 80's coordinate system with the FE model, since the lower accuracy of the Photon 80 makes it difficult to accurately locate the mounting structure's features.

After the data has been oriented to the correct coordinate system, the Photon 80 scan points are exported. Because the data is hard to manually manipulate with its large number of points, the data is imported into Rapidform® 3D. The Rapidform® program allows the points to be converted into a surface mesh. From the mesh, a surface is lofted, as shown in Fig. 3.35. This lofted surface is then imported directly into FEMAP for visual comparison of the surface shape.

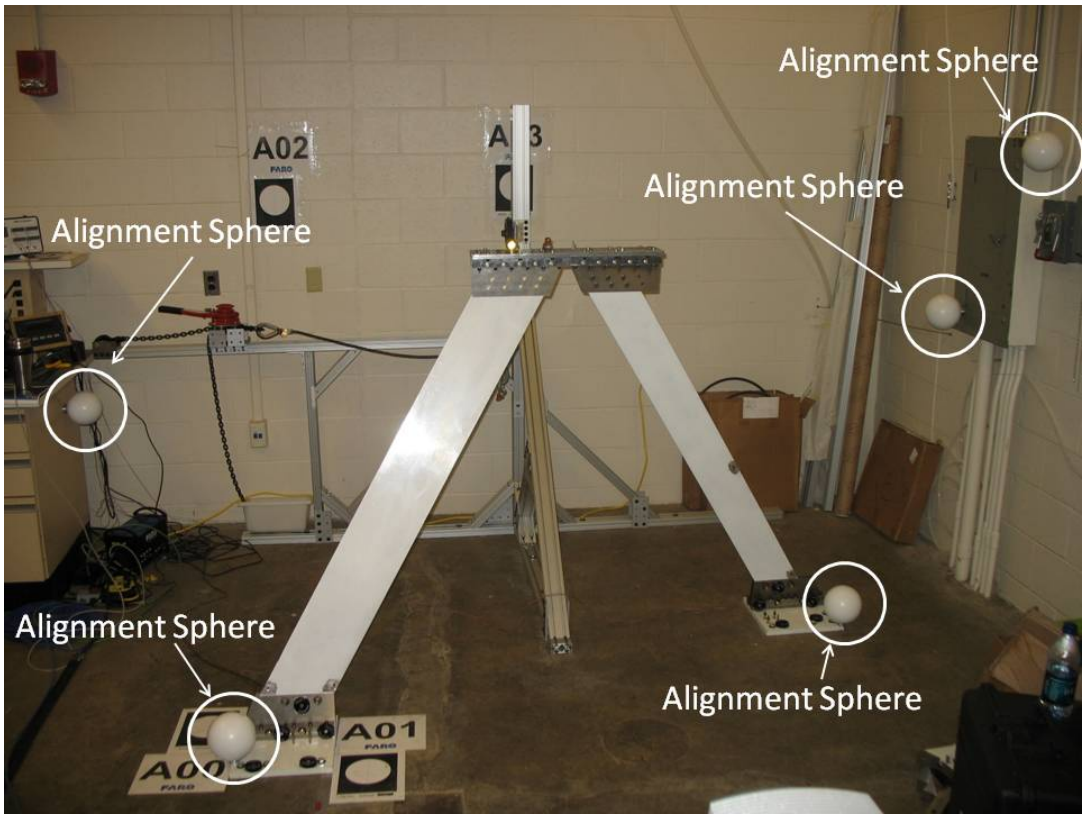

Figure 3.33: Spherical Alignment Targets.

This surface is sliced into several sections. The end points of these sections are compared to the closest node in the FE model, as shown in Fig. 3.34. This node is determined by selecting the corresponding points between the undeformed model and unloaded test article surface. The distance between these corresponding points is calculated and all the distances are averaged together using:

$$ADE = \frac{\sum_{i=1}^{n} \left(\sqrt{(g_{x,n} - s_{x,n})^2 + (g_{y,n} - s_{y,n})^2 + (g_{z,n} - s_{z,n})^2} \right)}{n} \tag{3.3}$$

where ADE is the average distance error, g_x is the x-direction position of the grid point, g_y is the y-direction position of the grid point, g_z is the z-direction position of the grid point, s_x is the x-direction position of the surface point, s_y is the y-direction position of the surface point, s_z is the z-direction position of the surface point, and n is the number of grid points (16 for the qualification model and 26 for the joined-wing model). This resultant number, the ADE, gives a quick feel of how well the surface shape matches the FE model; the larger the number, the worse the correlation.

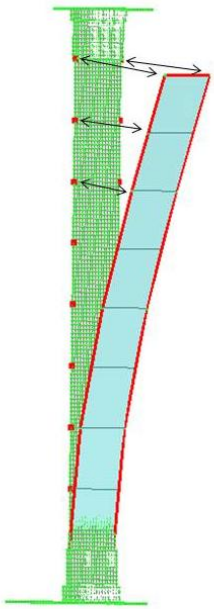

Figure 3.34: Example of a Sliced Surface for Calculating the ADE.

At this point, the Laser Tracker's point data can be directly compared to the same location in the FE model, and plots of deflections can be created.

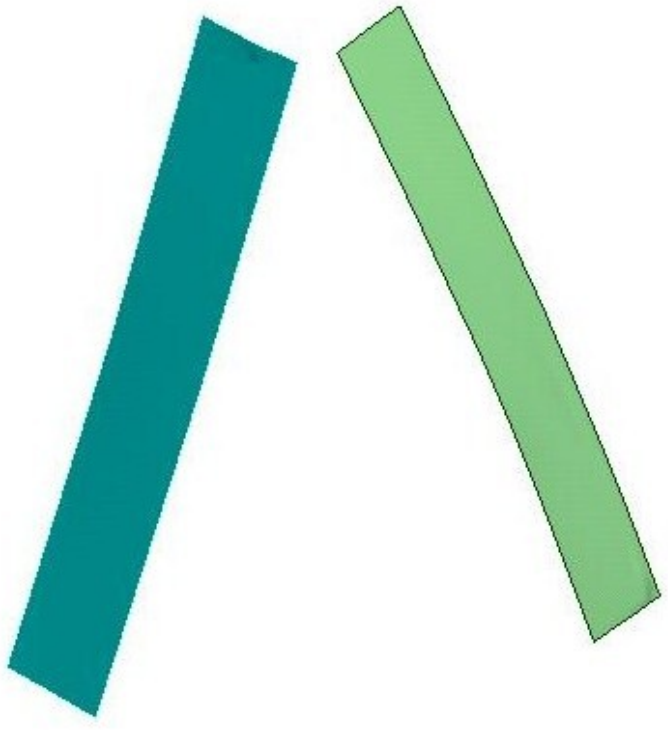

Figure 3.35: Example of Joined-wing Lofted Surface.

IV. Results and Analysis

Although three qualification and three joined-wing test articles were designed, only the solid and hollow qualification and the solid joined-wing test articles were constructed in time for this research. This chapter will present the data collected and model correlation efforts.

4.1 Material Properties

The modulus of elasticity of the 6061 aluminum used in the solid wing was measured at 9.9E6 psi which agrees closely with other reported values. [5] This modulus is used in all the FE models. Five samples were tested in the MTS tensile test system, although not all provided clean data due to equipment malfunctions. Figure 4.1 shows the load versus elongation curves for one of the samples. The curve also shows a yield around 4,500 $\mu\epsilon$. In order to include margin for error with respect to permanent deformation of the test article, 4,000 $\mu\epsilon$ is used as the yield limit. This margin will also take into account that the strain gages may not be at the highest stress locations even though the gages are placed at or as close as possible to the highest stress locations.

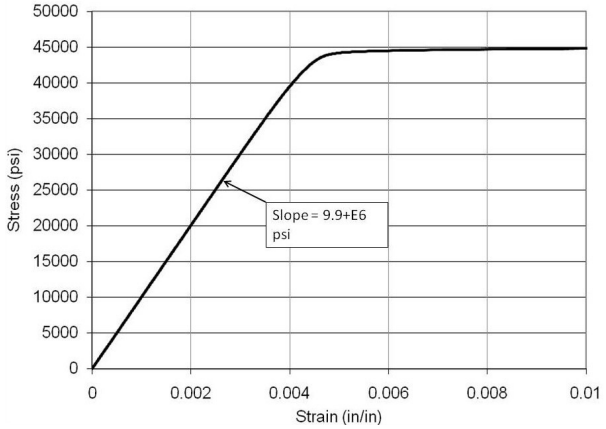

Figure 4.1: Measured Stress-strain Curve

4.2 Solid Qualification Wing

The experimental results show that the initial FE models were too stiff. Further analysis showed that the cause was primarily due to the rigid links in the top mounting structure. Thus, the rigid links of the top and bottom mounting structure were changed

to 6DOF spring elements. This change allowed the stiffness of the bolted connections to be modeled more accurately and the FE model could now be easily tuned by selecting spring stiffness coefficients. Incidentally, the experiment was designed around the less flexible FE model predictions and the loading structure was almost positioned too close to the test article to allow full test deflection. All qualification test article data has been transformed so that the following coordinate system is used: x is in the forward direction or direction towards the front of the aircraft, y is out of the wing tip, and z is in the load direction or upward with respect to the aircraft; shown in Fig. 4.2.

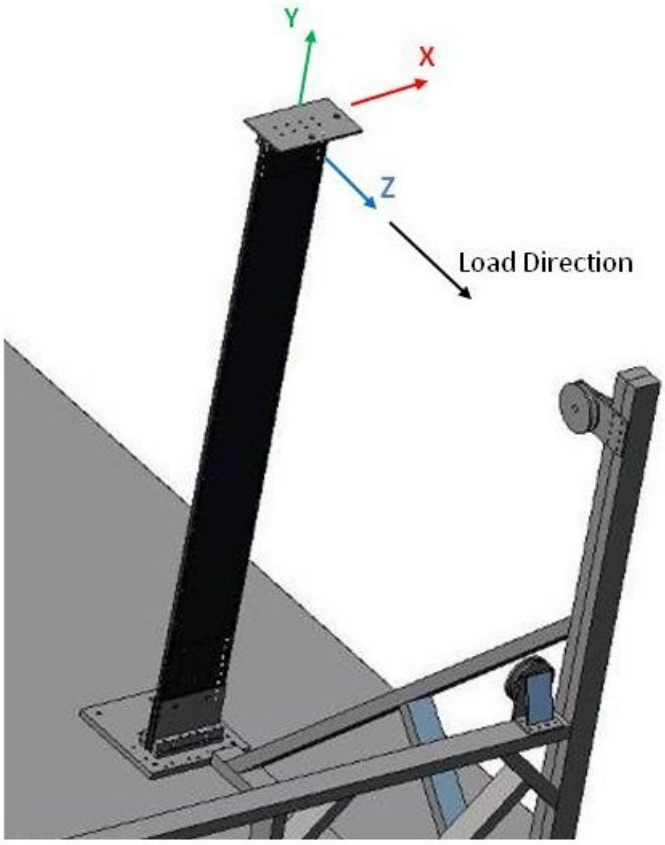

Figure 4.2: Qualification Wing Coordinate System

4.2.1 Deflection Curves. The solid qualification test article was loaded along both bending axes as explained in Section 3.1.1.

4.2.1.1 Lateral Bending. With the Laser Tracker, a tracker point was measured near the top of the test article, as shown in Fig. 4.3. There are four data

sets of the measured displacements of the point: x-, y-, and z-displacements with load and the root-mean-squared (RMS) or total displacement. The displacement plots are shown in Figs. 4.4, 4.5, 4.6 and 4.7. The diamonds represent the experimental results; the solid line represents the non-linear FE model solution; and the dashed line represents the linear FE model solution.

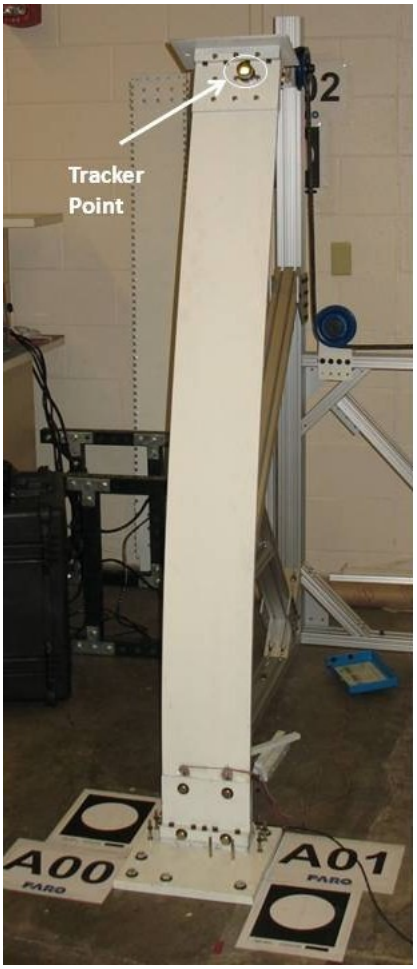

Figure 4.3: Solid Qualification - Lateral Bending - Tracker Point.

As expected, the agreement between the FE model displacement predictions and measured displacements in the x-direction is poor. This was due to alignment issues and resolved with a change to the PolyWorks® software before the joined-wing testing. Without re-testing the qualification model, the alignment could not be improved. While the measured data is in close agreement to the FE models, the y- and z-direction error is due to the change in load direction in the test article. In the FE model, the load is assumed to stay along the z-direction. In reality, the load direction varied greatly, as

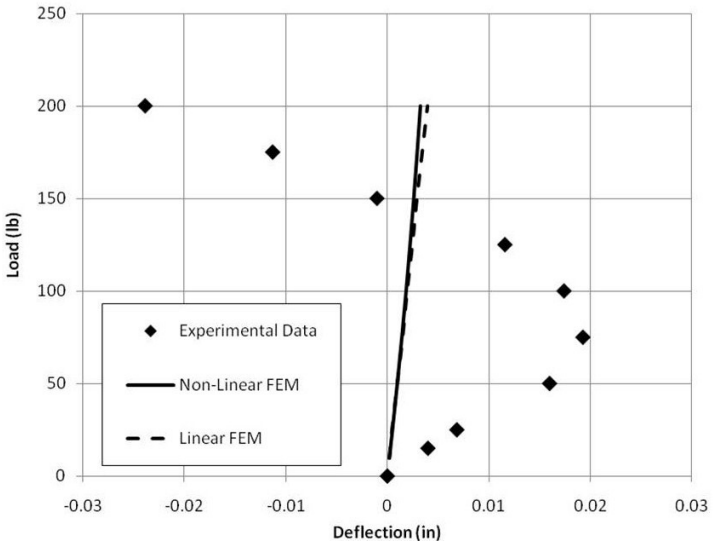

Figure 4.4: Solid Qualification - Lateral Bending - X Direction.

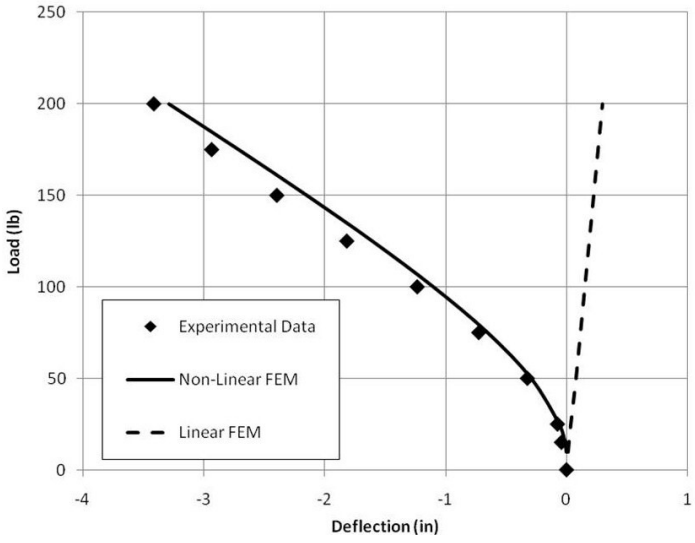

Figure 4.5: Solid Qualification - Lateral Bending - Y Direction.

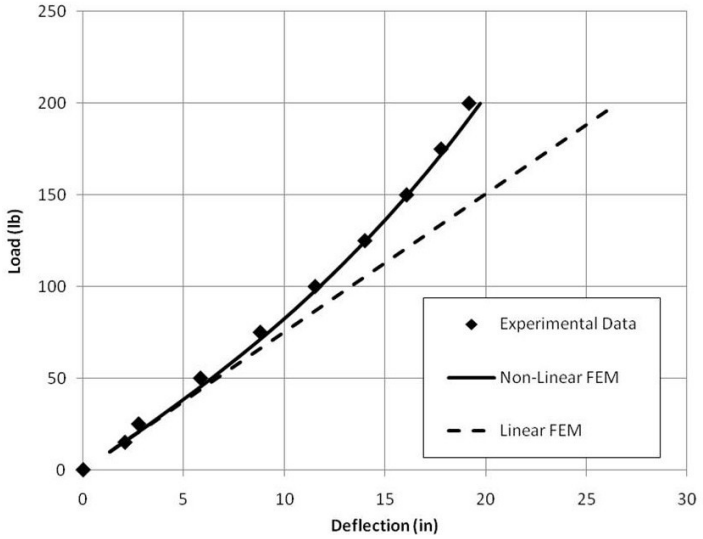

Figure 4.6: Solid Qualification - Lateral Bending - Z Direction.

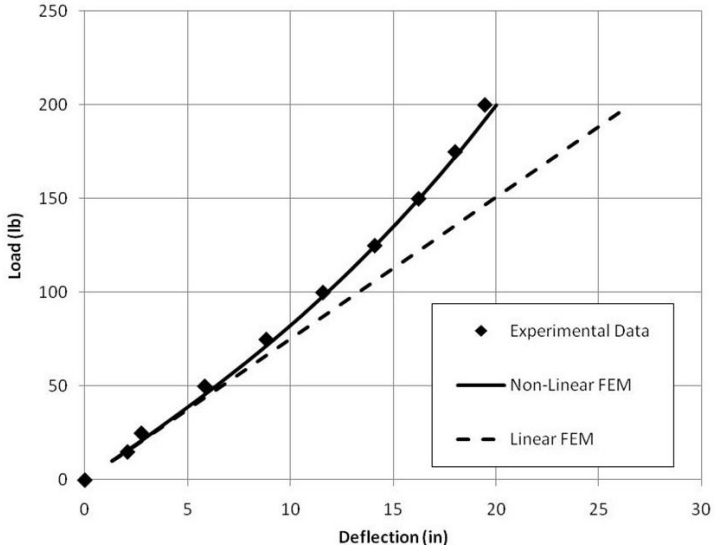

Figure 4.7: Solid Qualification - Lateral Bending - RMS.

shown in Fig. 4.8. While the actual load direction could be simulated, it was felt that the agreement was close enough for this data. It is also worth noting that the beam is extremely flexible; at a 200 lb load, the beam has deflected 20 in or 28% of its 72 in length.

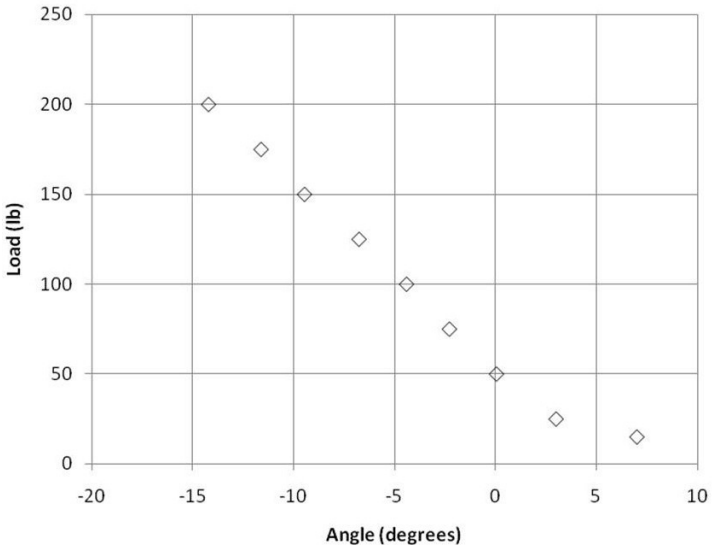

Figure 4.8: Solid Qualification - Lateral Bending - Applied Load Angle.

4.2.1.2 Transverse Bending. A tracker point was measured near the top of the test article, as shown in Fig. 4.9. There are four data sets of the measured displacements of the point: x-, y-, and z-displacements with load and the root-mean-squared (RMS) or total displacement. The plots are shown in Figs. 4.10, 4.11, 4.12 and 4.13. The diamonds represent the experimental results; the solid line represents the non-linear FE model solution; and the dashed line represents the linear FE model solution.

Agreement between predicted and measured displacements in the transverse bending test is not as good as the lateral bending test for several reasons. First, alignment was difficult because of software incompatibilities, as explained in the lateral bending section; and second, the applied force was not along the z-direction. The applied force was angled 4 deg toward the x-axis because the load application structure was oriented for the lateral bending qualification test and could not be moved to properly align with

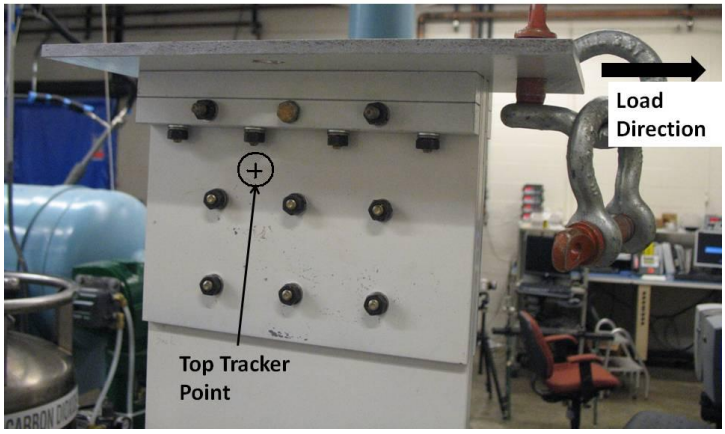

Figure 4.9: Solid Qualification - Transverse Bending - Top Tracker Point.

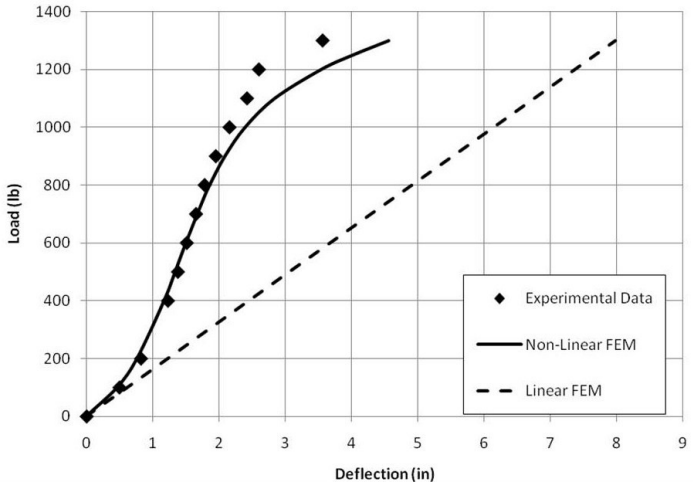

Figure 4.10: Solid Qualification - Transverse Bending - X Direction.

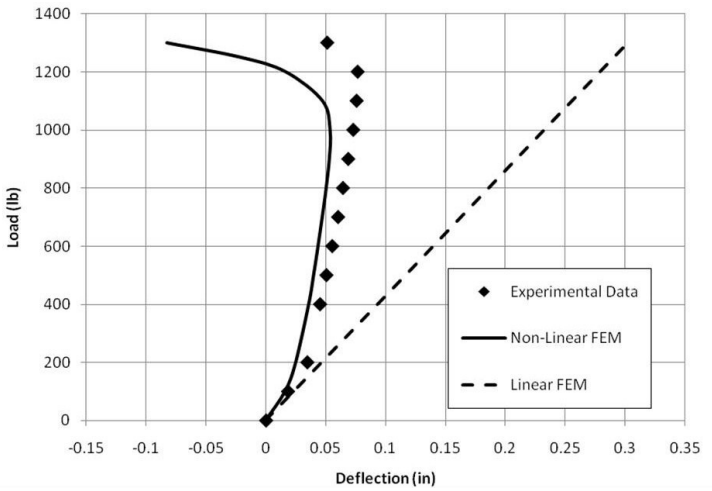

Figure 4.11: Solid Qualification - Transverse Bending - Y Direction.

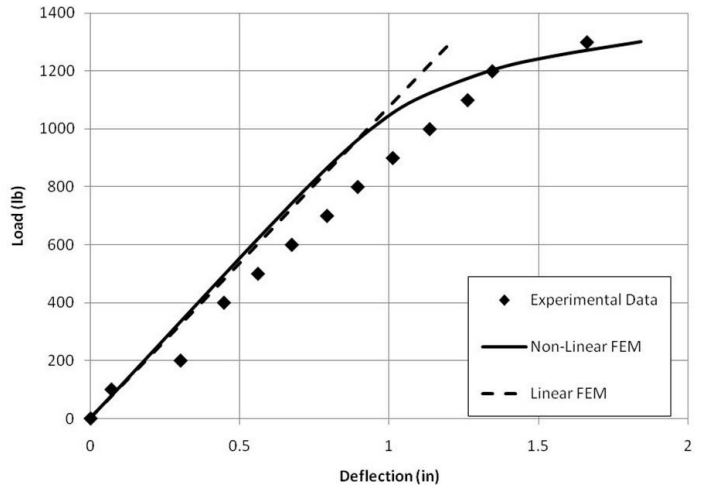

Figure 4.12: Solid Qualification - Transverse Bending - Z Direction.

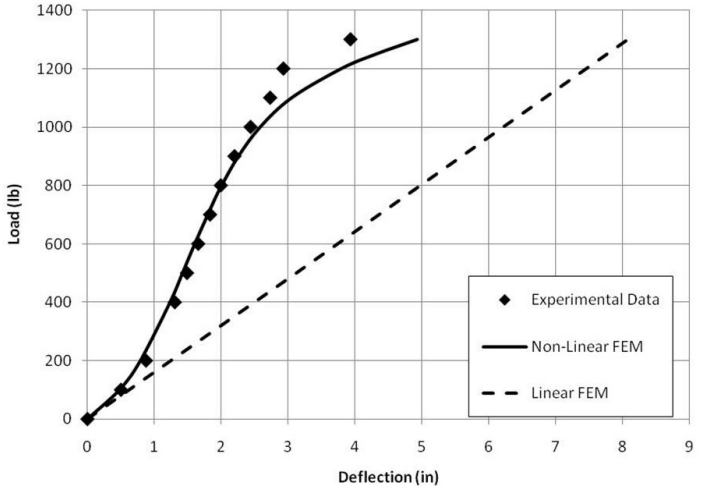

Figure 4.13: Solid Qualification - Transverse Bending - RMS.

the load point. This added an extra layer of complexity to the FE model. A loading structure that could adjust the load direction would be required to improve correlation.

4.2.2 Surface Matching.

4.2.2.1 Lateral Bending. For the qualification test articles, the surface data from the Photon 80 allowed the FE models to be quickly tuned. It was hoped that these tuned values would work well as a first order approximation of the needed values for the corresponding joined-wing. As will be discussed in the upcoming joined-wing section, this was not the case. The tuning of the qualification models was not a wasted activity; it provided needed experience for quickly tuning the joined-wing models.

Due to an average alignment between the scanner and FE coordinate systems, an ADE of 0.034 in shows that the FE model predicted and scanned surfaces closely align, as shown in Fig. 4.14. For the 150 lb load case, the non-linear solution, Fig. 4.15(b), has an ADE of 0.19 in and the linear solution, Fig. 4.15(a), has an ADE of 1.75 in. The non-linear FE model predicted displacements closely match the measured at 16 points along the surface, showing that the overall surface shape was matched. Comparisons of measured and predicted surfaces for other load cases are provided in Appendix A.

4.2.2.2 Transverse Bending. Due to a good alignment between the scanner and FE coordinate systems, a ADE of 0.0009 in shows that the FE model predicted and scanned surfaces closely align, as shown in Fig. 4.16. For the 1,000 lb load case, the non-linear solution, Fig. 4.17(b), has an ADE of 0.32 in and the linear solution, Fig. 4.17(a), has an ADE of 1.35 in. This shows that for this type of loading, a non-linear solution is required. A twisting was also seen but not shown here, signifying that the beam is buckling as expected. Comparisons of measured and predicted surfaces for other load cases are provided in Appendix A.

4.2.3 Strain.

4.2.3.1 Lateral Bending. As detailed in Section 3.1.5 and shown here again in Fig. 4.18, there are three strain gages on the solid qualification test article. The

Figure 4.14: Solid Qualification - Lateral Bending - 0 lb Surface Matching.

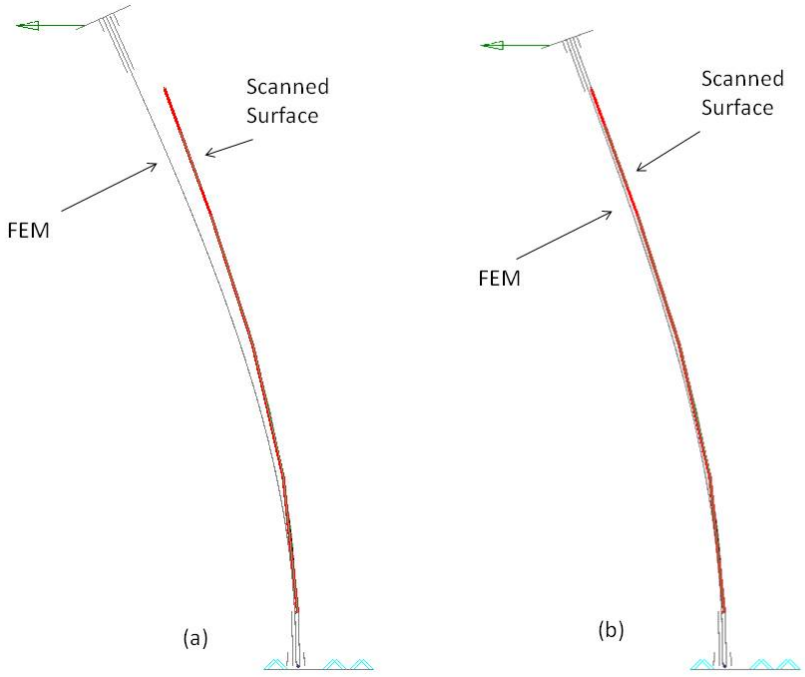

Figure 4.15: Solid Qualification - Lateral Bending - 150 lb Surface Matching - (a) Linear and (b) Non-Linear.

Figure 4.16: Solid Qualification - Transverse Bending - 0 lb Surface Matching.

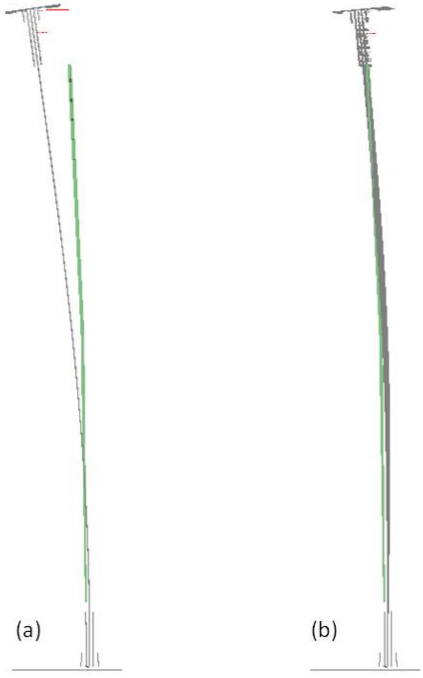

Figure 4.17: Solid Qualification - Transverse Bending - 1,000 lb Surface Matching - (a) Linear and (b) Non-Linear.

recorded strains are shown in Fig. 4.19. Gage 1 and 2 track together as expected, which signifies that the test article was not twisting about the y-axis as it was loaded. Low values of strain were recorded at Gage 3, which would indicate that the test article was also bending in around the z-axis, but the displacement data in Section 4.2.1.1 above does not support that conclusion. Likely, Gage 3 was not exactly on the neutral axis of the beam, which would explain the low amount of strain recorded.

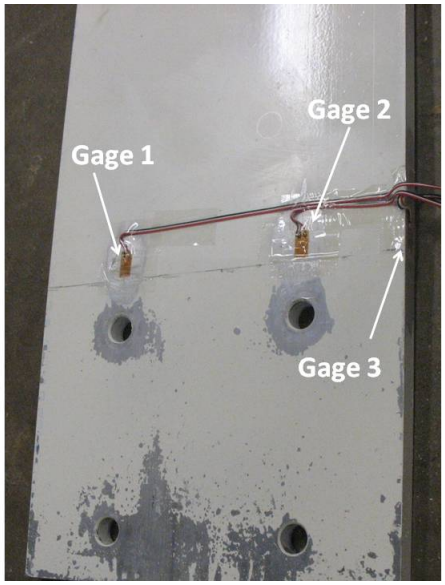

Figure 4.18: Solid Qualification Test Article with Gages.

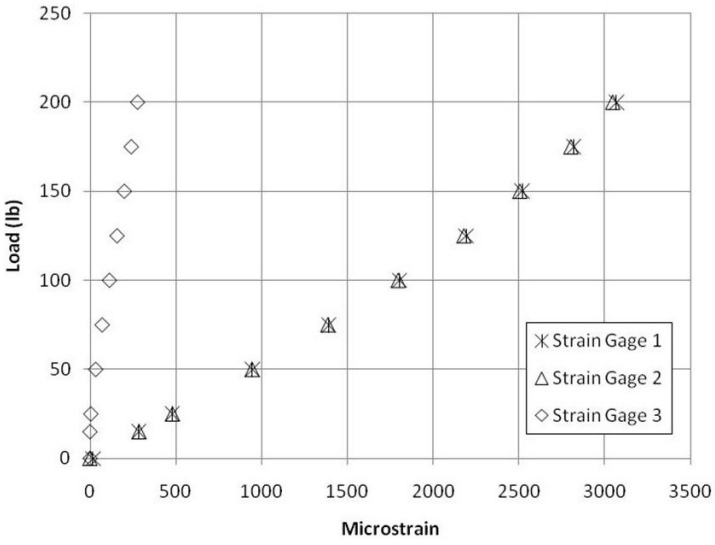

Figure 4.19: Solid Qualification - Lateral Bending - Recorded Strain.

4.2.3.2 Transverse Bending. When the solid qualification test article is loaded such that it bends in the transverse bending direction, the resulting strain, as shown in Fig. 4.20, indicates the expected buckling. At the low load levels, Gage 1 strains indicate increasing compression and Gage 2 strains indicate increasing tension. After 900 lb, Gage 1 strain values changes from increasing to decreasing. This change indicates the onset of the beam buckling. The only way Gage 1 could reduce its strain is for the beam to start rotating about the y-axis. It was predicted in Eq. 3.1 that buckling would occur at 1,000 lb. The earlier buckling is due to the load angle as explained in Section 4.2.1.2 above.

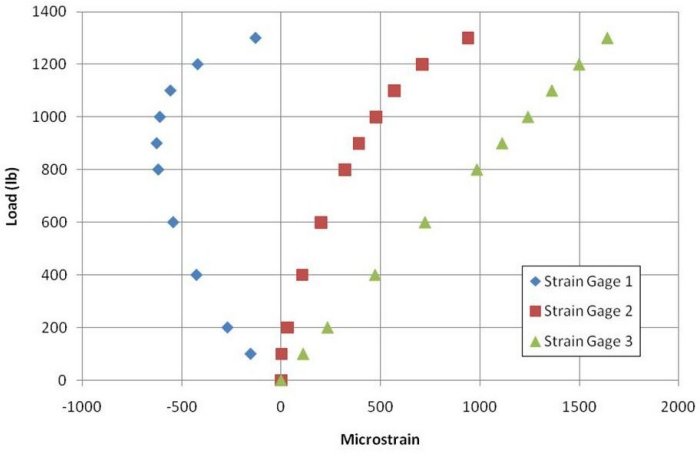

Figure 4.20: Solid Qualification - Transverse Bending - Recorded Strain.

4.2.4 Base Movement. As a first attempt to quantify the movement of the base during the testing, a tracker point (Fig. 4.21) was placed on the connector block during the transverse bending tests. Figure 4.22 shows the movement of this point during the experiment. The recorded movement was generally negligible for this point, since it was on the connector block. The tracker point really needed to be located on the base plate to accurately quantify base movement, which was done in the joined-wing test article. Base movement will be further discussed in the joined-wing test article section.

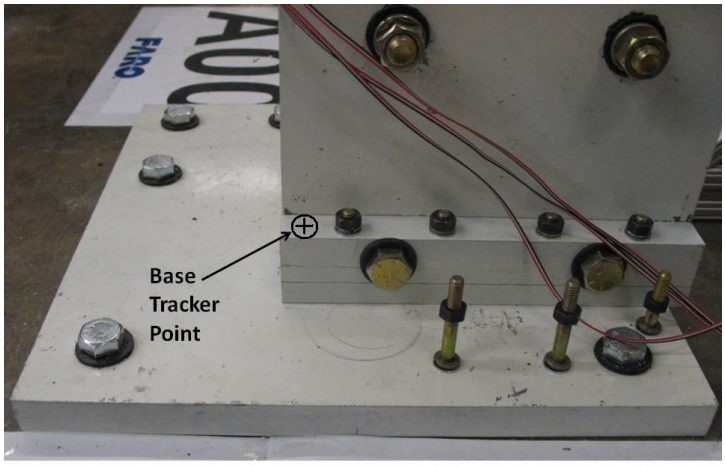

Figure 4.21: Solid Qualification Test Article - Transverse Bending - Connector Block Tracker Point.

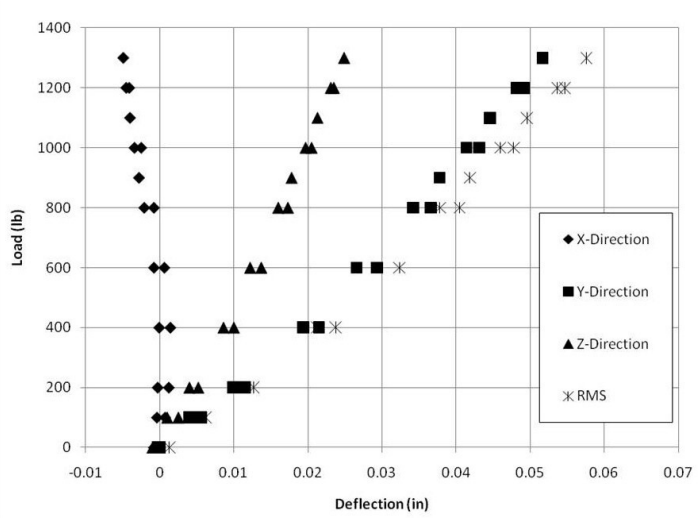

Figure 4.22: Solid Qualification - Transverse Bending - Connector Block Movement.

4.3 Hollow Qualification Wing

4.3.1 Deflection Curves. With the Laser Tracker, a tracker point was measured near the top of the test article, as shown in Fig. 4.23. There are four data sets of the measured displacements of the point: x-, y-, and z-displacements with load and the root-mean-squared (RMS) or total displacement. The plots are shown in Figs. 4.24, 4.25, 4.26 and 4.27. The diamonds represent the experimental results; the solid line represents the non-linear FE model solution; and the dashed line represents the linear FE model solution.

Figure 4.23: Hollow Qualification - Tracker Point.

All the data shows poor correlation. Also, the non-linear solution would only converge to a 15 lb load; all solution attempts above this load failed. Nastran had trouble solving this FE model because of significant skin buckling, which I will touch on later. Additional data on this test article can be found in Appendix B.

4.3.2 Surface Matching. The predicted and measured displacement surfaces match for the 0 lb load set, Fig. 4.28, showing that the scan data and FE model are aligned. The non-linear solution for the 15 lb load set, Fig. 4.29(b), visually align. The linear solution for the 15 lb load set, Fig. 4.29(a), does not visually align. This shows

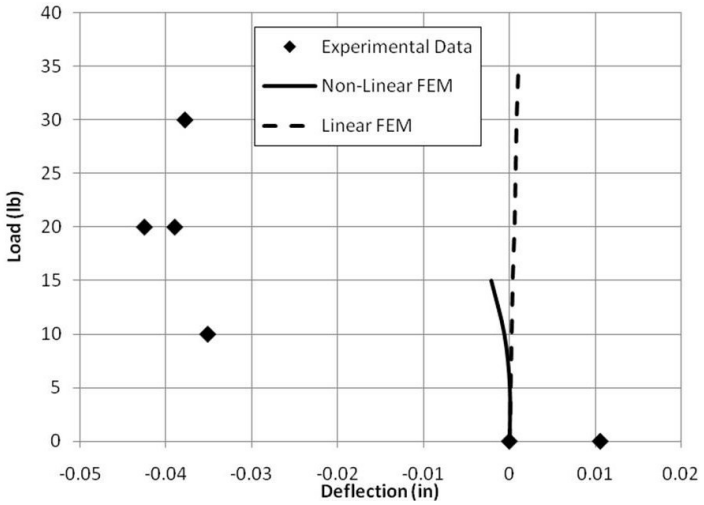

Figure 4.24: Hollow Qualification - X-Direction.

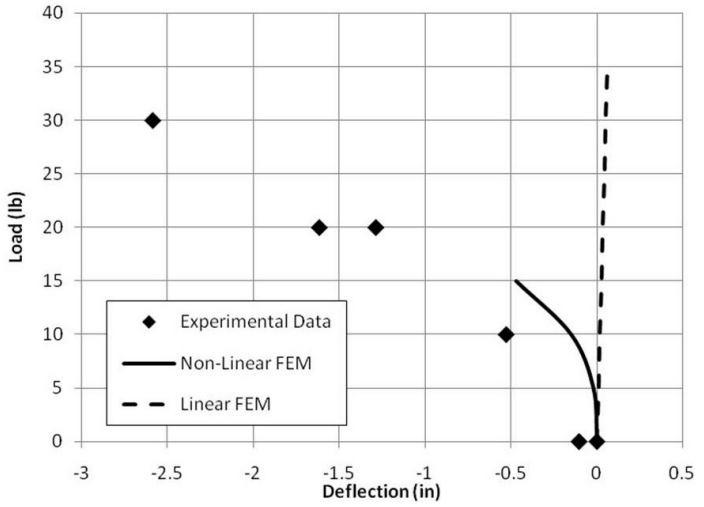

Figure 4.25: Hollow Qualification - Y-Direction.

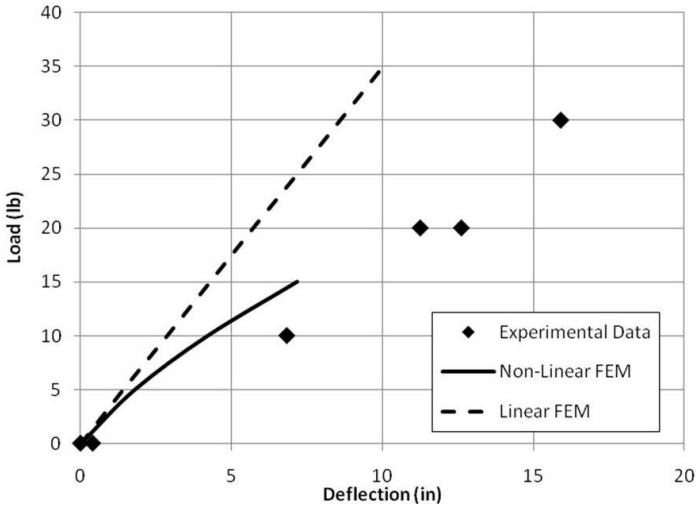

Figure 4.26: Hollow Qualification - Z-Direction.

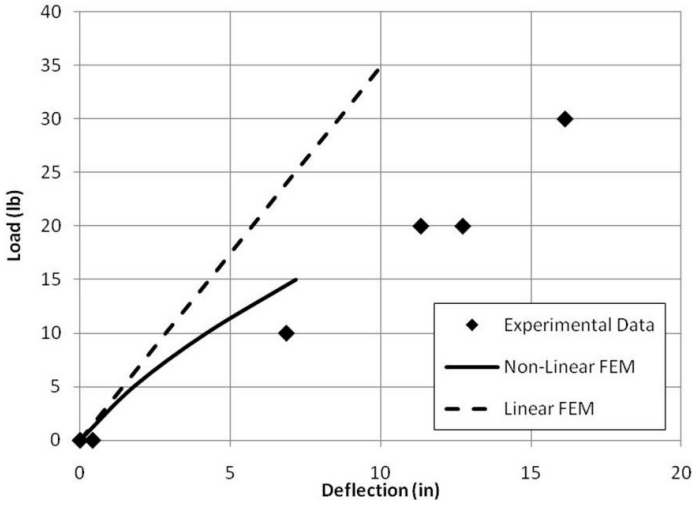

Figure 4.27: Hollow Qualification - RMS.

that for this amount of deflection of the beam, a non-linear solution is required. While the point data is poorly correlated above, the surface data matched well for the solved non-linear cases. The ADE was not calculated for this case. Additional surfaces for this model are in Appendix B.

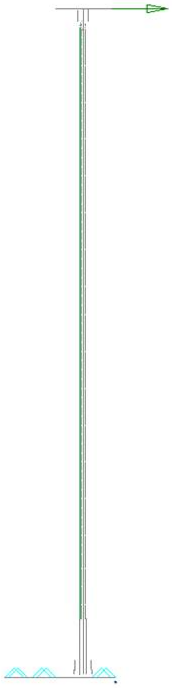

Figure 4.28: Hollow Qualification - 0 lb Surface Matching.

4.3.3 Strain. There were two strain gages on the hollow qualification test article, as described in Section 3.1.5 and shown here again in Fig. 4.30. Figure 4.31 shows strain values from these gages for two sets of tests. Neither set of strain data matches extremely well, especially Gage 2. Also, the very low loads (under 30 lb) introduced a large amount of error because the measurement system was designed for significantly higher loads. Accurate repeatability at such low loads is difficult because of the error in the measurement system.

4.3.4 Skin Buckling. As expected, skin buckling was experienced in the hollow qualification test article. Figure 4.32(a) shows the compression skin buckling predicted by the FE model. Figure 4.32(b) is a photograph of the test article under load. As indicated in Fig. 4.32, the wavelength of the skin buckling is different between the FE

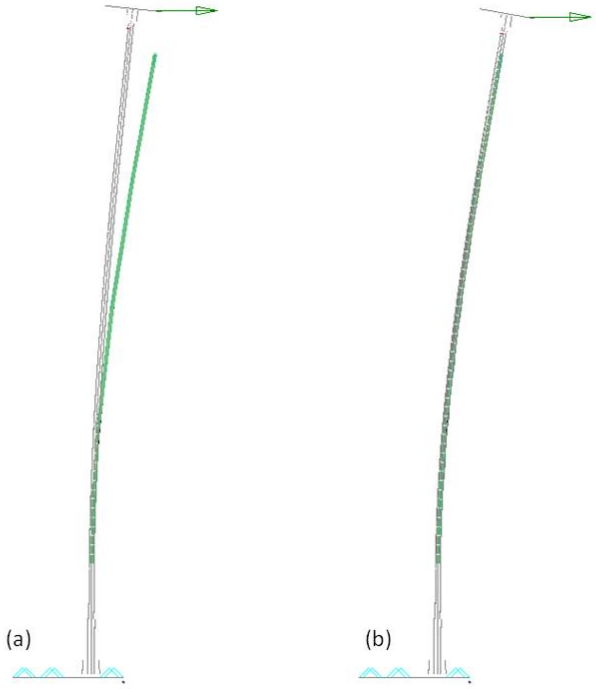

Figure 4.29: Hollow Qualification - 15 lb Surface Matching - (a) Linear and (b) Non-Linear.

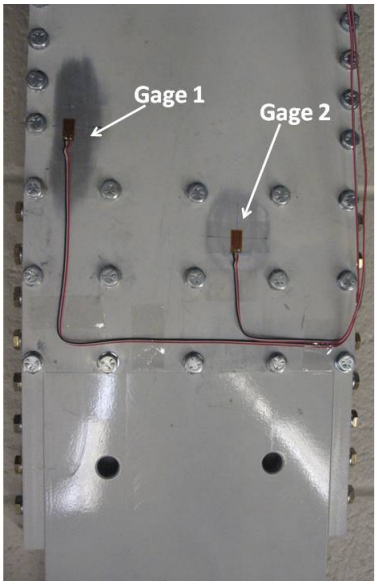

Figure 4.30: Hollow and Foam-filled Qualification Test Article with Gages.

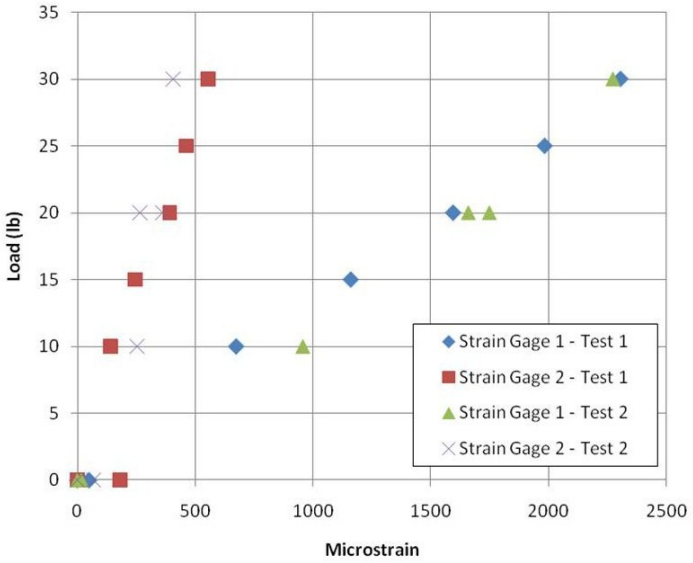

Figure 4.31: Hollow Qualification - Recorded Strain.

model and test article, signifying that the FE model is not fully correlated. Likely, modeling the bolts holding the skin to the ribs as rigid links is over-constraining the solution. Due to the inability of Nastran to converge for most of the non-linear load cases, a different solver may be needed to accurately model the skin buckling.

The tension side of the test article and the FE model also exhibited similar skin buckling, this time seen as a single vertical line, as seen in Fig. 4.33. This is a result of the significant total deformation of the test article and the skin buckling on the opposite side of the test article.

4.4 Solid Joined-Wing

The solid joined-wing test article was designed with the express purpose of clearly demonstrating the non-linear bend-twist couple inherent with the joined-wing design, as described previously. Three data sets were collected during the experiment using the laser systems: top deflections (Laser Tracker), surface shape (Photon 80), and base movement (Laser Tracker). The strains and angles were also recorded. All data has been transformed so that the following coordinate system is used: x is in the forward direction or direction towards the front of the aircraft, y is out of the wing tip, and z is in the load direction or upward with respect to the aircraft; shown in Fig. 4.34.

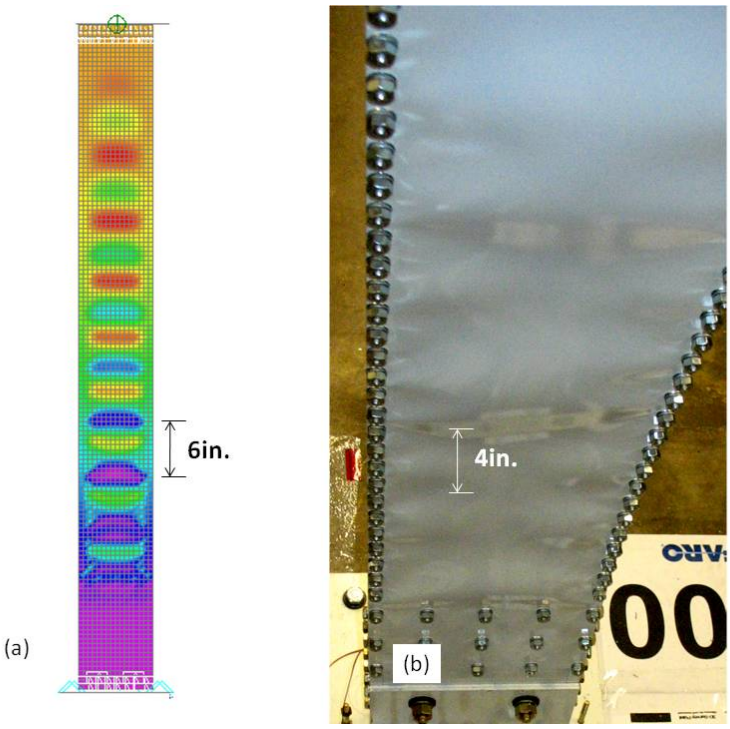

Figure 4.32: Hollow Qualification - (a) FE Model and (b) Test Article Compression Buckling.

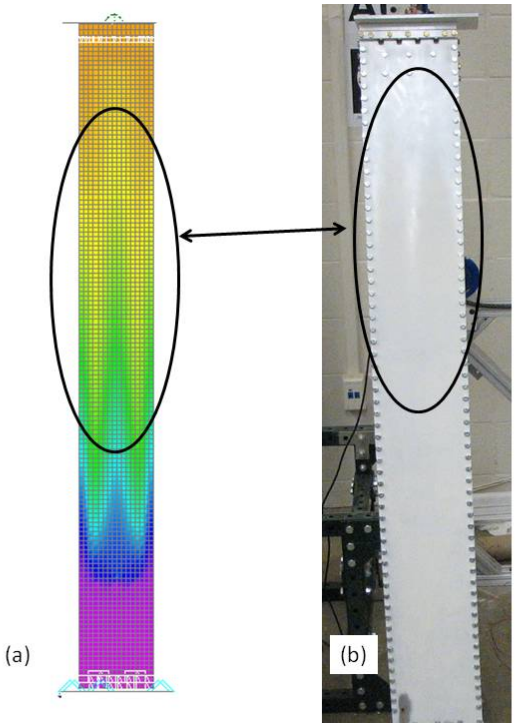

Figure 4.33: Hollow Qualification - (a) FE Model and (b) Test Article Tension Buckling.

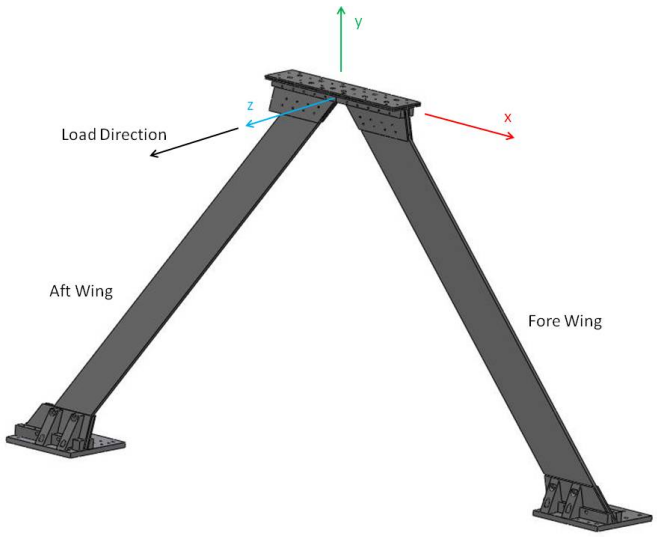

Figure 4.34: Solid Joined-wing Coordinate System

For the FE model, the hand-tuned stiffness coefficients of the 6DOF springs from the solid qualification model were used as a starting point for the stiffness coefficient values for the 6DOF springs in the joined-wing. These values produced a joined-wing FE model that was not rigid enough when compared to measured responses. Therefore, the qualification FE model 6DOF coefficients were not used in the joined-wing FE models. Instead, the same trial and error method as used for the qualification FE models was used for the joined-wing FE models.

4.4.1 Deflection Curves. With the Laser Tracker, four points were tracked during the experiments. The locations of the points on the test article are shown in Fig. 4.35. Point 1 also shows the SMR at the point location. The points are offset 1 in from the surface, which is the center of a mounted SMR. Corresponding points were created in the FE model, shown in Fig. 4.36.

The tuned FE model produced accurate predictions in the non-linear range of the experimental results. All the x-, y-, z-, and RMS-displacement plots of this section use the following symbols: the diamonds represent the experimental results, the solid line represents the non-linear FE model solution, and the dashed line represents the linear FE model solution.

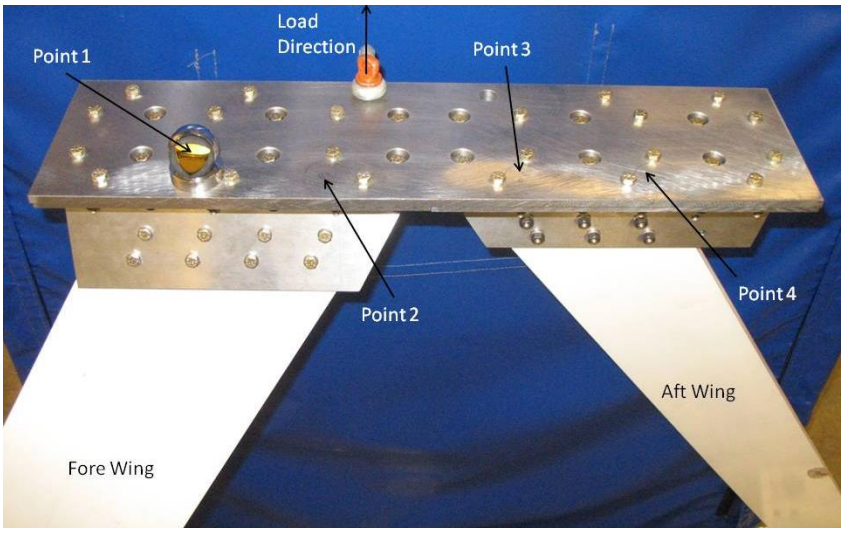

Figure 4.35: Solid Joined-wing Tracker Points.

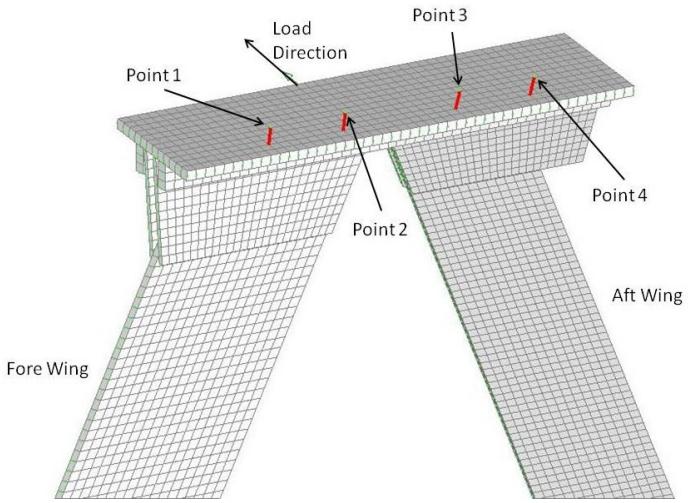

Figure 4.36: Solid Joined-wing FE Model Points.

4.4.1.1 Point 1. There are four data sets of the measured displacements at Point 1: x-, y-, and z-displacements with load and the root-mean-squared (RMS) or total displacement. The plots are shown in Figs. 4.37, 4.38, 4.39, and 4.40. These plots show that the solution most clearly matches the non-linear solution, as expected. Table 4.1 shows the percent error at each point with the non-linear FE model. The z-direction shows particularly low error in the 300 to 1,100 lb range, since the model was tuned using this range of data. The z-direction is also the greatest change in movement, shown in the values and the fact that the RMS values and error closely track the z-direction, seen in Figs. 4.39 and 4.40 and Tab. 4.1. The y-direction has the poorest correlation. The poor correlation shows that the FE model is not adequately tuned, but the disagreement between y-values is also the smallest, and therefore the error has the least effect on the overall deflection and shape of the FE model. Figure 4.38 shows that the FE model is predicting larger deflections in the y-direction, which for this point means that the top plate is slightly over-rotating in the FE model. Additional measurements at this point can be found in Appendix C.

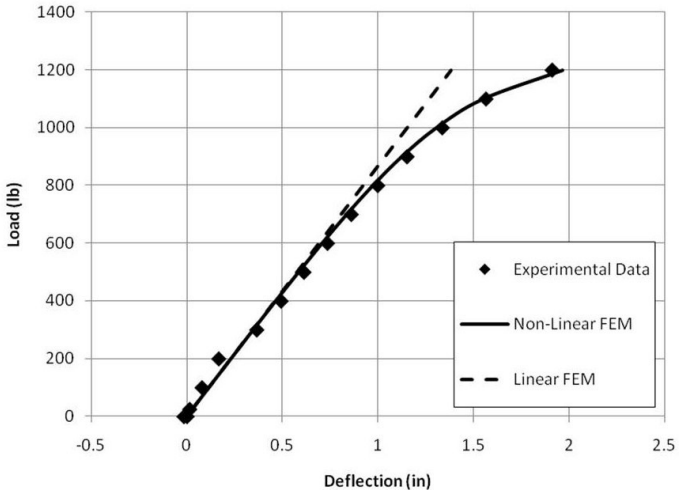

Figure 4.37: Solid Joined-wing - Point 1 - X-Direction.

4.4.1.2 Point 2. The second point data is shown in Figs. 4.41, 4.42, 4.43, and 4.44. Table 4.2 shows the percent error at each point with the non-linear FE model. The same trend is evident with Point 2 as with Point 1 above. The error is particularly low in the z-direction between 300 and 1,100 lb, as seen in Fig. 4.43 and

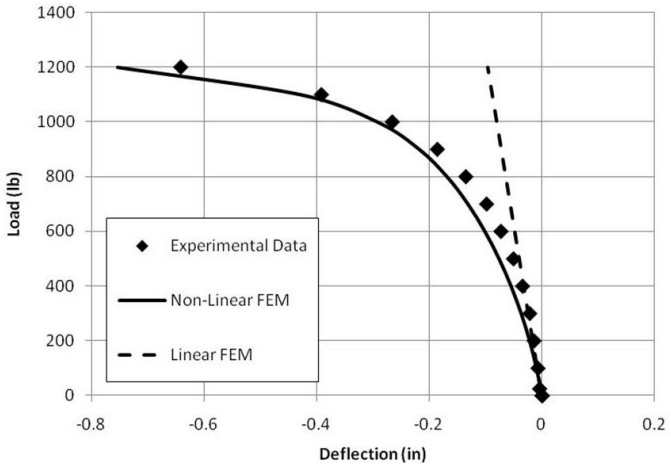

Figure 4.38: Solid Joined-wing - Point 1 - Y-Direction.

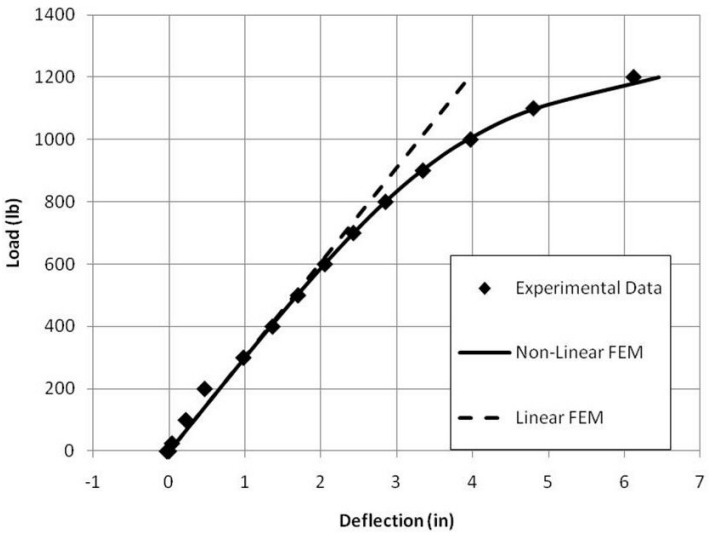

Figure 4.39: Solid Joined-wing - Point 1 - Z-Direction.

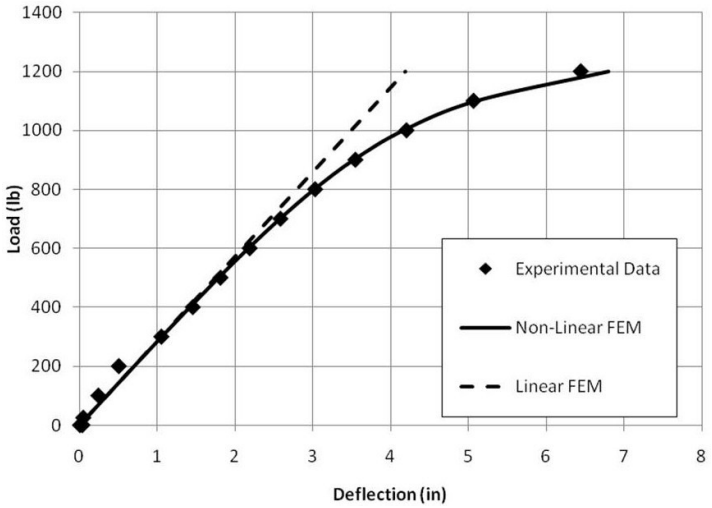

Figure 4.40: Solid Joined-wing - Point 1 - RMS.

Table 4.1: Solid Joined-wing - Point 1 - Percent Error Between Non-Linear FE Model Solutions and Measured Results.

Load (lb)	x (%)	y (%)	z (%)	RMS (%)
25	116	46	105	105
100	47	38	48	48
200	39	58	40	40
300	5	71	1	1
400	6	59	2	2
500	5	51	1	1
600	4	39	0	1
700	3	34	0	0
800	3	25	0	0
900	2	17	0	1
1000	2	10	1	1
1100	1	10	1	1
1200	3	18	6	6

Tab. 4.2. The y-direction tracks fairly well in Fig. 4.42. Interestingly, the linear solution diverges very quickly at this point because the direction of the displacement changes. Additional measurements at this point can be found in Appendix C.

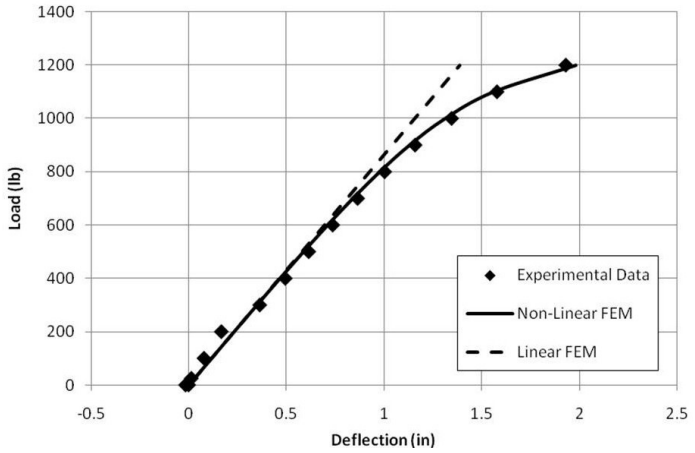

Figure 4.41: Solid Joined-wing - Point 2 - X-Direction.

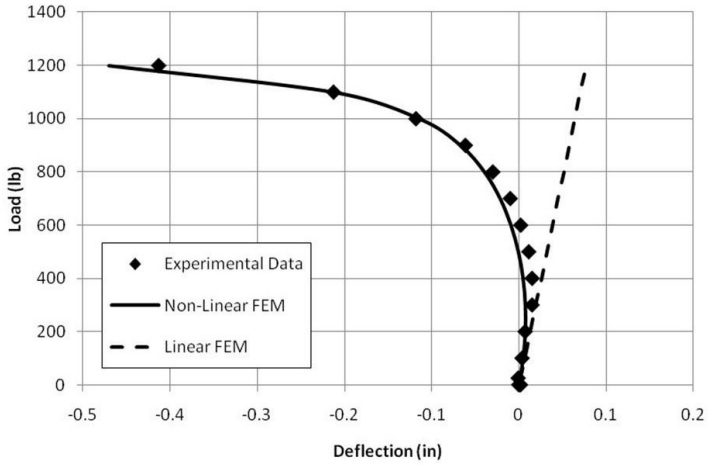

Figure 4.42: Solid Joined-wing - Point 2 - Y-Direction.

4.4.1.3 Point 3. The third point data is shown in Figs. 4.45, 4.46, 4.47, and 4.48. Table 4.3 shows the percent error at each point with the non-linear FE model. As with Points 1 and 2, Point 3 shows very good correlation in the x- and z-directions between 300 and 1,100 lb, shown in Figs. 4.45 and 4.47. The y-direction is overshot in the non-linear FE model by a high percentage, shown in Fig. 4.46 and Tab. 4.3. This

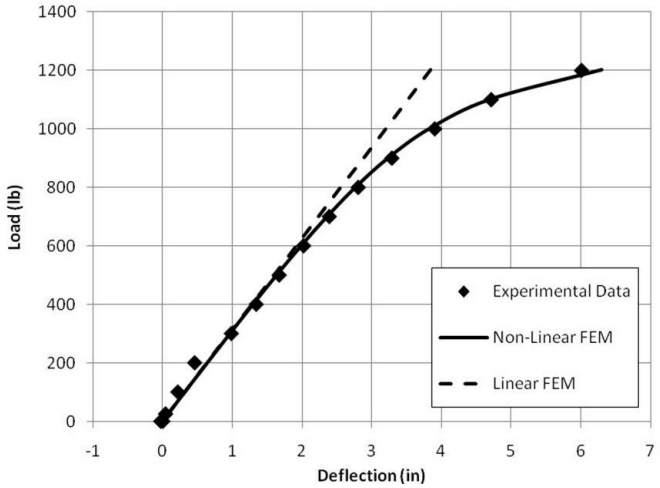

Figure 4.43: Solid Joined-wing - Point 2 - Z-Direction.

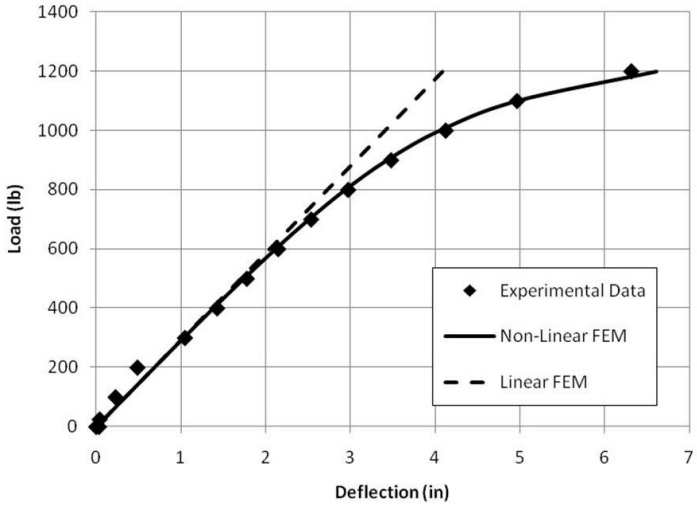

Figure 4.44: Solid Joined-wing - Point 2 - RMS.

Table 4.2: Solid Joined-wing - Point 2 - Percent Error Between Non-Linear FE Model Solutions and Measured Results.

Load (lb)	x (%)	y (%)	z (%)	RMS (%)
25	115	395	108	108
100	47	31	49	49
200	38	4	41	40
300	4	50	2	2
400	6	67	3	3
500	4	102	2	2
600	4	477	1	2
700	3	121	1	1
800	2	32	1	1
900	2	9	1	1
1000	2	4	2	2
1100	1	0	0	0
1200	3	14	5	5

is still due to the fact that FE model's top plate is rotating more than the test article. Additional measurements at this point can be found in Appendix C.

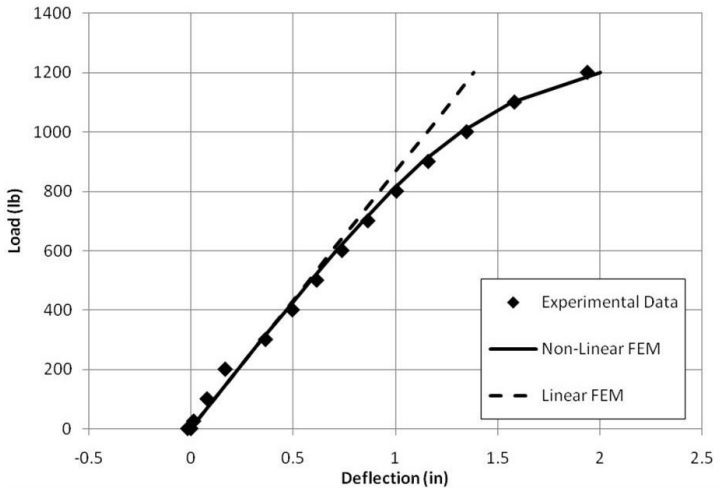

Figure 4.45: Solid Joined-wing - Point 3 - X-Direction.

4.4.1.4 Point 4. The fourth point data is shown in Figs. 4.49, 4.50, 4.51, and 4.52. Table 4.4 shows the percent error at each point with the non-linear FE model. As with the previous points, Point 4 also has very good correlation in the x- and z-directions, Figs. 4.49 and 4.51, in the 300 to 1,100 lb range. The y direction is still

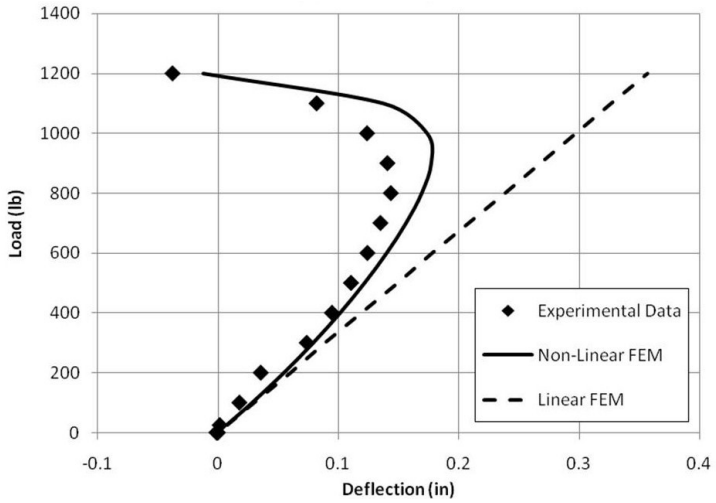

Figure 4.46: Solid Joined-wing - Point 3 - Y-Direction.

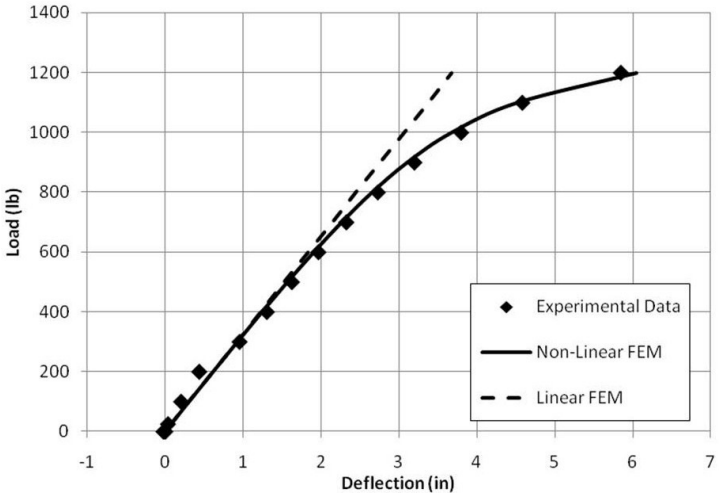

Figure 4.47: Solid Joined-wing - Point 3 - Z-Direction.

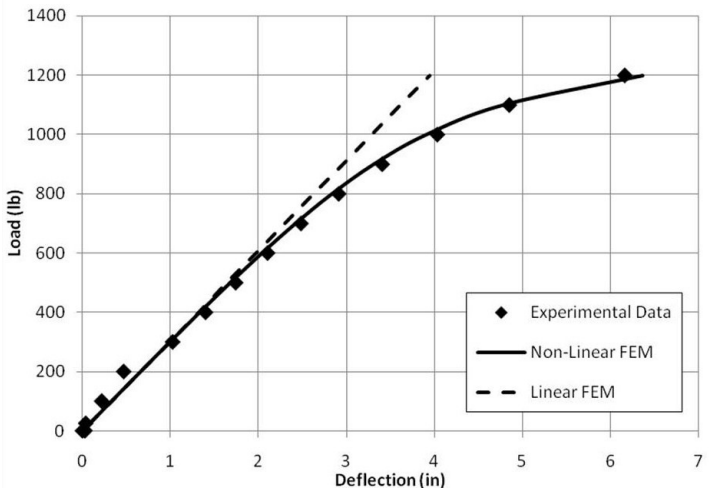

Figure 4.48: Solid Joined-wing - Point 3 - RMS.

Table 4.3: Solid Joined-wing - Point 3 - Percent Error Between Non-Linear FE Model Solutions and Measured Results.

Load (lb)	x (%)	y (%)	z (%)	RMS (%)
25	111	374	121	120
100	46	60	51	51
200	38	55	41	41
300	5	8	3	3
400	6	7	5	5
500	5	10	4	4
600	4	13	3	3
700	3	16	3	3
800	2	18	3	3
900	2	26	3	3
1000	2	41	3	3
1100	1	68	2	2
1200	3	68	3	3

off due to the excessive FE model top plate rotation, shown in Fig. 4.50 and Tab. 4.4. Additional measurements at this point can be found in Appendix C.

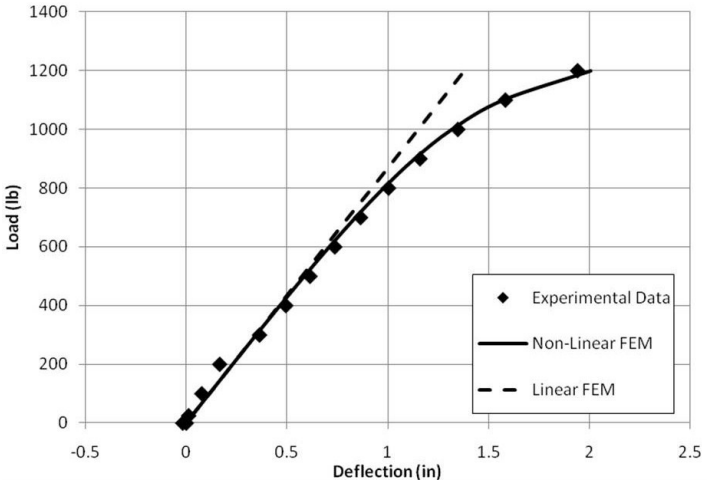

Figure 4.49: Solid Joined-wing - Point 4 - X-Direction.

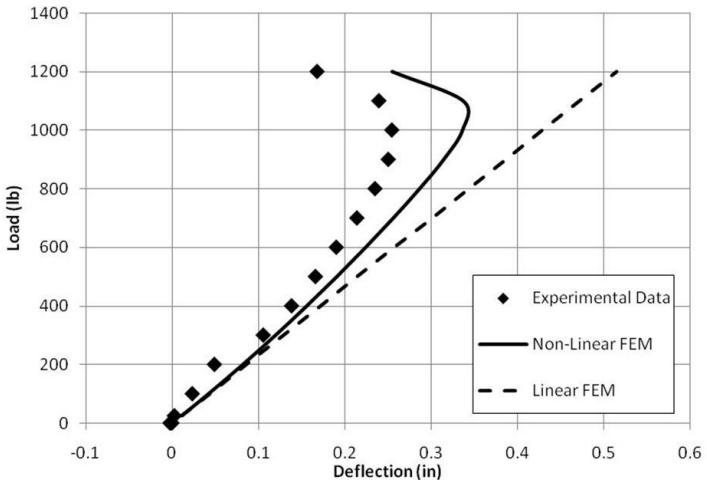

Figure 4.50: Solid Joined-wing - Point 4 - Y-Direction.

It is important to note that the maximum translation at 1,200 lb is only 6 in, or 11% of the wing's 57 in height. This highlights the reason the joined-wing concept is being considered as a HALE aircraft design despite the complex geometric couplings seen; the joined-wing design is extremely stiff.

4.4.2 Surface Shape. The Photon 80 surface scanner data, in the form of lofted surfaces, is compared to the FE model to verify that the FE model is correlated. It is not enough to match the tip deflection, as was done in the previous section with the tracker

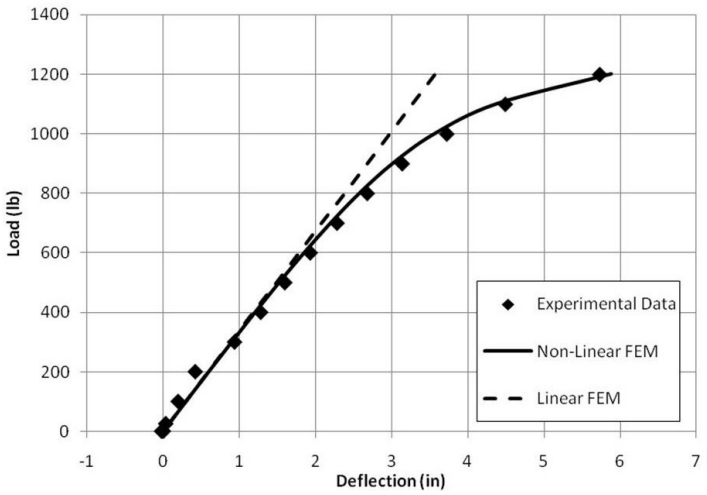

Figure 4.51: Solid Joined-wing - Point 4 - Z-Direction.

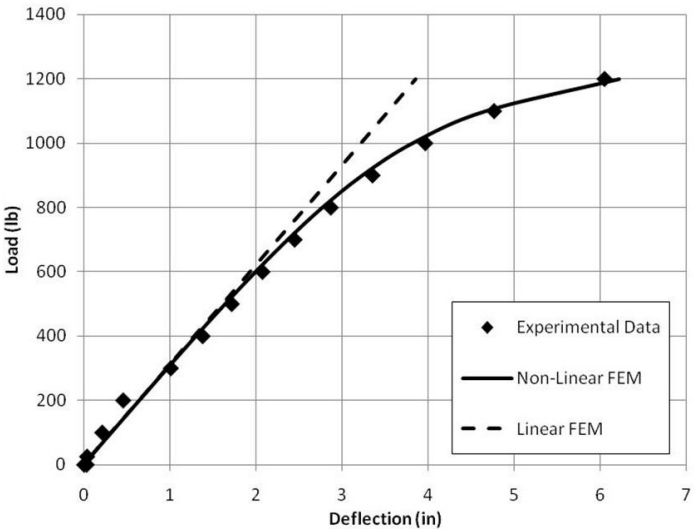

Figure 4.52: Solid Joined-wing - Point 4 - RMS.

Table 4.4: Solid Joined-wing - Point 4 - Percent Error Between Non-Linear FE Model Solutions and Measured Results.

Load (lb)	x (%)	y (%)	z (%)	RMS (%)
25	144	267	134	137
100	49	77	54	53
200	39	66	42	42
300	5	13	4	4
400	6	12	6	5
500	5	15	5	4
600	4	18	4	4
700	3	19	4	3
800	3	22	4	3
900	2	25	4	4
1000	2	32	4	4
1100	1	40	3	2
1200	3	51	3	3

data; the full bend-twist couple must be evident to determine if the FE model is indeed correlated. From the side-view of the test article, Fig. 4.53 shows the actual test article and Fig. 4.54 shows the FE model and scanned surface for the undeformed test article. Due to a proper alignment between the scanner and FE coordinate systems, an ADE of 0.23 in shows that the FE model and scanned surfaces closely align.

Figure 4.55 shows the test article under a 1,000 lb load. Figure 4.56 shows the linear (Fig. 4.56(a)) and non-linear (Fig. 4.56(b)) FE model compared to the surface data. It is clear that the linear solution does not align well with the surface shape, whereas the non-linear solution aligns quite well. The linear case has an ADE of 0.42 in, and the non-linear case has an ADE of 0.25 in. Likewise, Figs. 4.57 and 4.59 show the test article under a 1,100 and 1,200 lb load, respectively. The 1,100 lb load has a linear ADE of 0.56 in (Fig. 4.58(a)) and a non-linear ADE of 0.25 in (Fig. 4.58(b)). The 1,200 lb load has a linear ADE of 0.77 in ((Fig. 4.60(a)) and a non-linear ADE of 0.18 in (Fig. 4.60(b)). Additional surfaces are presented in Appendix D.

Figure 4.59 clearly shows the aft wing in a bend-twist deformation. This highlights that this joined-wing test article was designed correctly. The test article was loaded to 1,200 lb three times and exhibited no permanent deformation. As will be explained later, the bend-twist coupling is not beam buckling in the conventional sense of the term.

Figure 4.53: Solid Joined-wing - Undeformed Test Article.

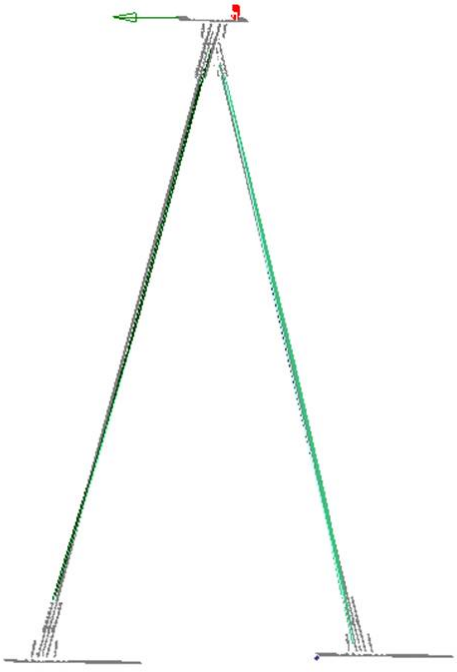

Figure 4.54: Solid Joined-wing - Undeformed FE Model.

Figure 4.55: Solid Joined-wing - Test Article under a 1,000 lb Load.

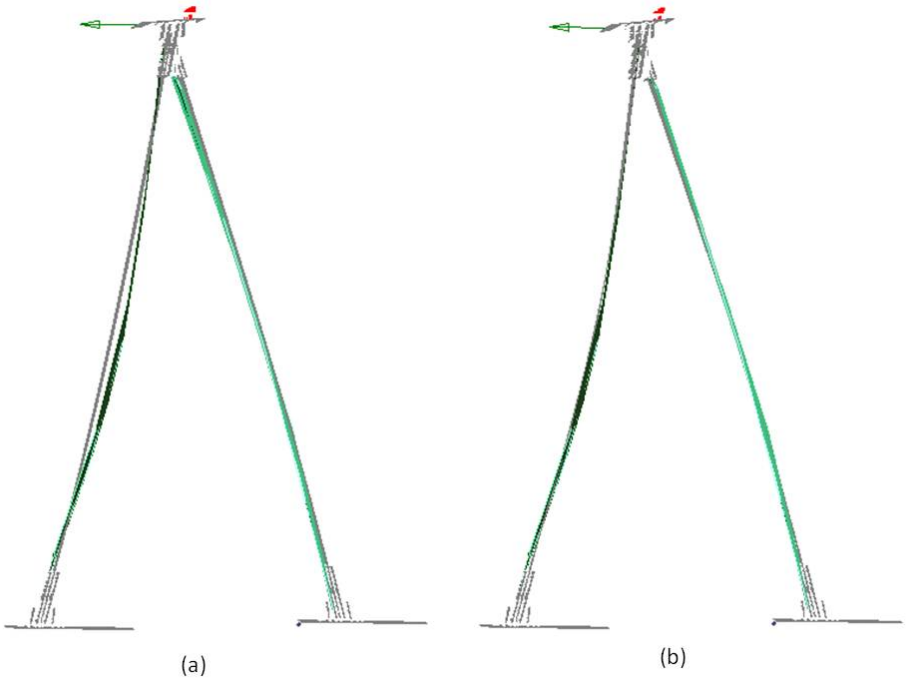

Figure 4.56: Solid Joined-wing - (a) Linear and (b) Non-linear FE Model under a 1,000 lb Load.

Figure 4.57: Solid Joined-wing - Test Article under a 1,100 lb Load.

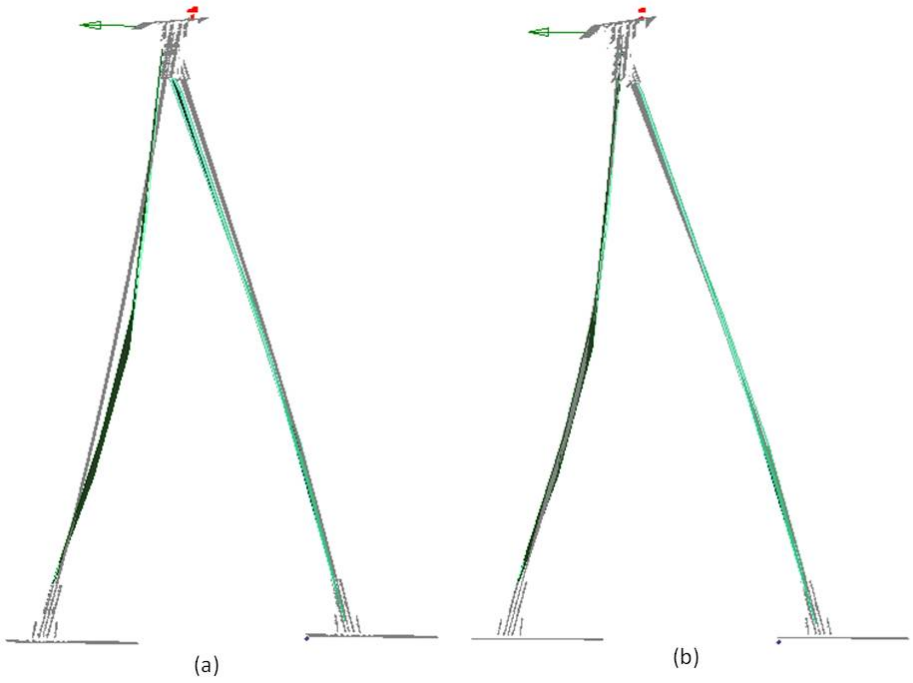

Figure 4.58: Solid Joined-wing - (a) Linear and (b) Non-linear FE Model under a 1,100 lb Load.

Figure 4.59: Solid Joined-wing - Test Article under a 1,200 lb Load.

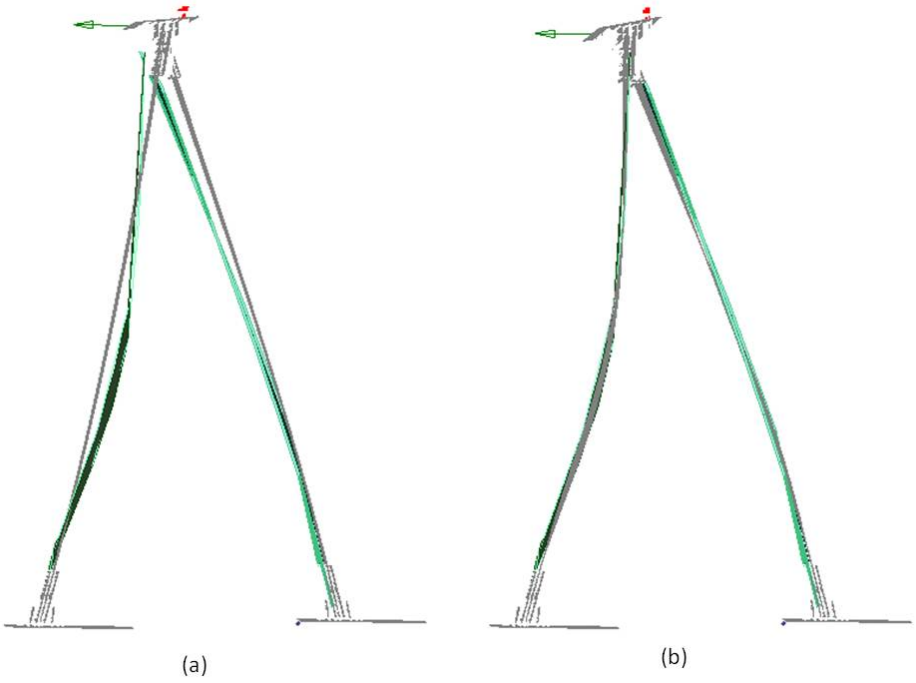

Figure 4.60: Solid Joined-wing - (a) Linear and (b) Non-linear FE Model under a 1,200 lb Load.

4.4.3 Strain. On the test article, the four strain gages, described in detail in Section 3.1.5 and shown here again in Fig. 4.61, were recorded during the experiment. The data is shown in Fig. 4.62. It is important to notice that during the high loads, where the aft wing is undergoing a significant bend-twist couple, it is holding a load comparable to the fore wing at the root. Typically, a joined-wing design like this experiment is considered buckling critical, but the wing does not buckle in the way most people would perceive as buckling. In a typical beam, when the structure buckles, it can no longer handle an increase in load. In a joined-wing, when the structure is undergoing its global buckling case or the bend-twist coupling, the beams are still resisting the load. Also worth noting is that the aft root experiences a stress relief because of the bend-twist coupling with the z-direction loading. Figure 4.62, combined with the material testing shown in Fig. 4.1, shows that the maximum load applied of 1,200 lb was the last load case before yielding, since the 4,000 $\mu\epsilon$ yield point would have been reached before 1,300 lb.

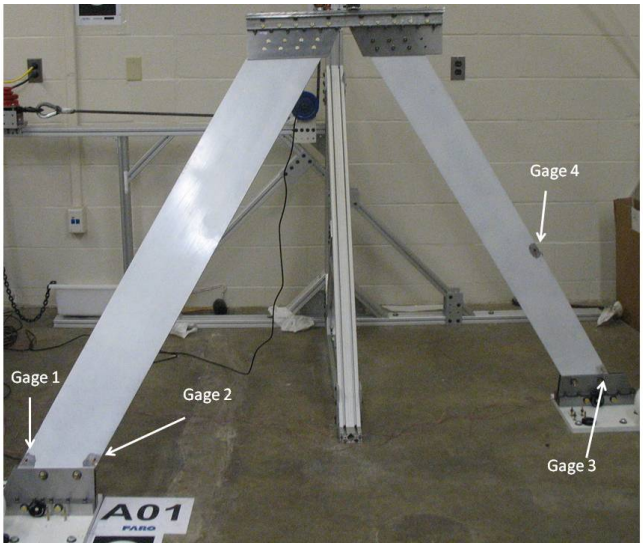

Figure 4.61: Solid Joined-wing Test Article with Gages.

4.4.4 Top Joint Constraint. The top mounting structure of the joined-wing test article was designed to allow a common load application point and to hold the fore and aft wings fixed relative to each other. After tuning the FE model, the stresses in the top mounting structure were evaluated to determine if these stresses were likely

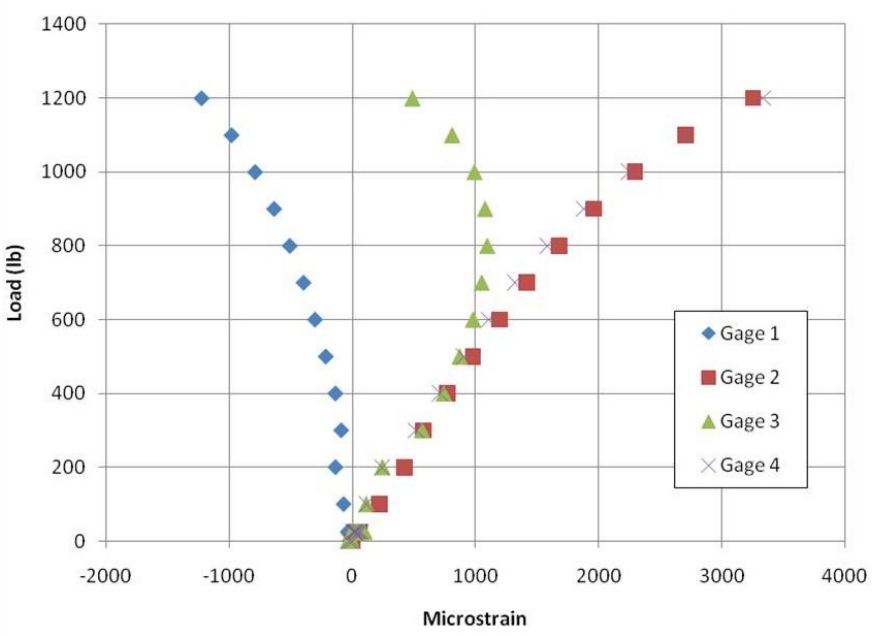

Figure 4.62: Solid Joined-wing - Recorded Strain.

to cause deformation of the steel. The bottom plate mean stress of the joined-wing FE model at 1,200 lb is shown in Fig. 4.63. The legend shows the stress in units of psi. As expected, the stress at the joint of the joined-wing is low, 0 psi to 9,000 psi in compression, compared to the stresses at the roots, 26,000 psi in tension and 35,000 psi in compression. Based on these results, no further investigation of the relative joint deformation is needed.

4.4.5 Base Movement. One of the concerns with the design of the joined-wing test article was movement of the base plates. In the FE model, these are constrained against all movement. In reality, this is at best, a fairly good assumption. Therefore, several Laser Tracker points were evaluated at specific locations on the base plates, shown in Figs. 4.64 and 4.65.

The main reference points are 1 and 2 for both the fore and aft base plates. Figures 4.66, 4.67, 4.68 and 4.69 show the movement of the base plates. Data from the other points is presented in Appendix E.

In general, this data shows that while the base does move, the displacement is under 0.003 in. The only direction greater than 0.003 in is in the y-direction of the fore

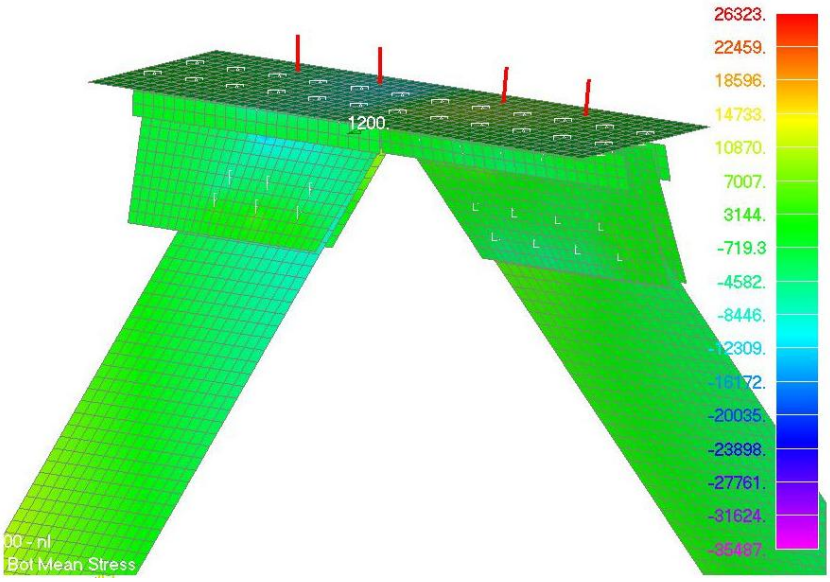

Figure 4.63: Solid Joined-wing FE Model - Stress at Top Mounting Structure.

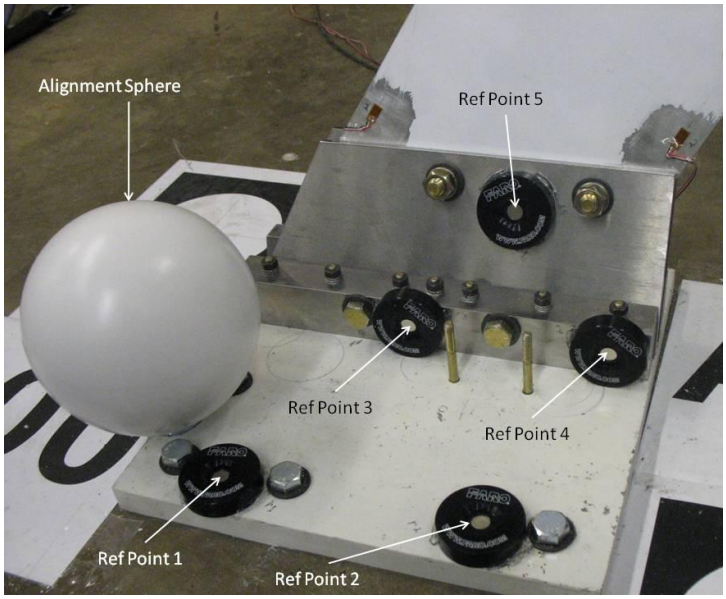

Figure 4.64: Solid Joined-wing - Fore Base Plate - Reference Points.

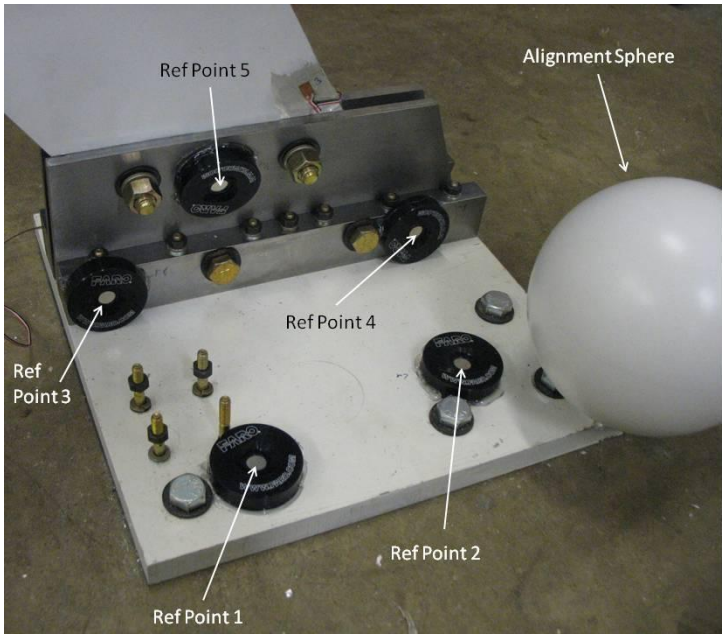

Figure 4.65: Solid Joined-wing - Aft Base Plate - Reference Points.

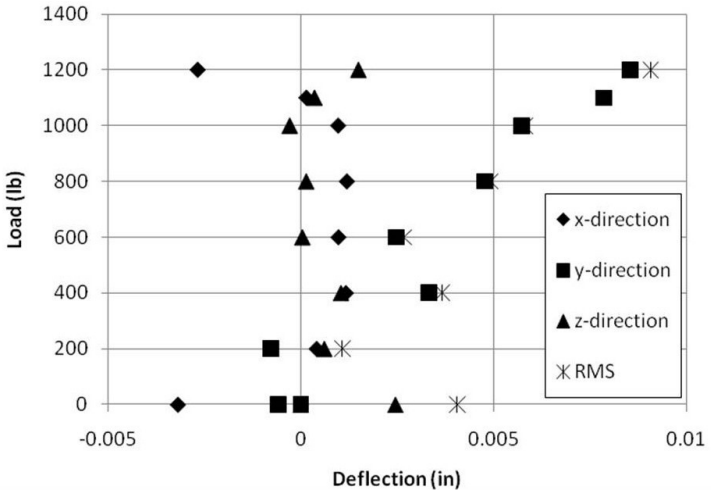

Figure 4.66: Solid Joined-wing - Fore Reference Point 1 - Movement.

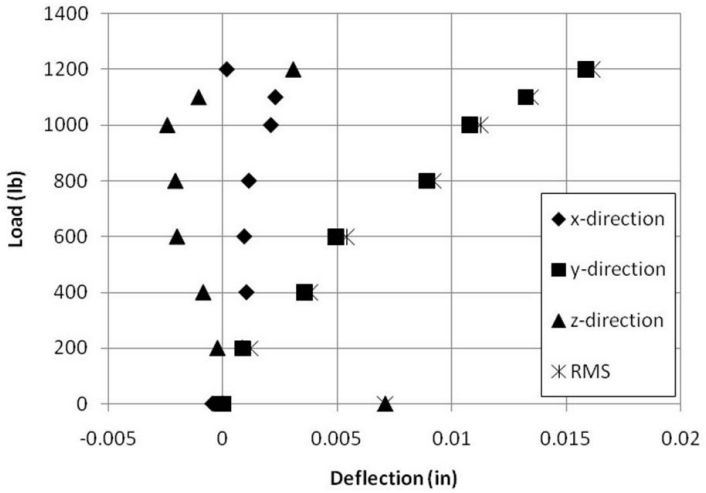

Figure 4.67: Solid Joined-wing - Fore Reference Point 2 - Movement.

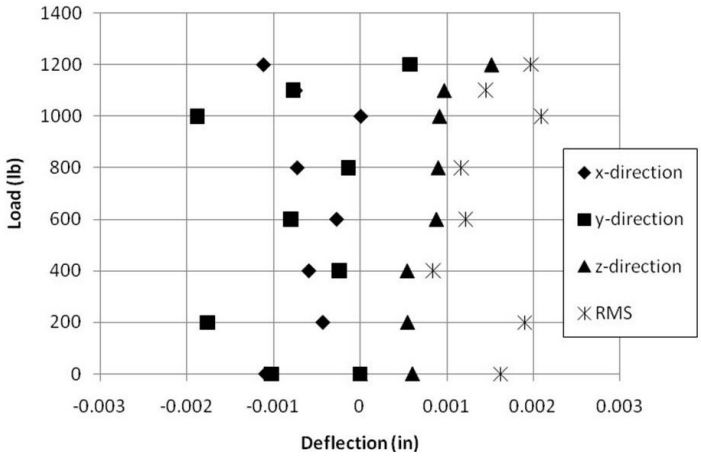

Figure 4.68: Solid Joined-wing - Aft Reference Point 1 - Movement.

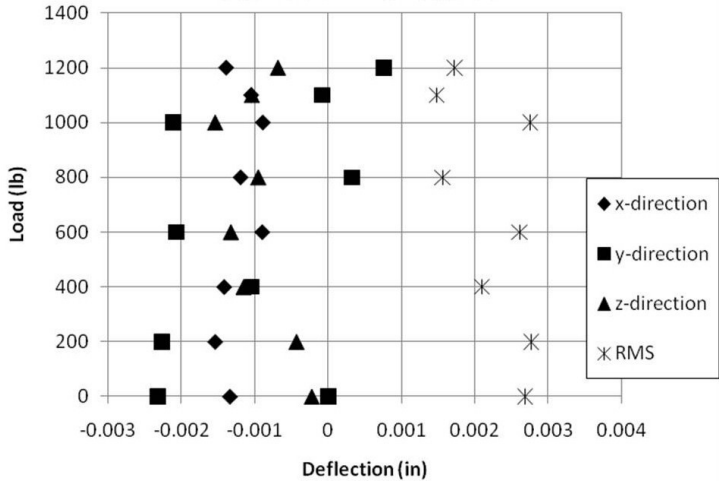

Figure 4.69: Solid Joined-wing - Aft Reference Point 2 - Movement.

base plate reference points, seen in Figs. 4.66 and 4.67. This signifies that the base plate is lifting slightly under high loads; however, this is still low enough that the assumption of no rotation is still valid, contributing to less that 2% error in tip deflection at a 1,200 lb load.

V. Conclusions

5.1 Summary

In Chapter 1, this research was introduced and the goals of this research were presented: provide experimental data on simple joined-wing test articles that will allow researchers to validate tools like GEBT for use in the design of joined-wing HALE aircraft, develop a standard set of experimental procedures for testing joined-wings in the lab, and compare experimental data with analytical results.

In Chapter 2, an overview of the joined-wing aircraft was presented. Previous experimental and analytical efforts were detailed. In particular, GEBT was presented and the need for accurate measurement data for validation of this new theory.

In Chapter 3, the experimental plan and design was detailed. The qualification stage of this experiment was focused on verifying all experimental procedures, resolving construction issues, and gaining confidence in data collection and analysis. The joined-wing stage was the primary experiment of this research effort and incorporated lessons learned from procedures evaluated during the qualification stage to facilitate ease of data collection and analysis. There were three types of qualification and joined-wings designed: solid, hollow, and foam-filled. However, only the solid and hollow qualification and solid joined-wing test articles were constructed in time for this research.

In Chapter 4, the results of the experimental testing of the solid and hollow qualification and solid joined-wing test articles were detailed, as well as the preliminary FEA results. Displacement data was collected with the FARO Laser Tracker. Surface shape scans were taken with the FARO Photon 80. These measurements were transformed to match the coordinate system of the FE model for easy data comparisons. It was shown that all the test articles exhibited non-permanent geometric non-linear deflections, requiring the use of time-intensive non-linear solvers. The movement of the base plates was tracked to ensure that the boundary assumptions were correct.

5.2 Results

The goals of this research were to provide experimental data on simple joined-wing test articles that will allow researchers to validate tools like GEBT for use in the design

of joined-wing HALE aircraft, to develop a standard set of experimental procedures for testing joined-wings in the lab, and to compare experimental data with analytical results. These goals were met: quality data was collected which is ready to use for optimization, the experimental procedures were verified and ready for further use, and the data was compared to preliminary FE models showing that non-linear analyses are required for the joined-wing design.

The solid qualification test article was tested with respect to both bending axes. Preliminary FE models showed fairly good correlation. Bending in the transverse direction produced the expected non-linear buckling. The hollow qualification test article proved to be extremely flexible and subject to extreme skin buckling. This skin buckling proved to be impossible to analyze in Nastran at the higher load levels.

The solid joined-wing test article was successfully tested. The joined-wing was designed to exhibited non-linear bend-twist before material yield and this was clearly observed and measured. Even though the aft wing started buckling, it was still able to carry a load equal to the fore wing root attachment point. This signifies that although a joined-wing can buckle, this buckling is not the same as a single wing buckling. A buckle-critical joined-wing can still carry a load, and this allows less stiff and potentially lighter wings to be built for an aircraft using the joined-wing concept. The FE model correlated well, although the FE model showed a higher amount of top plate rotation than the experimental results. The surface scans aligned with the non-linear FE model results as the load was increased, matching the deflections in both the fore and aft wing as well as the bend-twist coupling. Strain measurements showed that during the non-linear bend-twist coupling of the joined-wing, the root of the aft wing experienced a stress relief.

The Photon 80 performed extremely well for capturing the surface shapes of the test articles. The Laser Tracker added the precision data needed to create accurate point tracks, verify that the base constraints were correct, and align the data to the FE model.

Besides a significant quality and quantity of collected data, it was shown the reason the joined-wing concept is popular for HALE aircraft despite its complicated geometric non-linearities: this design is extremely stiff. The solid qualification test article experi-

enced 28% deflection compared to length at only a 200 lb load, where as the joined-wing test article experienced only 11% deflection compared to length at 6 times the load. Further, at a 200 lb load, the joined-wing experienced $\leq$1% deflection compared to length. This allows a similarly designed joined-wing HALE aircraft to devote significantly less structure to the wings as a single wing HALE aircraft.

5.3 Future Work

Further testing needs to be performed on the solid joined-wing test article, particularly with varying applied load directions. The hollow and foam-filled joined-wing test articles need to be constructed and tested as well. These additional test articles are closer in design to real aircraft wings and will bridge the gap between a solid cross-section and actual wings with ribs, spars and skin. Additional joined-wing test articles should be built with composite materials, since most HALE aircraft are constructed from composite materials.

The load application structure needs to be modified to allow the load direction to be changed. It may be possible to cause the fore wing to begin twisting before the aft wing. Also, follower forces should be investigated to better approximate air loads.

The joined-wing test articles should be vibrationally tested to measure the natural frequencies and modes of each test article. This testing should be done at both zero and non-zero load cases to help in dynamic analyses. This data can be used for further FE model optimization and GEBT validation.

Further, full field strain measurements should be considered in order to collect a better picture of the strain field over the entire test article. This will aid in the validation and correlation of the FE models and code as well as verify the predicted strain field. It would also allow non-contact strain measurements over the entire structure without the error of finite length gages.

The recorded data should be used to validate GEBT code, allowing GEBT to optimize further iterations of test articles. Also, the existing data should be used to

correlate the FE models using optimization routines. This will increase the confidence of using the FE models to develop the test plans for future joined-wing experiments.

Appendix A. Solid Qualification - Lateral Bending - Test Article Data

The following figures and tables supplement and expand on the data presented in Chapter 4.

Table A.1: Solid Qualification - Lateral Bending - Percent Error of Non-Linear FEM.

Load (lb)	x (%)	y (%)	z (%)	RMS (%)
15	93	70	5	5
25	93	22	19	19
50	94	11	9	9
75	93	11	4	4
100	89	11	2	2
125	81	12	0	0
150	353	11	0	0
175	126	8	1	1
200	114	4	3	3

Table A.2: Solid Qualification - Lateral Bending - Percent Error of Linear FEM.

Load (lb)	x (%)	y (%)	z (%)	RMS (%)
15	93	154	4	4
25	93	150	21	21
50	94	123	14	14
75	92	115	13	13
100	89	112	15	15
125	79	110	19	18
150	390	109	24	23
175	131	109	31	29
200	117	109	39	36

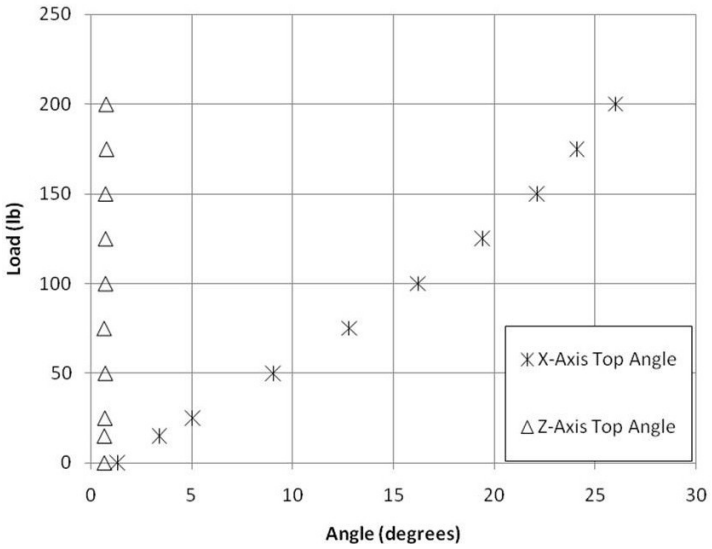

Figure A.1: Solid Qualification - Lateral Bending - Top Plate Angles

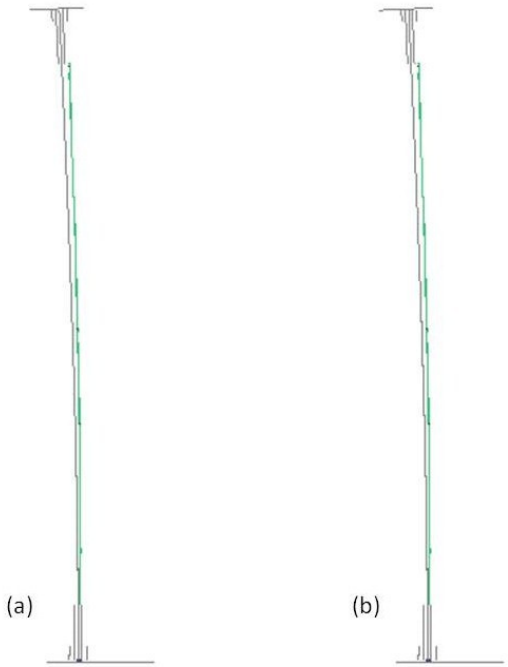

Figure A.2: Solid Qualification - Lateral Bending - 15 lb Surface Matching - (a) Linear and (b) Non-Linear.

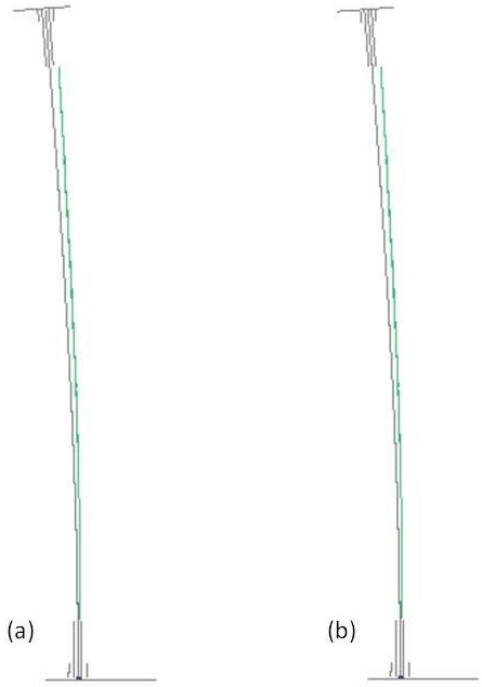

Figure A.3: Solid Qualification - Lateral Bending - 25 lb Surface Matching - (a) Linear and (b) Non-Linear.

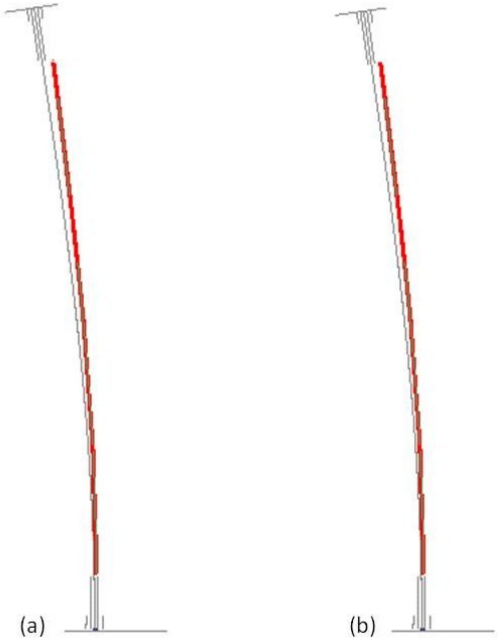

Figure A.4: Solid Qualification - Lateral Bending - 50 lb Surface Matching - (a) Linear and (b) Non-Linear.

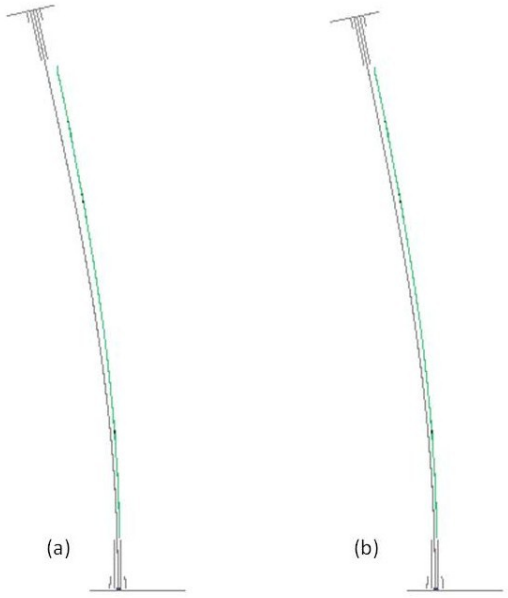

Figure A.5: Solid Qualification - Lateral Bending - 75 lb Surface Matching - (a) Linear and (b) Non-Linear.

Figure A.6: Solid Qualification - Lateral Bending - 100 lb Surface Matching - (a) Linear and (b) Non-Linear.

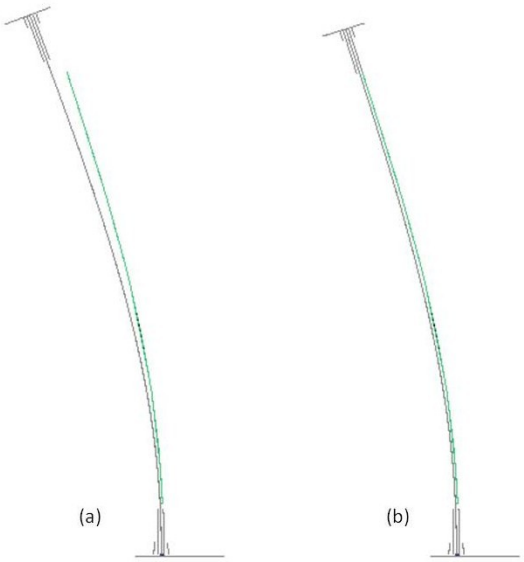

Figure A.7: Solid Qualification - Lateral Bending - 125 lb Surface Matching - (a) Linear and (b) Non-Linear.

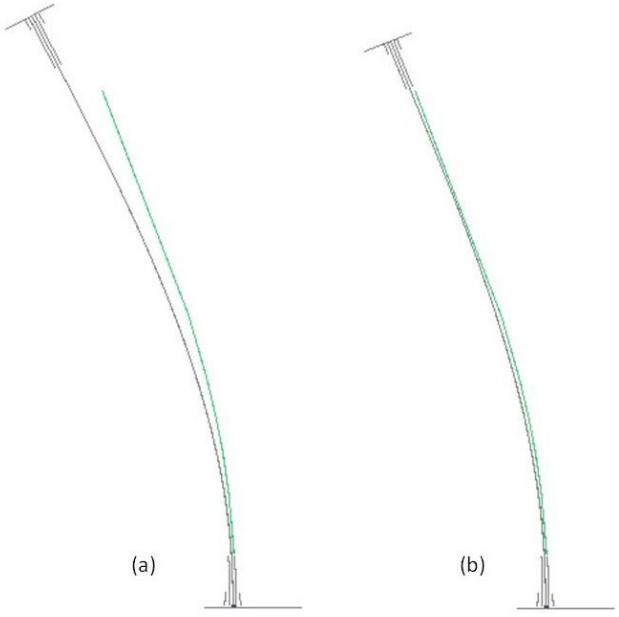

Figure A.8: Solid Qualification - Lateral Bending - 175 lb Surface Matching - (a) Linear and (b) Non-Linear.

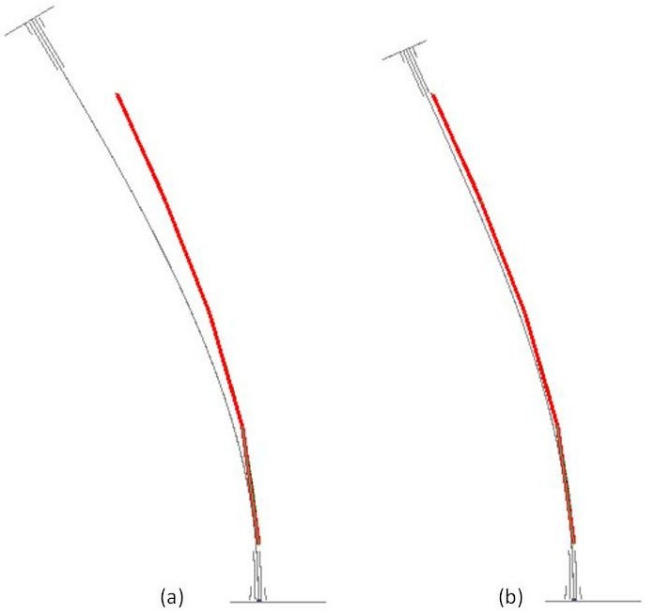

Figure A.9: Solid Qualification - Lateral Bending - 200 lb Surface Matching - (a) Linear and (b) Non-Linear.

Appendix B. Solid Qualification - Transverse Bending - Test Article Data

The following figures and tables supplement and expand on the data presented in Chapter 4.

Table B.1: Solid Qualification - Transverse Bending - Percent Error of Non-Linear FEM.

Load (lb)	x (%)	y (%)	z (%)	RMS (%)
100	6	13	32	5
200	7	28	40	10
400	4	21	19	6
500	3	21	19	5
600	1	21	19	3
800	5	22	18	0
900	7	23	18	2
1000	11	27	17	6
1100	17	38	14	11
1200	36	78	0	29
1300	28	261	11	25

Table B.2: Solid Qualification - Transverse Bending - Percent Error of Linear FEM.

Load (lb)	x (%)	y (%)	z (%)	RMS (%)
100	24	26	34	24
500	122	130	17	108
1000	184	218	18	155
1300	124	490	27	105

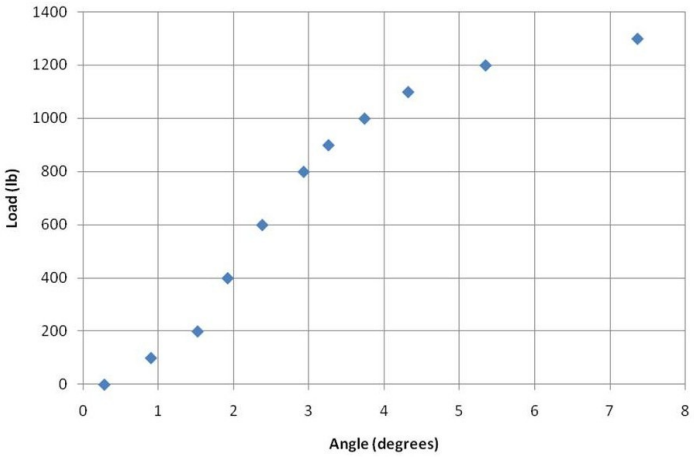

Figure B.1: Solid Qualification - Transverse Bending - Top Plate Angle

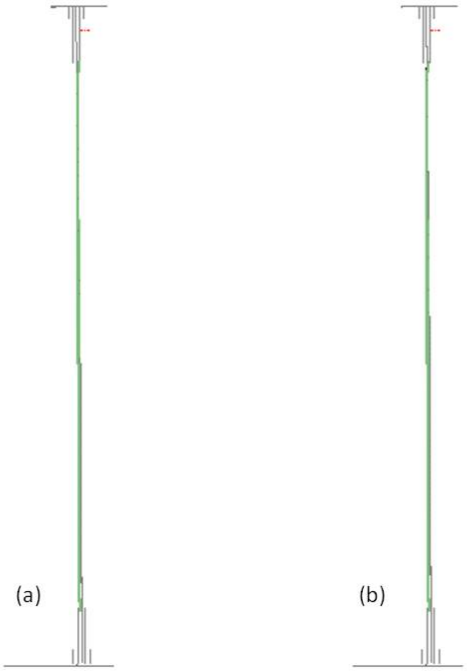

Figure B.2: Solid Qualification - Transverse Bending - 100 lb Surface Matching - (a) Linear and (b) Non-Linear.

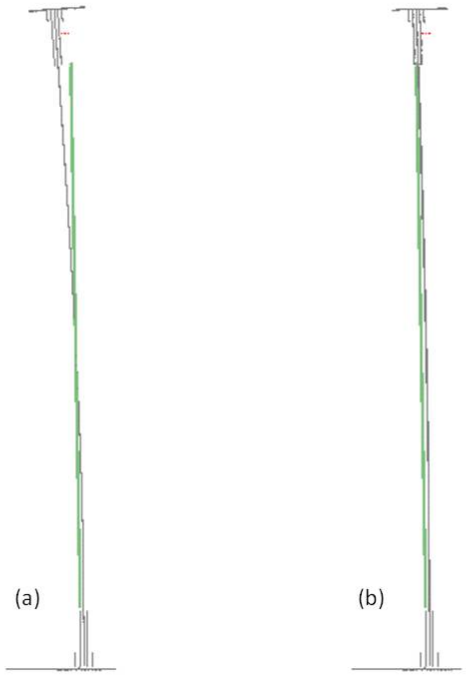

Figure B.3: Solid Qualification - Transverse Bending - 500 lb Surface Matching - (a) Linear and (b) Non-Linear.

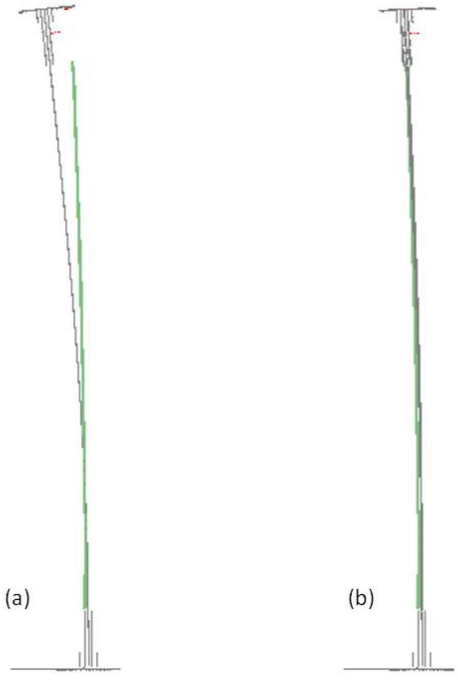

Figure B.4: Solid Qualification - Transverse Bending - 750 lb Surface Matching - (a) Linear and (b) Non-Linear.

Figure B.5: Solid Qualification - Transverse Bending - 800 lb Surface Matching - (a) Linear and (b) Non-Linear.

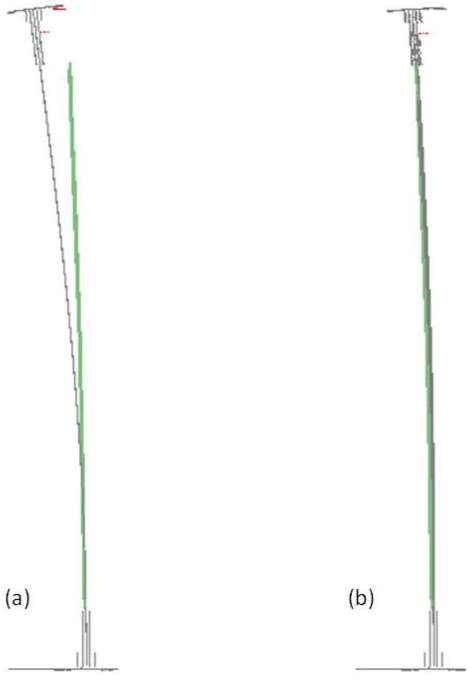

Figure B.6: Solid Qualification - Transverse Bending - 900 lb Surface Matching - (a) Linear and (b) Non-Linear.

Figure B.7: Solid Qualification - Transverse Bending - 1100 lb Surface Matching - (a) Linear and (b) Non-Linear.

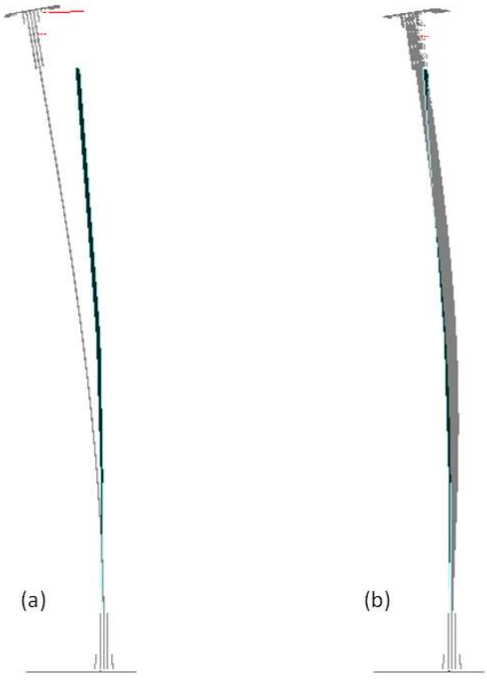

Figure B.8: Solid Qualification - Transverse Bending - 1250 lb Surface Matching - (a) Linear and (b) Non-Linear.

Appendix C. Hollow Qualification Test Article Data

The following figures and tables supplement and expand on the data presented in Chapter 4.

Table C.1: Hollow Qualification - Percent Error of Non-Linear FEM.

Load (lb)	x (%)	y (%)	z (%)	RMS (%)
10	98	72	39	39

Table C.2: Hollow Qualification - Percent Error of Linear FEM.

Load (lb)	x (%)	y (%)	z (%)	RMS (%)
10	101	103	58	58
20	102	102	55	55
30	102	102	46	47

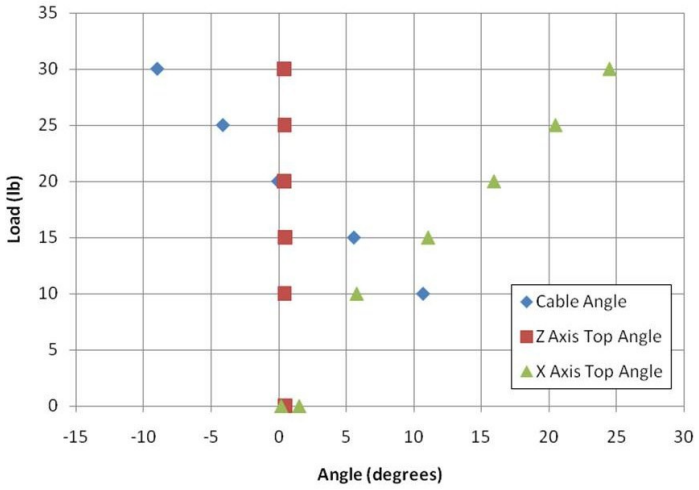

Figure C.1: Hollow Qualification - Top Plate Angle

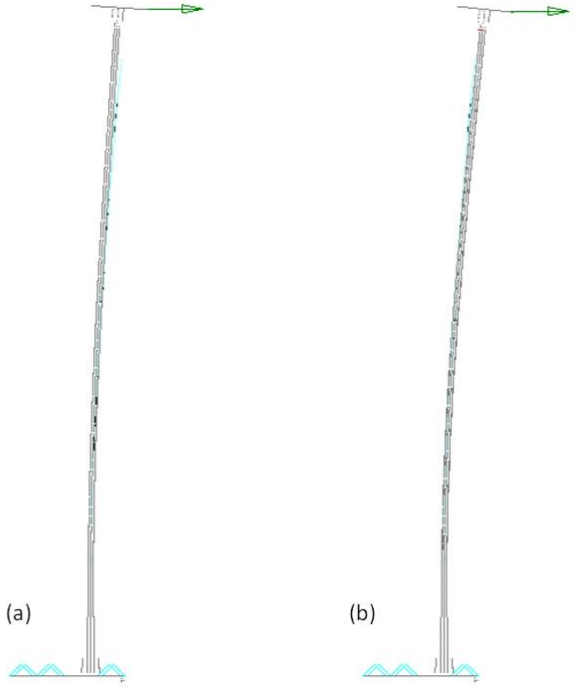

Figure C.2: Hollow Qualification - 10 lb Surface Matching - (a) Linear and (b) Non-Linear.

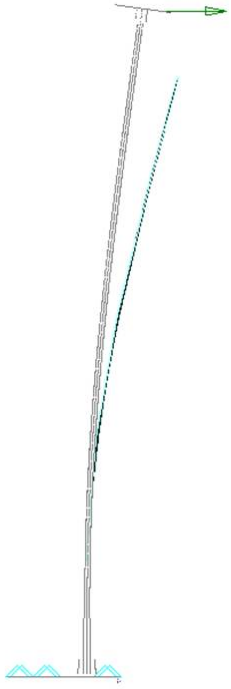

Figure C.3: Hollow Qualification - 20 lb Surface Matching - Linear.

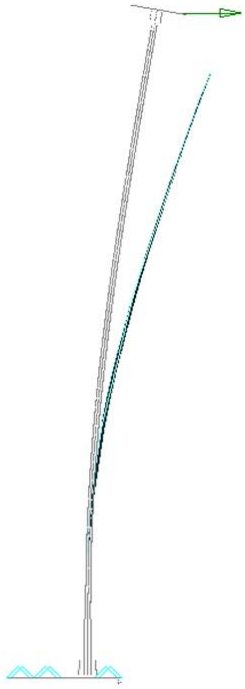

Figure C.4: Hollow Qualification - 25 lb Surface Matching - Linear.

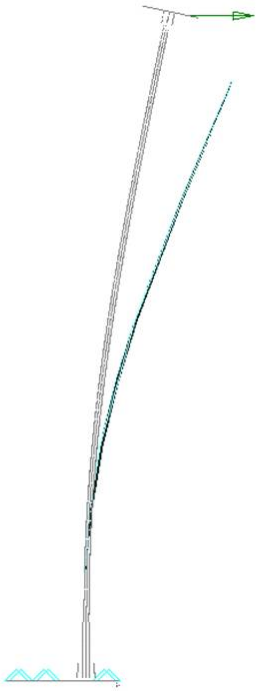

Figure C.5: Hollow Qualification - 30 lb Surface Matching - Linear.

Appendix D. Solid Joined-wing Test Article Data

The following figures and tables supplement and expand on the data presented in Chapter 4.

Table D.1: Solid Joined-wing - Point 1 - Percent Error of Linear FEM.

Load (lb)	x (%)	y (%)	z (%)	RMS (%)
25	116	48	105	105
100	47	17	48	48
200	39	17	40	40
300	5	12	1	0
400	6	7	3	4
500	6	21	3	3
600	6	34	4	4
700	6	43	5	5
800	8	53	8	8
900	10	61	11	11
1000	14	70	17	17
1100	19	78	24	24
1200	28	85	35	35

Table D.2: Solid Joined-wing - Point 2 - Percent Error of Linear FEM.

Load (lb)	x (%)	y (%)	z (%)	RMS (%)
25	115	411	108	109
100	47	64	49	49
200	38	74	40	40
300	5	25	2	2
400	6	67	4	5
500	6	177	4	4
600	6	1562	5	5
700	6	571	6	6
800	8	273	8	8
900	10	195	12	12
1000	14	155	18	17
1100	19	133	25	25
1200	28	119	36	35

Table D.3: Solid Joined-wing - Point 3 - Percent Error of Linear FEM.

Load (lb)	x (%)	y (%)	z (%)	RMS (%)
25	111	378	121	120
100	46	67	51	51
200	38	67	41	41
300	5	21	4	4
400	7	26	6	6
500	6	35	6	6
600	6	44	6	6
700	7	55	8	7
800	8	66	10	10
900	10	91	14	13
1000	14	141	19	18
1100	20	300	26	25
1200	29	1051	37	36

Table D.4: Solid Joined-wing - Point 4 - Percent Error of Linear FEM.

Load (lb)	x (%)	y (%)	z (%)	RMS (%)
25	144	269	134	137
100	49	81	53	53
200	39	74	42	42
300	5	21	5	4
400	7	24	7	7
500	6	29	7	6
600	6	35	8	7
700	7	40	9	8
800	8	46	11	10
900	11	54	15	14
1000	15	68	20	19
1100	20	97	27	26
1200	29	206	38	36

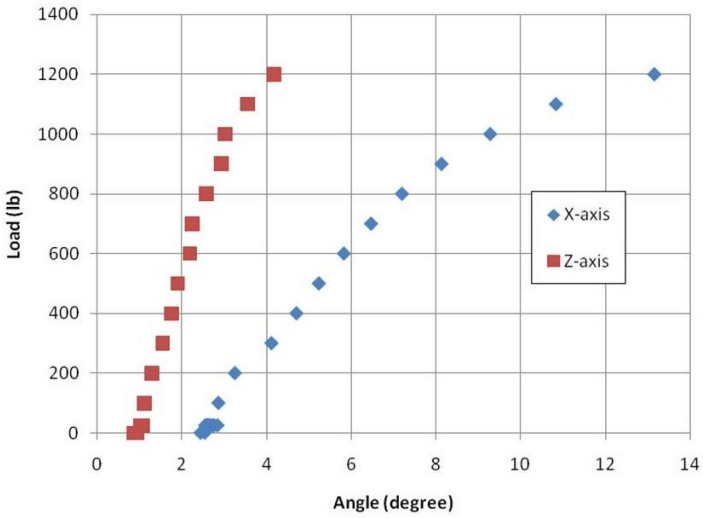

Figure D.1: Solid Joined-wing - Top Plate Angles

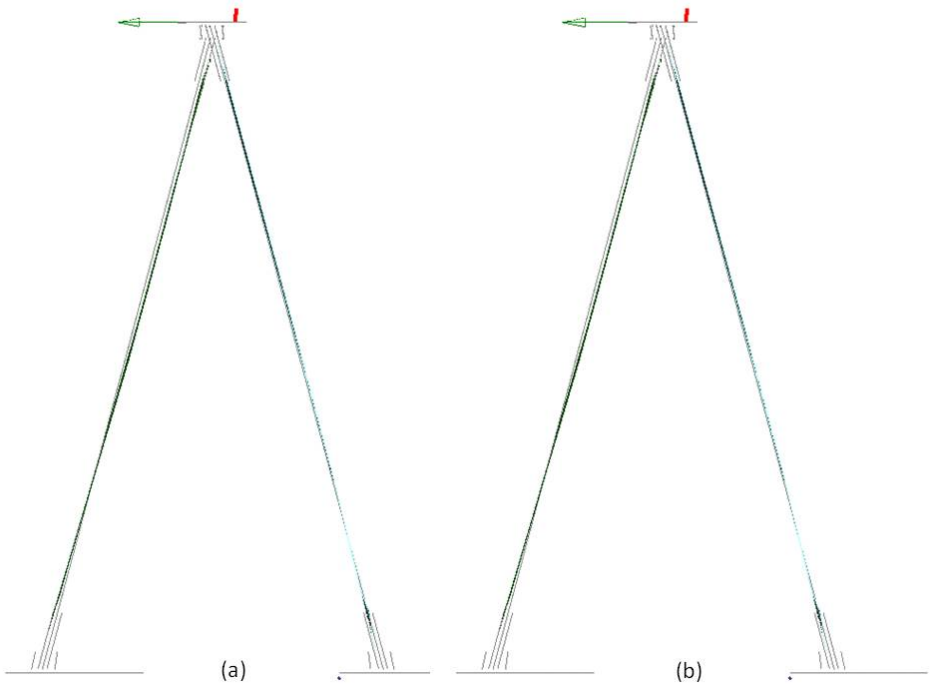

Figure D.2: Solid Joined-wing - 25 lb Surface Matching - (a) Linear and (b) Non-Linear.

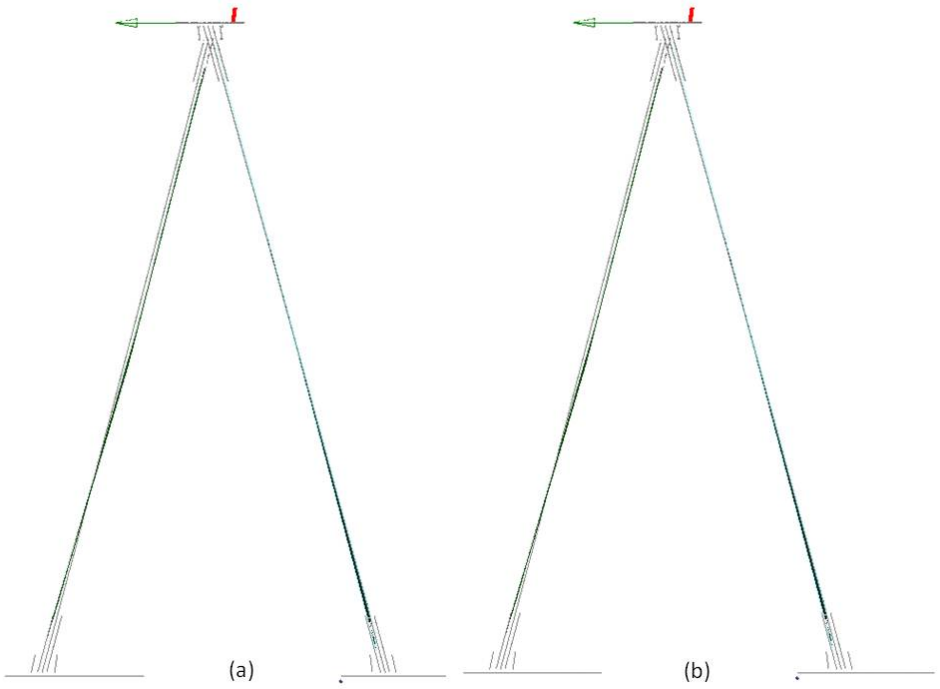

Figure D.3: Solid Joined-wing - 100 lb Surface Matching - (a) Linear and (b) Non-Linear.

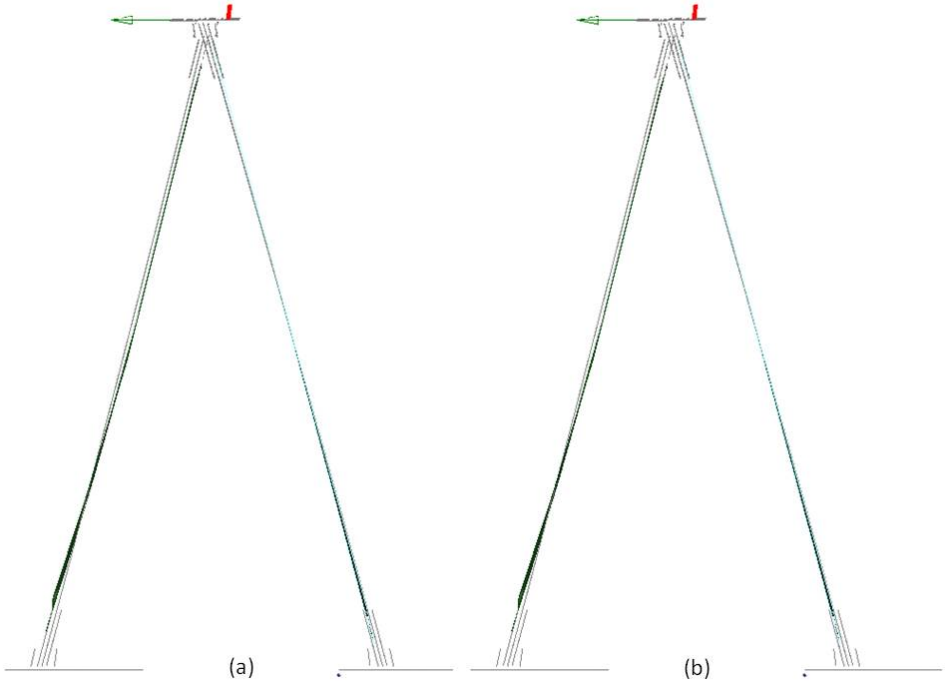

Figure D.4: Solid Joined-wing - 200 lb Surface Matching - (a) Linear and (b) Non-Linear.

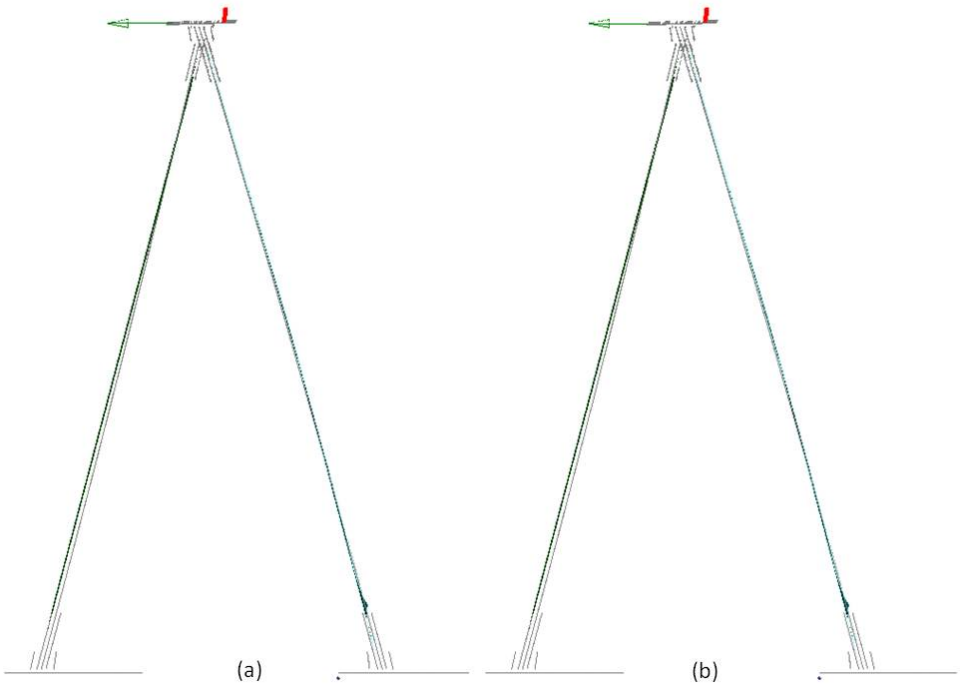

Figure D.5: Solid Joined-wing - 300 lb Surface Matching - (a) Linear and (b) Non-Linear.

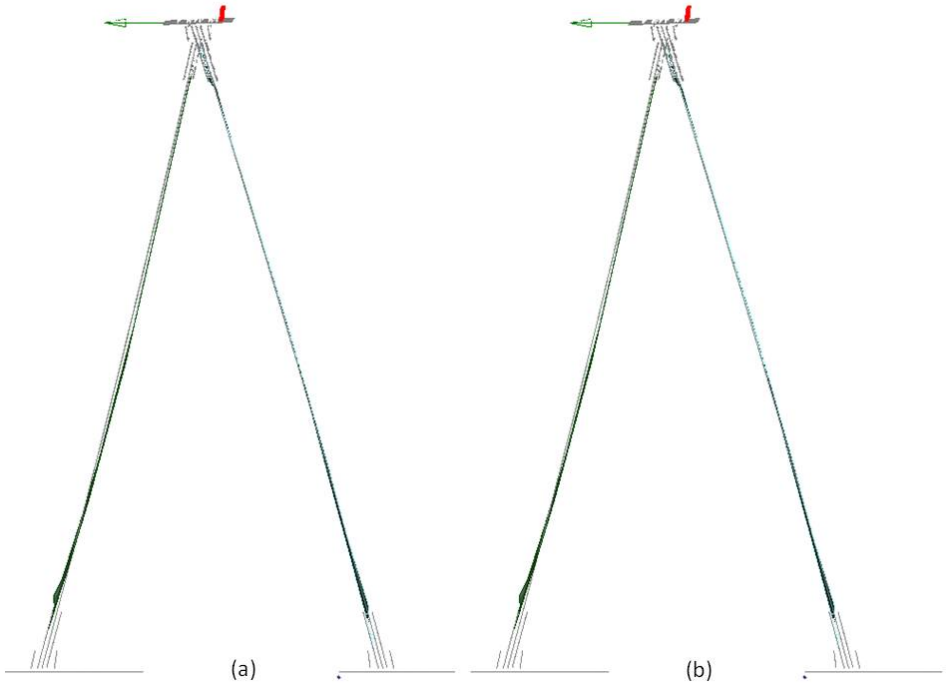

Figure D.6: Solid Joined-wing - 400 lb Surface Matching - (a) Linear and (b) Non-Linear.

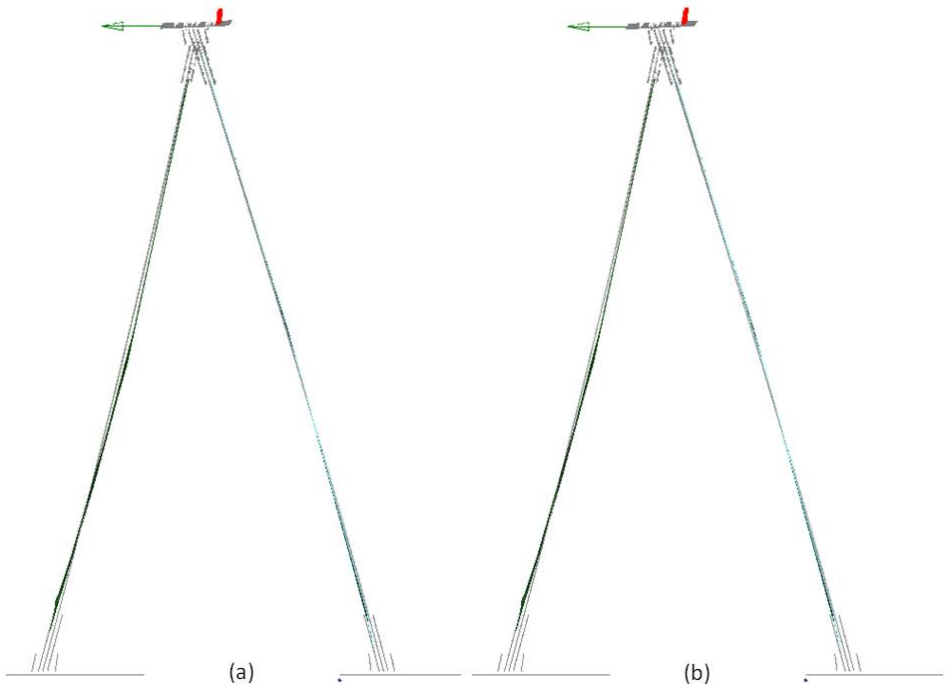

Figure D.7: Solid Joined-wing - 500 lb Surface Matching - (a) Linear and (b) Non-Linear.

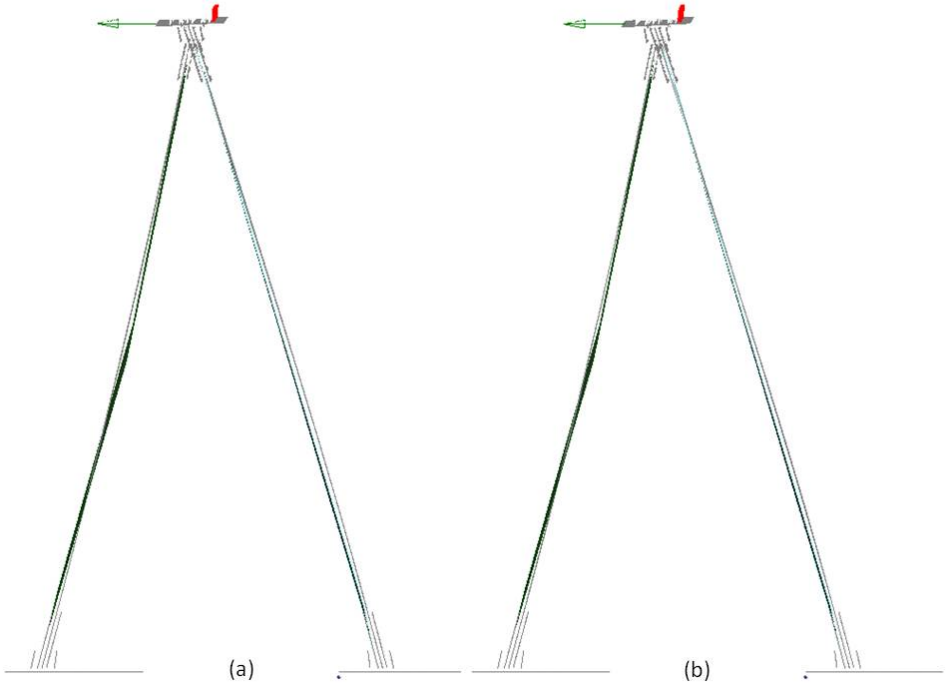

Figure D.8: Solid Joined-wing - 600 lb Surface Matching - (a) Linear and (b) Non-Linear.

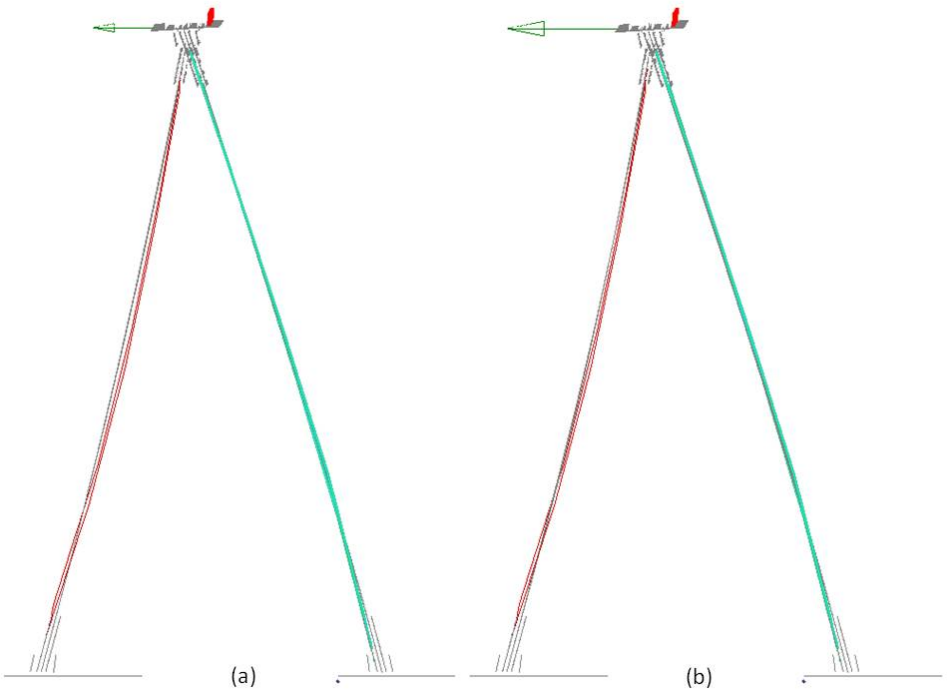

Figure D.9: Solid Joined-wing - 700 lb Surface Matching - (a) Linear and (b) Non-Linear.

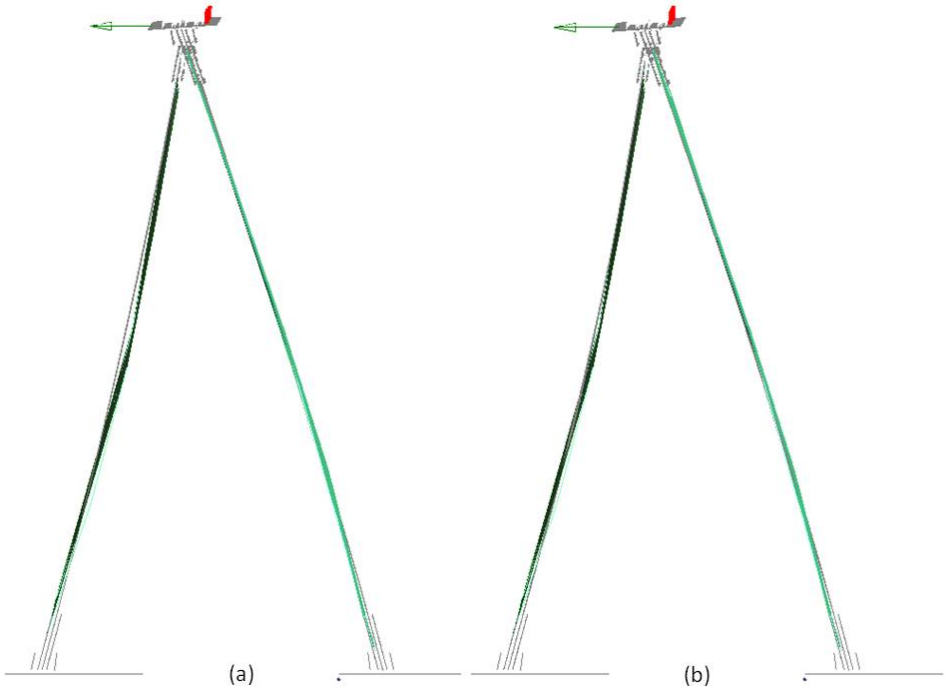

Figure D.10: Solid Joined-wing - 800 lb Surface Matching - (a) Linear and (b) Non-Linear.

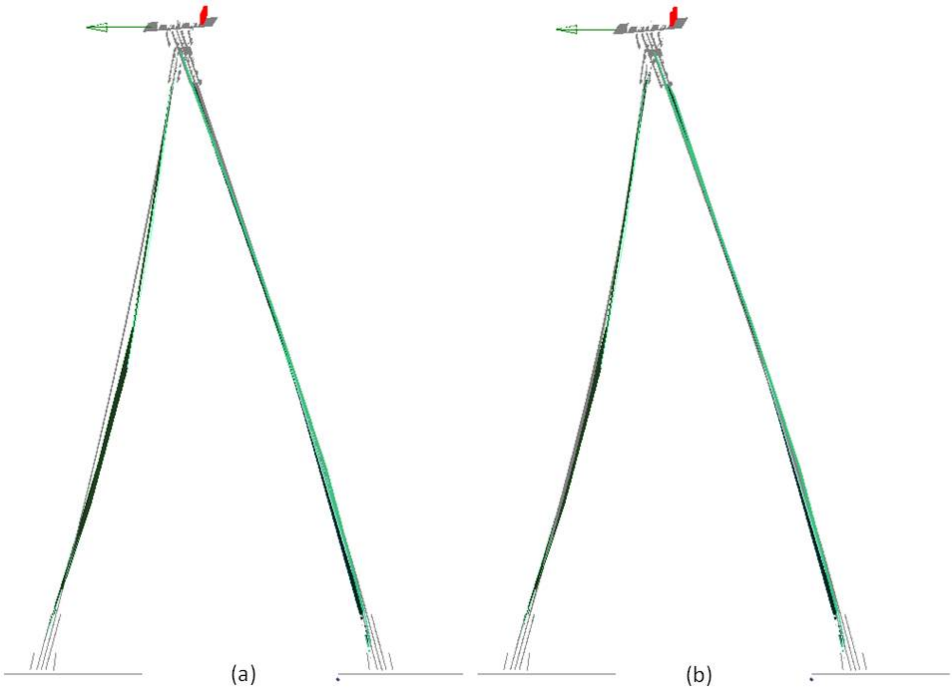

Figure D.11: Solid Joined-wing - 900 lb Surface Matching - (a) Linear and (b) Non-Linear.

Appendix E. Base Reference Point Data

The following figures and tables supplement and expand on the data presented in Chapter 4.

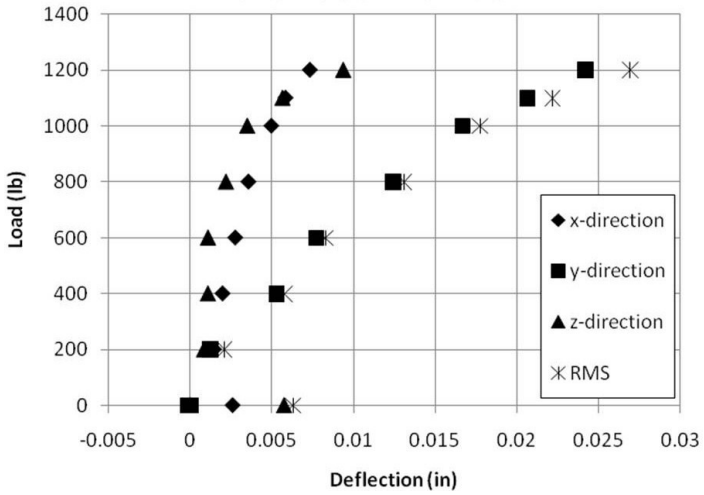

Figure E.1: Solid Joined-wing - Fore Reference Point 3 - Movement.

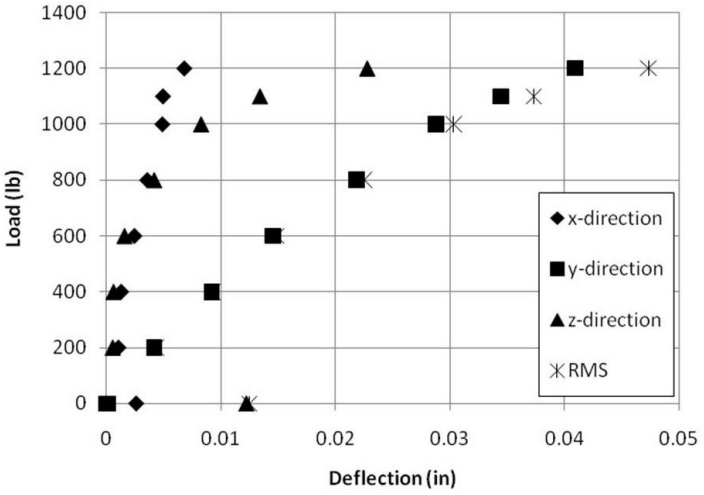

Figure E.2: Solid Joined-wing - Fore Reference Point 4 - Movement.

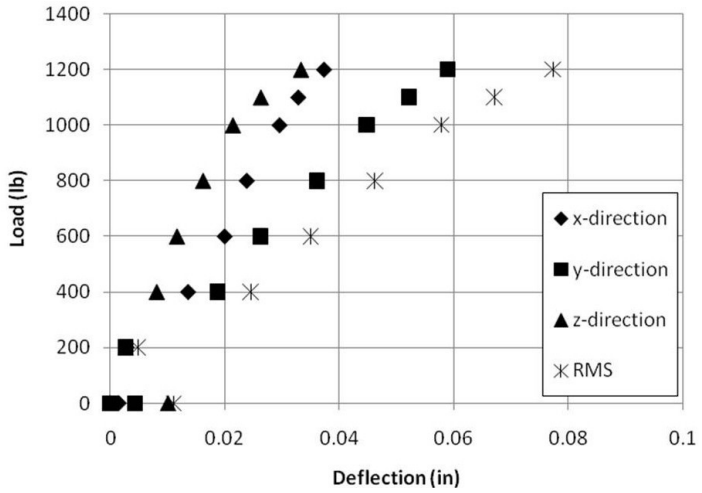

Figure E.3: Solid Joined-wing - Fore Reference Point 5 - Movement.

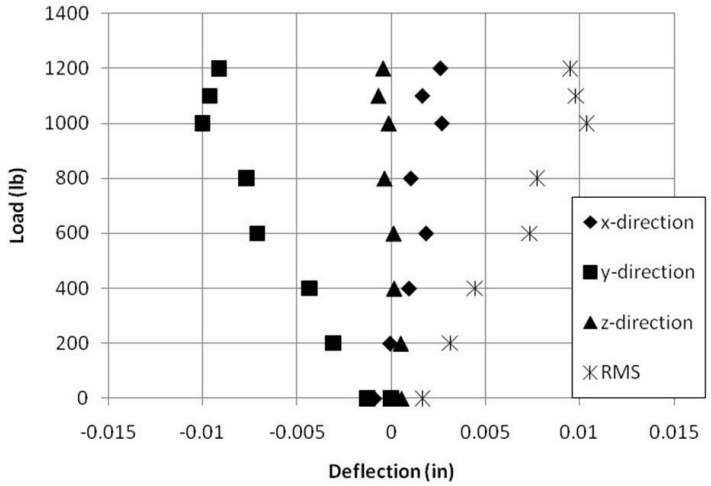

Figure E.4: Solid Joined-wing - Aft Reference Point 3 - Movement.

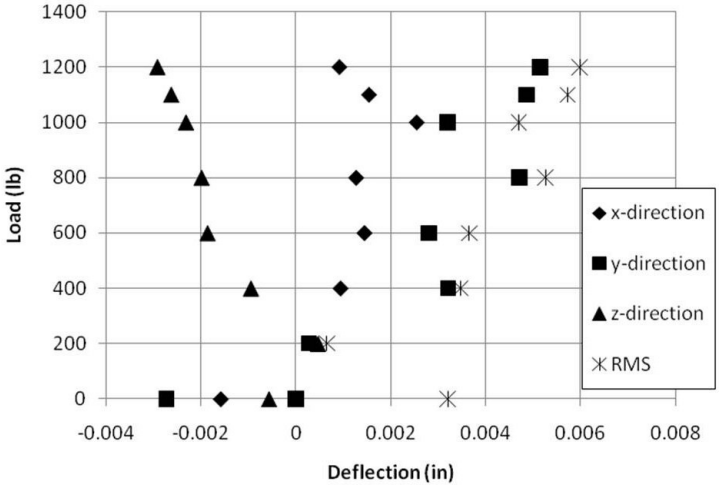

Figure E.5: Solid Joined-wing - Aft Reference Point 4 - Movement.

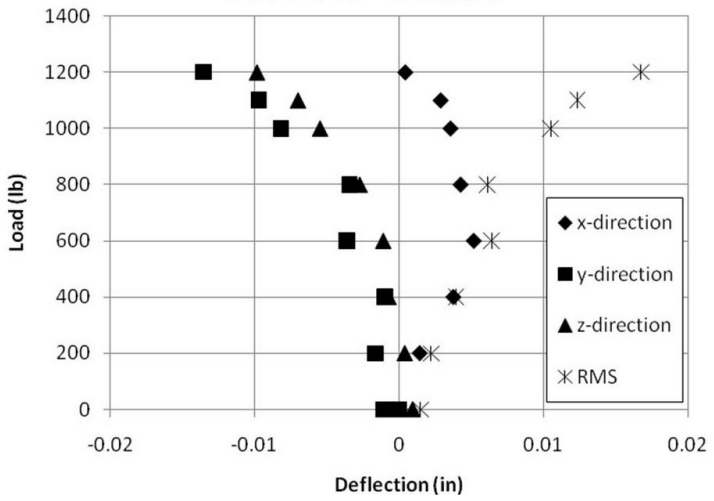

Figure E.6: Solid Joined-wing - Aft Reference Point 5 - Movement.

Bibliography

1. Adams, Brandon J. *Structural Stability of a Joined-Wing SensorCraft*. Master's thesis, Air Force Institute of Technologies, Jun 2007.

2. Blair, Maxwell, Robert A. Canfield, and Roberts Ronald W., Jr. "Joined-Wing Aeroelastic Design with Geometric Non-Linearity". *Journal of Aircraft*, 42(4):832–848, 2005.

3. Bond, Vanessa L. *Flexible Twist for Pitch Control in a High Altitude Long Endurance Aircraft with Nonlinear Response*. Ph.D. thesis, Air Force Institute of Technologies, Dec 2008.

4. Boston, Jonathan, Nicholas S. Green, and Nick Keller. "Mech 542 Aluminum Joined-Wing Experiment", Mar 2009. Final Report for Mech 542, AFIT.

5. Chairman, MIL-HDBK-5 Coordination Activity. *Metallic Materials and Elements for Aerospace Vehicle Structures, MIL-HDBK-5H*. Department of Defense, 1998.

6. FARO Technologies, Inc. "FARO Laser Tracker Xi Datasheet". `http://www.faro.com/FaroIP/Files/File/TechsheetsDownload/04REF201_038_LASER_TRACKER_Xi.pdf`, 2008.

7. FARO Technologies, Inc. "FARO Photon 80/20 Datasheet". `http://www.faro.com/pdf/FARO_Photon_en.pdf`, 2009.

8. Gallman, John W. and Ilan M. Kroo. "Structural Optimization for Joined-Wing Synthesis". *Journal of Aircraft*, 33(1):214–223, 1996.

9. Gallman, John W., Stephen C. Smith, and Ilan M. Kroo. "Optimization of Joined-Wing Aircraft". *Journal of Aircraft*, 30(6):897–905, 1993.

10. Green, Nicholas S. *Structural Optimization of Joined-Wing Beam Model with Bend-Twist Coupling Using Equivalent Static Loads*. Master's thesis, Air Force Institute of Technologies, Jun 2009.

11. Hartog, J.P. *Advanced Strength of Materials*. McGraw-Hill Book Company, Inc., 1952.

12. Hodges, D. H. "A Mixed Variational Formulation Base on Exact Intrinsic Equations for Dynamics of Moving Beams". *International Journal of Solids and Structures*, 26:832–848, 1990.

13. Kaloyanova, Valentina D., Karman N. Ghia, and Urmila Ghia. "Structural Modeling and Optimization of the Joined Wing of a High-Altitude Long-Endurance (HALE) Aircraft". *AIAA Aerospace Sciences Metting and Exhibit*, AIAA 2005-1087. Reno, Nevada, Jan 2005.

14. Marisarla, Soujanya. *Structural Analysis of an Equivalent Box-Wing Representation of Sensorcraft Joined-Wing Configuration for High-Altitude, Long-Endurance (HALE) Aircraft*. Master's thesis, University of Cincinnati, Mar 2005.

15. Narayanan, Vijay. *Structural Analysis of Reinforced Shell Wing Model for Joined-Wing Configuration*. Master's thesis, University of Cincinnati, Mar 2005.

16. Omar, E. *Sensor Integration Study for Sensor Craft UAV Mid-Term Review*. Presentation Material Contract: F33613-00-D-3052, Delivery Order: 0019, The Boeing Company, Washington, Sept 9-10, 2003.

17. Patil, Mayuresh J. "Nonlinear Aeroelastic Analysis of Joined-Wing Aircraft". *AIAA/ASME/ASCE/AHS Structures, Structural Dynamics, and Materials Conference*, AIAA 2003-1487. Norfolk, Virginia, Apr 2003.

18. Rasmussen, Cody C., Robert A. Canfield, and Maxwell Blair. "Optimization Process for Configuration of Flexible Joined-Wing". *AIAA/ISSMO Multidisciplinary Analysis and Optimization Conference*, AIAA 2004-4330. Albany, New York, Aug 2004.

19. Wolkovitch, Julian. "The Joined Wing: An Overview". *Journal of Aircraft*, 23(3):161–178, 1986.

20. Yu, Wenbin and Maxwell Blair. "GEBT: A General-Purpose Tool for Nonlinear Analysis of Composite Beams". *51st AIAA/ASME/ASCE/AHS/ASC Structures, Structural Dynamics, and Materials Conference*, AIAA 2010-3019. Orlando, Florida, Apr 2010.

REPORT DOCUMENTATION PAGE

Form Approved
OMB No. 0704–0188

1. REPORT DATE (DD–MM–YYYY)	2. REPORT TYPE	3. DATES COVERED *(From — To)*
25-03-2010	Master's Thesis	Jan 2009 - Mar 2010

4. TITLE AND SUBTITLE
Experiments with Geometric Non-Linear Coupling for Analytical Validation

5a. CONTRACT NUMBER

5b. GRANT NUMBER

5c. PROGRAM ELEMENT NUMBER

6. AUTHOR(S)
Boston, Jonathan D., YD-1, USAF, ASC/EN

5d. PROJECT NUMBER
09ENY340

5e. TASK NUMBER

5f. WORK UNIT NUMBER

7. PERFORMING ORGANIZATION NAME(S) AND ADDRESS(ES)
Air Force Institute of Technology
Graduate School of Engineering and Management (AFIT/ENY)
2950 Hobson Way
WPAFB OH 45433-7765

8. PERFORMING ORGANIZATION REPORT NUMBER
AFIT/GAE/ENY/10-M04

9. SPONSORING / MONITORING AGENCY NAME(S) AND ADDRESS(ES)
Dr. Maxwell Blair
US Air Force Research Laboratory/RBSD
2130 Eighth Street, Building 146
Wright-Patterson AFB 45433-7542
937-255-8430 (DSN:785-8430)

10. SPONSOR/MONITOR'S ACRONYM(S)
AFRL/RBSD

11. SPONSOR/MONITOR'S REPORT NUMBER(S)

12. DISTRIBUTION / AVAILABILITY STATEMENT
APPROVED FOR PUBLIC RELEASE; DISTRIBUTION UNLIMITED

13. SUPPLEMENTARY NOTES

14. ABSTRACT

This study was focused on obtaining accurate experimental data for the validation of the geometrically exact beam theory from a series of experiments in which high quality surface shape and deflection data was collected. Many previous experiments have experienced issues with data collection or test articles which the researchers were unable to overcome. The test program was performed in two stages: qualification and joined-wing. The qualification stage validated the experimental procedures on simple 72 in long aluminum beams with 8 in x 0.5 in cross-sections. The joined-wing stage was the primary experiment focused on obtaining quality data for use in validation and each joined-wing had an overall length of 57 in. The fore wing was designed with a chord of 8 in and a thickness of 0.5 in; the aft wing was designed with a chord of 6 in and a thickness of 0.5 in. These dimensions were chosen so the joined-wing produced a non-linear bend-twist couple before permanent deformation. The bend-twist couple in a solid cross-section aluminum joined-wing was successfully captured with surface shape, deflection points, and strain data.

15. SUBJECT TERMS
Joined-wing, GEBT, geometric coupling, experimental methods, bend-twist coupling

16. SECURITY CLASSIFICATION OF:			17. LIMITATION OF ABSTRACT	18. NUMBER OF PAGES	19a. NAME OF RESPONSIBLE PERSON
a. REPORT	b. ABSTRACT	c. THIS PAGE	UU	131	Eric D. Swenson, Lt Col, USAF (ENY)
U	U	U			19b. TELEPHONE NUMBER (Include Area Code) (937)255-3636, ext 7479 eric.swenson@afit.edu